

INTERDISCIPLINARY SPACE LOGISTICS OPTIMIZATION FRAMEWORK FOR LARGE-SCALE SPACE EXPLORATION

A Dissertation
Presented to
The Academic Faculty

by

Hao Chen

In Partial Fulfillment
of the Requirements for the Degree
Doctor of Philosophy in the
College of Engineering
Daniel Guggenheim School of Aerospace Engineering

Georgia Institute of Technology
May 2021

COPYRIGHT © 2021 BY HAO CHEN

INTERDISCIPLINARY SPACE LOGISTICS OPTIMIZATION FRAMEWORK FOR LARGE-SCALE SPACE EXPLORATION

Approved by:

Dr. Koki Ho, Advisor
School of Aerospace Engineering
Georgia Institute of Technology

Dr. Brian Gunter
School of Aerospace Engineering
Georgia Institute of Technology

Dr. E. Glenn Lightsey
School of Aerospace Engineering
Georgia Institute of Technology

Dr. Christopher Carr
School of Aerospace Engineering
Georgia Institute of Technology

Dr. Harrison Hyung Min Kim
Department of Industrial and Enterprise
Systems Engineering
University of Illinois at Urbana-Champaign

Date Approved: April 16, 2021

All civilizations become either spacefaring or extinct.
Carl Sagan

For my wife Dingyue

ACKNOWLEDGEMENTS

I would like to thank everyone I met, talked, and discussed my work with during my five-year Ph.D. study at both the University of Illinois at Urbana-Champaign and Georgia Tech. I always think I'm one of the luckiest guys on this planet. Without the tremendous support, help, and advice from them, I could not have completed all the fantastic work introduced in this thesis.

First of all, I can't describe how thankful I am to my advisor, Prof. Koki Ho. Without his great advice and support, I could not have completed all of my achievements during my Ph.D. study. I still remember our first meeting on the third floor of the Talbot lab, where I selected space logistics as my research direction without any hesitation, not realizing that it would be my life-long focus and career. It was an afternoon in the spring, just like today.

In addition, I would like to express my thanks to my other committee members. Prof. Harrison Kim provided me a lot of support when I was at UIUC, especially during my multiple application processes to the CSE fellowship program. I also appreciate the help and support from Prof. Glenn Lightsey and Prof. Brian Gunter after I arrived at Georgia Tech. Valuable mission operation information and data received from Prof. Christopher Carr were useful not only for this thesis but also for my future studies in space exploration. I'm also grateful to Prof. Melkior Ornik and Prof. Paul Grogan for their consistent advice during my research.

Moreover, I want to thank all my friends in the Space Systems Optimization Group (SSOG), Hang Woon, Tristan, Kento, etc. Without your help, my Ph.D. studies wouldn't have been that smooth. I cannot forget our drifting along a river the name of which I can no longer remember. That was one of my happiest memories in Champaign.

I would like to pay special thanks to my wife, parents, and relatives for their continuous encouragement of my work and life in the US. Their support has fueled my hope, optimism, and enthusiasm.

Before I forget, I also would like to thank all the tasty restaurants in both Champaign and Atlanta, i.e., BoBo China, Tang Dynasty, Royal China, etc. The delicious foods there provided me endless energy to nourish me so that I could complete this thesis.

Having been a student for over twenty years, it's time to add a period and start a new journey. Like any end, this is just another beginning.

TABLE OF CONTENTS

ACKNOWLEDGEMENTS	iv
LIST OF TABLES	viii
LIST OF FIGURES	x
NOMENCLATURE	xii
SUMMARY	xvi
CHAPTER 1. Introduction	1
1.1 Motivation and Objective	1
1.2 Research Contributions	3
1.2.1 Contribution 1: Mixed-Integer Nonlinear Programming (MINP) Formulation for Integrated Space Logistics and Spacecraft Design	4
1.2.2 Contribution 2: Periodic Time-Expanded Network (TEN) for Regular Interplanetary Mission	4
1.2.3 Contribution 3: Multi-Fidelity Mission Planning Framework for Infrastructure Design and Resource Logistics	5
1.2.4 Contribution 4: Decision Rules for Flexibility Management	6
1.3 Thesis Overview	7
CHAPTER 2. LITERATURE REVIEWS	8
2.1 MINP for Integrated space logistics and spacecraft design	8
2.2 Periodic TEN for Regular Interplanetary Mission	10
2.3 Multi-Fidelity Mission Planning Framework for Infrastructure Design and Resource Logistics	13
2.4 Flexibility Management for Space Logistics via Decision Rules	15
CHAPTER 3. Integrated Space Logistics and Spacecraft Design	20
3.1 Methodology	21
3.1.1 Modeling	21
3.1.2 Optimization Methods	35
3.2 Results and Analysis	42
3.2.1 Model Validation	42
3.2.2 Campaign-level Space Logistics Design	46
3.3 Chapter Summary	63
CHAPTER 4. Regular Interplanetary Mission	65
4.1 Methodology	65
4.1.1 Generalized Multicommodity Network Flow	65
4.1.2 Partially Periodic TEN	67
4.1.3 Properties of Partially Periodic TEN	71
4.2 Case Study Results and Analysis	76
4.2.1 Mars Transportation Mission	76

4.2.2	Spacecraft design model	79
4.2.3	Comparison of Optimization Formulations	80
4.2.4	Analysis of Partially Periodic GMCNF Results	83
4.3	Chapter Summary	85
CHAPTER 5. Infrastructure Design and Resource Logistics		87
5.1	Prefixed Space Infrastructure Optimization Formulation	88
5.2	Full-Size Space Infrastructure Optimization Formulation	91
5.2.1	ISRU system modeling	91
5.2.2	Full-Size Space Logistics Formulation	96
5.2.3	Relationship with the Prefixed Formulation	101
5.2.4	Limitations of the Full-Size Formulation	102
5.3	Multi-Fidelity Space Infrastructure Optimization Formulation	102
5.3.1	Constraint Aggregation and Variable Packing	104
5.3.2	Preprocessing Algorithm for Automatic Commodity Packing	110
5.4	Case Study and Analysis	116
5.4.1	Mission Scenario	116
5.4.2	Comparison of Optimization Formulations	122
5.5	Chapter Summary	129
CHAPTER 6. Flexibility Management via Decision Rules		131
6.1	Methodology	131
6.1.1	Problem Setting	131
6.1.2	Scenario Generation Model	134
6.1.3	Flexibility Management Background and Overview	134
6.1.4	Mission Cost Evaluation through Space Logistics	138
6.1.5	Operating Time Loss Evaluation through Decision Rules	140
6.1.6	Flexibility Management Framework for Space Logistics	145
6.2	Case Study: Space Station Resupply Logistics	146
6.2.1	Space Station Resupply Mission Background	146
6.2.2	Space Station Resupply Mission Analysis and Results	150
6.3	Chapter Summary	156
CHAPTER 7. Conclusion		158
7.1	Thesis Summary	158
7.2	Broader Applications	159
7.3	Future Work	160
APPENDIX A. Parametric Spacecraft Model		164
APPENDIX B. Probability Distribution Generation for the Case Study		166
REFERENCES		171

LIST OF TABLES

Table 1	- Definition of indices, variables, and parameters.	27
Table 2	- Spacecraft sizing comparison.	31
Table 3	- Spacecraft used in Apollo 17.	43
Table 4	- Demand and supply of Apollo 17 mission.	43
Table 5	- Mass differences comparison at Earth orbit insertion.	46
Table 6	- Demand and supply of lunar mission.	48
Table 7	- Summary of parameters and assumptions.	48
Table 8	- Spacecraft design of a single mission design.	49
Table 9	- Spacecraft design of the multi-mission campaign design solution (interval: one year).	51
Table 10	- Comparison of different optimization methods (interval: one year).	57
Table 11	- Computational complexity comparison.	72
Table 12	- Demand and supply of Mars transportation mission.	77
Table 13	- Summary of parameters and assumptions.	78
Table 14	- Lunar exploration demands and supplies.	118
Table 15	- Spacecraft design parameters.	119
Table 16	- ISRU infrastructure design models. [73]	121
Table 17	- Mission operation parameters and assumptions.	122
Table 18	- Comparison of formulation performances w.r.t. ISRU productivity.	124
Table 19	- Optimization formulation performance comparison.	125
Table 20	- Comparison of formulation performances w.r.t. the launch frequency.	127
Table 21	- Sensitivity analysis of ISRU storage system sizing.	129

Table 22	- ISS CRS Cargo Manifest Mass by Category (Dec. 2015 to Jun. 2017).	148
Table 23	- Demand and Supply of the Resupply Mission.	149
Table A1	- List of fuel and corresponding parameters used for spacecraft models.	164
Table A2	- List of spacecraft data used for spacecraft model.	165
Table B1	- Summary of FPIP Planning Dates.	167

LIST OF FIGURES

Figure 1	- Earth-Moon-Mars transportation network	3
Figure 2	- Integrated optimization framework ([adapted from [7, 52-54]])	23
Figure 3	- Full time-expanded network [53]	25
Figure 4	- Nonuniform time-step time-expanded network.	30
Figure 5	- The oxygen production level normalized by ISRU system mass [7].	33
Figure 6	- The oxygen production normalized by ISRU system mass.	34
Figure 7	- Piecewise function and its epigraph as the union of polyhedra.	36
Figure 8	- Flow chart of SA-based approach.	41
Figure 9	- Apollo 17 network model.	42
Figure 10	- Apollo 17 example.	45
Figure 11	- Commodity flows in the optimal solution.	45
Figure 12	- Single lunar mission solution.	50
Figure 13	- Commodity flows of single lunar mission.	50
Figure 14	- Multi-mission lunar campaign solution (interval: one year).	53
Figure 15	- Commodity flows of the multi-mission lunar campaign solution (interval: one year).	54
Figure 16	- Results of multi-mission lunar campaign design with respect to mission interval.	55
Figure 17	- Comparison of IMLEO results by MILP and SA method.	60
Figure 18	- Results of multi-mission lunar campaign design with respect to ISRU productivity (interval: one year).	61
Figure 19	- Results of multi-mission lunar campaign design with respect to spacecraft structure mass (interval: one year).	62
Figure 20	- Partially periodic TEN.	69

Figure 21	- Earth-moon-Mars transportation network model.	77
Figure 22	- Mission IMLEO comparison among GMCNF formulations.	82
Figure 23	- Problem-solving time cost comparison among GMCNF formulations.	83
Figure 24	- Mars regular space transportation mission planning (10-mission case).	84
Figure 25	- Relationship between average mission IMLEO and ISRU productivities.	85
Figure 26	- Integrated ISRU modeling flow chart.	96
Figure 27	- An example of the full-size space infrastructure optimization formulation.	97
Figure 28	- Cis-lunar transportation network model.	117
Figure 29	- How delay and safety stock influence space missions (an example).	133
Figure 30	- Space Station Resupply Mission Plan.	149
Figure 31	- Expected Operating Time Loss vs. Expected IMLEO Pareto Front.	152
Figure 32	- Decision Rule Result Variance.	153
Figure 33	- Pareto Fronts Comparison with Respect to the Number of Launches.	154
Figure 34	- Pareto Fronts for Different Percentages of Crew Operating Time for Science.	156
Figure B1	- Historical Error in CRS Launch Date Planning (within 1 Year of Planned Launch).	168
Figure B2	- Historical Error in CRS Launch Date Planning (within 90 days of planned launch).	170
Figure B3	- Launch Delay Cumulative Distribution Function.	170

NOMENCLATURE

Symbols

- \mathcal{A} set of directed arcs
- A coefficient matrix for linear programming
- B remaining stock, kg
- b spacecraft flow vector (binary)
- \mathcal{C}_c continuous commodity set
- \mathcal{C}_d discrete commodity set
- C spacecraft payload capacity, kg
- D delay length, days
- d demand or supply vector, kg
- e continuous variable denotes payload or propellant capacity, kg
- f spacecraft fuel type (integer)
- \mathcal{G} network graph
- G space mission cost
- g_0 gravitational acceleration on Earth, 9.8 m/s^2
- H concurrency matrix
- h crew time loss, days
- I_{sp} specific impulse, sec
- i node index ($\in \mathcal{N}$)
- J objective function
- j node index ($\in \mathcal{N}$)
- \mathcal{K} scenario set

- K total number of regular space missions
- k regular space mission index
- \mathcal{L} rocket launch set
- L storage length, days
- l number of concurrency constraints
- \mathcal{M} a large constant
- M spacecraft propellant capacity, kg
- M_O oxygen in situ resource utilization plant mass, kg
- M_{UB} upper bound of propellant capacity, kg
- \mathcal{N} set of nodes
- N ISRU hourly productivity, kg/hr
- N_O oxygen in situ resource utilization plant production, kg
- N_M oxygen in situ resource utilization plant productivity, kg/hr/kg plant
- \mathcal{P} union of polyhedra
- P polyhedron formed by epigraph of piecewise function
- P_I infrastructure power demand, kW
- P_0 power system output power, kW
- p types of commodities
- Q transformation matrix
- Q_I infrastructure operating length per solar day, h
- Q_p power system working time per solar day, h
- Q_u commodity packing index subsets
- q scenario probability
- \mathcal{R} recession cone

R safety stock decision rule
 r available safety stock, kg
 S_k commodity index partition subsets
 s spacecraft structure mass
 \mathcal{T} set of time steps
 T maximum time horizon
 t time index ($\in \mathcal{T}$)
 t_b spacecraft impulsive burn time, sec
 t_0 length of the setup phase
 t_p length of each cycle in periodic phase
 U branching scheme
 u additional supply, kg
 \mathcal{V} set of spacecraft
 V set of breakpoints
 v spacecraft-type index ($\in \mathcal{V}$)
 \mathcal{W} set of time windows
 \mathcal{X} variable vector for linear programming
 \mathbf{x} payload flow vector
 y spacecraft flow variable (integer)
 Z mission performance
 α structural fraction
 β consumption rate, kg/hr/kg plant
 γ the specific mass of energy storage systems
 ε energy storage efficiency

σ reactor productivity, kg/hr/kg plant
 μ_1 safety stock availability (binary)
 μ_2 additional supply necessity (binary)
 φ weighting coefficient
 η commodity consumption rate, kg/day
 ψ commodity shortage penalty, day/kg
 Δt time of flight, day
 ΔV change of velocity, km/s
 $\tilde{\zeta}$ commodity packing index set
 ζ rocket launch time function
 ϕ propellant mass fraction

Superscripts and Subscripts

$(\cdot)_i$ node i
 $(\cdot)_j$ node j
 $(\cdot)_t$ time step t
 $(\cdot)_v$ spacecraft v
 $(\cdot)_\xi$ mission scenario ξ
 $(\cdot)_\theta$ rocket launch θ

SUMMARY

As low-cost rocket launch technologies and space resource utilization systems emerge, human space exploration is attracting increasing interest from industry, government, and academia. To extend the domain of human activity beyond the low-Earth orbit and maintain a long-term human presence in cislunar space and eventually Mars, we need to build a sustainable and affordable interplanetary space transportation system. It requires a campaign-level perspective for space mission design in addition to the conventional mission-level perspective. This thesis first proposes an integrated space logistics framework to enable concurrent optimization of space transportation scheduling, spacecraft sizing, space infrastructure design and deployment. Then, a periodic time-expanded network is built to resolve the scalability issue in the time dimension for long-term space exploration missions. After establishing efficient space logistics optimization frameworks, we switch our focus to space infrastructure technology trade studies to consider space infrastructure design from the subsystem level. A multi-fidelity optimization method is introduced to guarantee optimization accuracy while improving computational efficiency. Finally, a flexibility management framework is proposed to handle uncertainties in space mission planning and operations. Multiple case studies for human lunar and Mars exploration campaigns are conducted leveraging the proposed methods and frameworks to demonstrate their values and potential impacts. This research resolves the grand challenge of space logistics mission design for future large-scale multi-mission space campaigns.

CHAPTER 1. INTRODUCTION

1.1 Motivation and Objective

As low-cost rocket launch technologies and space resource utilization systems emerge, human space exploration is attracting increasing interest from industry, government, and academia. To extend the domain of human activity beyond the low-Earth orbit and maintain a long-term human presence in cislunar space and eventually Mars, there are at least three fundamental questions to answer regarding space logistics:

- 1) How can we design a sustainable and affordable space transportation system?
- 2) How can we perform efficient mission planning optimization for large-scale multi-mission space campaigns?
- 3) How can we handle uncertainties in space mission planning and space infrastructure design?

These questions relate to broad fields in space system engineering, including space vehicle design, space transportation, space resource utilization, and related supporting technologies. A series of interdisciplinary design and optimization frameworks and tools are critical to performing large-scale space mission planning, optimizing spacecraft and space infrastructure designs, and mitigating the impact of uncertainties. The objective of this thesis is to fulfill the demands of human space exploration by developing integrated space logistics frameworks, focusing on space vehicle design, space transportation scheduling, space infrastructure design, and flexibility management by leveraging state-of-the-art space logistics and space system engineering.

These frameworks are developed based on a network-based space logistics optimization model, which considers the space mission planning problem as a multi-commodity network flow problem. The network-based space logistics approach is a common and fundamental model for the proposed frameworks. However, depending on the specific application and the problem, they investigate different perspectives of space logistics and focus on resolving different challenges. For space vehicle design, a piecewise linear approximation method is proposed to consider nonlinear spacecraft design models. For long-term space transportation scheduling, a partially periodic time expanded network is introduced leveraging the repeating nature of regular transportation missions. For space infrastructure design, a new space infrastructure design concept is developed that considers infrastructure subsystems' internal interactions and their external synergistic effects with space logistics simultaneously. For flexibility management, a decision rule formulation is integrated into the network-based space logistics framework to handle uncertainties in space mission planning.

An example of the Earth-moon-Mars transportation network model is shown in Figure 1. In the network, nodes represent planets or orbits; arcs represent trajectories. Spacecraft, propellant, crew, and all other payloads are considered as commodities flowing along arcs in the network.

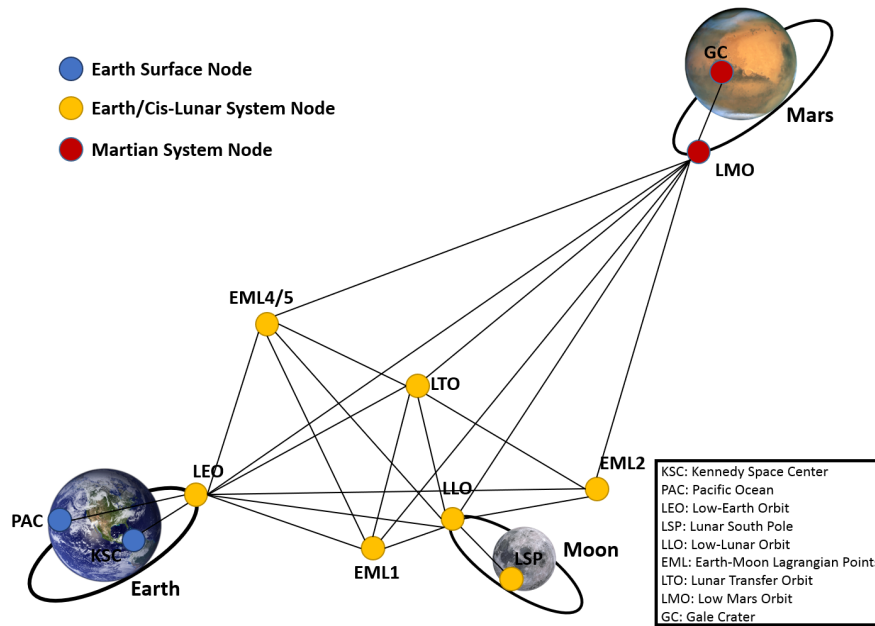


Figure 1 - Earth-Moon-Mars transportation network

The proposed frameworks based on the network-based space logistics model significantly enhance the current state-of-the-art of space logistics. This model is an important step forward in providing practical space mission planning tools under different mission scenarios. It is also particularly useful for space architecture performance evaluations for large-scale mission planning, space vehicle design, and flexibility management in future space logistics.

1.2 Research Contributions

The proposed research seeks to address the practical challenges of large-scale human space exploration considering multiple space missions at the same time. The proposed methods create new directions in campaign-level mission planning to enable effective space system optimization for space vehicle design, space infrastructure deployment, and space transportation scheduling in future space exploration. The research activities

described in this thesis for the development of integrated space logistics frameworks have the following four achievements.

1.2.1 Contribution 1: Mixed-Integer Nonlinear Programming (MINP) Formulation for Integrated Space Logistics and Spacecraft Design

Chapter 3 establishes the theory and methods to enable effective space mission planning for future long-term deep space human exploration. A campaign-level space logistics optimization framework that simultaneously considers mission planning and spacecraft design is developed utilizing mixed-integer nonlinear programming. In the mission planning part of the framework, deployment and utilization of in-orbit infrastructures, such as in-orbit propellant depots or in situ resource utilization plants are also taken into account.

This work provides an important step to close the gap in the past literature and reveals an integrated optimization formulation, considering both mission planning (including in-orbit infrastructure design) and spacecraft design using a mixed-integer programming formulation. The developed formulation can be particularly useful for evaluating the cost and benefit of cislunar infrastructure and for developing concrete space mission schedules for future long-term space exploration.

1.2.2 Contribution 2: Periodic Time-Expanded Network (TEN) for Regular Interplanetary Mission

Chapter 4 creates a computationally efficient and scalable mission planning optimization method for regular space transportation missions, defined as a set of repeating

and periodic interplanetary transportation missions over a long time horizon after one or a few setup missions. As more long-term human missions to Mars are being conceptualized, the need for a sustainable interplanetary transportation system has become increasingly prominent. However, planning regular transportation missions with existing space mission planning optimization formulations has a limitation in computational scalability in the time dimension. The proposed partially periodic time-expanded network can address this limitation of the past studies; it is shown to be computationally scalable and capable of generating solutions that are practically preferred. Thus, the proposed mission planning framework can provide a practical and computationally efficient method for long-term interplanetary transportation mission planning.

1.2.3 Contribution 3: Multi-Fidelity Mission Planning Framework for Infrastructure Design and Resource Logistics

To build a sustainable space transportation system for human space exploration, the design and deployment of space infrastructure, such as in-situ resource utilization plants, in-orbit propellant depots, and on-orbit servicing platforms, are critical. The design analysis and trade studies for these space infrastructure systems require the consideration of not only the design of the infrastructure elements themselves but also their supporting systems (e.g., storage, power) and logistics transportation while exploring various architecture options (e.g., location, technology). Chapter 5 proposes a system-level space infrastructure and logistics design optimization framework to perform architecture trade studies. A new space infrastructure logistics optimization problem formulation is proposed that considers the internal interactions of infrastructure subsystems and their external synergistic effects with space logistics simultaneously.

The proposed framework has four technical innovations. First, an interdisciplinary space infrastructure optimization formulation that considers the internal interactions of infrastructure subsystems and their external synergistic effects with space logistics transportation simultaneously is proposed. This is a new problem in space logistics for high-fidelity space infrastructure trade studies. Second, since the full-size version of this proposed problem formulation can be computationally prohibitive for large-scale space infrastructure design problems, a new multi-fidelity optimization formulation is developed that can provide an approximate solution to the full-size formulation at a significantly reduced computational cost with little sacrifice in the solution quality. The idea behind this multi-fidelity formulation is to vary the granularity of the commodity type definition over the network graph; this technique is referred to as commodity packing based on its physical meaning. Third, in order to identify where and when to pack the commodities for the multi-fidelity optimization formulation, a preprocessing algorithm is introduced for commodity packing. This method enables an automated implementation of the multi-fidelity formulation in the context of dynamic generalized multicommodity network flow. Fourth, the relationship between the solutions of the multi-fidelity, full-size, and prefixed formulations is established. This relationship enables us to find the approximate solution of the computationally prohibitive full-size formulation with the knowledge about the worst possible approximation error.

1.2.4 Contribution 4: Decision Rules for Flexibility Management

Chapter 6 develops a flexibility management framework for space logistics mission planning under uncertainty through decision rules and multi-stage stochastic programming. It aims to add built-in flexibility to space architectures in the phase of early-stage mission

planning. The proposed framework integrates the decision rule formulation into a network-based space logistics optimization formulation model. It can output a series of decision rules and generate a Pareto front between the expected mission cost (i.e., initial mass in low-Earth orbit) and the expected mission performance (i.e., effective crew operating time) considering the uncertainty in the environment and mission demands. The generated decision rules and the Pareto front plot can help decision-makers create implementable policies immediately when uncertainty occurs during space missions.

The proposed method provides an important step to make space mission planning and architecture design flexible to counter potential uncertainties in space missions. The proposed methodology is particularly useful for evaluating the performance of space infrastructure design under stochastic mission environments and developing a reliable space mission schedule for future campaign-level space exploration.

1.3 Thesis Overview

The remainder of this thesis is organized as follows. Chapter 2 provides a literature review of the research. Chapter 3 introduces the network-based mission planning framework for integrated space logistics optimization. Chapter 4 proposes a periodic time-expanded network (TEN) for regular interplanetary missions. Chapter 5 establishes a multi-fidelity mission planning framework to enable system-level infrastructure design. Chapter 6 creates a flexibility management framework based on decision rules to handle uncertainties in space missions. Case studies are also conducted to demonstrate the values and performances of the proposed frameworks in each chapter. Chapter 7 concludes the thesis with a summary and recommendations for future work.

CHAPTER 2. LITERATURE REVIEWS

2.1 MINP for Integrated space logistics and spacecraft design

As space exploration projects become increasingly complex, the campaign-level logistics perspective becomes more important for human space mission planning. In many past human space programs such as Apollo, every mission was logistically independent using a so-called carry-along strategy. This was efficient for short-term missions to a relatively close destination. However, for a longer-duration multi-mission space exploration campaign, reusable in-orbit infrastructures can be more attractive. For example, it can be beneficial to have an in-orbit propellant depot and/or a lunar in-situ resource utilization (ISRU) plant to refuel human missions to Mars or near-Earth objects (NEOs) in return for their emplacement cost and the required maintenance. There are pros and cons for the operation of those infrastructures. Therefore, it is important to perform an integrated campaign-level analysis considering both mission planning and infrastructure design to evaluate whether it pays off to deploy those infrastructures.

In addition, we need a paradigm shift in vehicle design as well. The conventional space programs such as Apollo delivered relatively similar payloads to the destination of each mission throughout the campaign, and therefore a few identical single-use vehicles were sufficient for their logistics. For example, each Apollo vehicle carried a similar amount of similar types of commodities (e.g., consumables, scientific payloads) in all missions. However, in a longer-duration multimission space exploration campaign with infrastructure deployment and utilization, we need to deliver different types and amounts of commodities to the destination throughout the campaign. For instance, at the beginning of the campaign, the spacecraft may need to carry ISRU plants, whereas later on in the campaign, it may need to carry the ISRU-generated propellants and its tank structure. Thus,

for such campaign-level mission design, it is critical to study and analyze the optimal fleet of multiuse vehicles, where each vehicle is flexible in its assigned function.

Many past studies have addressed space logistics mission planning, but few of them have considered in-orbit infrastructure design and spacecraft model concurrently at a reasonable level of fidelity. One of the most recent studies that analyzed space mission optimization is the generalized multicommodity network flow (GMCNF) formulation developed by Ishimatsu et al. [1]. Their research modeled the space logistics planning problem as a linear programming problem using a graph-theoretic approach, but this method did not include the emplacement cost for the in-orbit infrastructures properly. Ho et al. improved the GMCNF by proposing a dynamic space logistics optimization formulation that removed “time paradoxes” existing in the static network [2], referring to the propellant produced by ISRU that could be used before the ISRU plants are deployed. In addition to this, Ho et al. considered the emplacement cost of the in-orbit infrastructure. However, the infrastructure and spacecraft model used in the analysis was a low-fidelity linear model, which could result in an unrealistic solution (e.g., an unrealistically small vehicle size). Other space logistic optimization models such as the interplanetary logistics model [3], the exploration architecture model for in-space and Earth-to-orbit tool [4], and the space system architectures model based on graph theory [5] have been proposed for space logistics mission planning, but these studies did not consider the possibilities of using propellant depots and ISRU plants, which can be critical for long-term space exploration.

On the other hand, various studies have focused on the detailed design of in-orbit infrastructures, but few of them have also addressed the global optimization of space mission planning concurrently. For example, Oeftering [6] studied detailed cislunar infrastructure design and Schreiner [7] performed a detailed system-level ISRU plant sizing analysis for the molten regolith electrolysis process. Also, there were numerous architectures proposed about on-orbit propellant depots from both technological

perspectives [8-10] and economical perspectives [11-13]. However, those studies only looked at the design of depot with its local transportation system rather than providing a design method considering global optimization for the entire space logistics system.

As shown previously, most of the past space logistics literature has not considered space mission planning, in-orbit infrastructure, and vehicle design concurrently at a reasonable fidelity. In response to this background, an optimization formulation considering mission planning, in-orbit infrastructure design, and spacecraft design simultaneously is proposed in Chapter 3, aiming to evaluate the cost and benefit of reusable in-orbit infrastructures and generalized designed spacecraft. The model is a mixed-integer nonlinear programming formulation based on a time-expanded GMCNF model. This model significantly advances Ho et al.'s previous model [2] and takes into account higher-fidelity in-orbit infrastructure design models, including propellant depots and ISRU. We also add new constraints for vehicles and crew members. This optimization framework consists mainly of two parts: mission planning including infrastructure design, and spacecraft design.

2.2 Periodic TEN for Regular Interplanetary Mission

In addition to the concurrent optimization of transportation planning, spacecraft design, and space infrastructure design proposed in Chapter 3, another challenge in large-scale multi-mission campaign design is to handle the long time horizon in a regular interplanetary transportation system. One example of such a system is the regular cargo route to Mars proposed by SpaceX using fully reusable rockets [14]. These space missions are designed to support the setup and periodic resupply for future Mars settlement in a similar way as the logistics vehicles for the International Space Station resupply. Meanwhile, reusable vehicles and in-orbit infrastructure technologies such as propellant depots and in situ resource utilization (ISRU) plants in the cislunar and Martian systems

have been proposed to support space exploration sustainably [6]. However, designing a long-term regular space transportation system involves greater complexity than designing a short-term single mission. Particularly, when we take into consideration the deployment and operation of in-orbit infrastructures that are used over many missions (e.g., ISRU plants), the analysis needs to consider a long time horizon, and thus requires extensive and sometimes prohibitive computational effort with conventional methods.

Many past studies have been conducted on the topic of space logistics. The space logistics optimization models such as the interplanetary logistics model [3], the Exploration Architecture Model for In-Space and Earth-to-Orbit (known as EXAMINE) tool [4], SpaceNet [15], and the graph theory-based space system architectures model [5] have been proposed for space logistics mission planning. However, these studies either lacked or had limited global optimization capability for complex mission design problems that involved deployment and utilization of propellant depots and ISRU plants. Moreover, these models were not formulated to consider the mission interdependency at the multimission campaign level. In response to this background, Ishimatsu et al. proposed a generalized multicommodity network flow (GMCNF) to optimize the space mission planning problem globally based on a static network [1]. However, due to the linear nature of the static network, vehicles could not be tracked through the network and the size of vehicles may change during the mission. Cornes and de Weck improved the optimization fidelity through mixed-integer linear programming (MILP) and a tracking algorithm [16]. To take into account space mission planning, spacecraft design, and in-orbit infrastructure design concurrently, Ho et al. [2] and Chen and Ho [17] further improved the GMCNF model by considering the time dimension (i.e., time-expanded GMCNF) and proposed an integrated space logistics mission planning framework. This framework enabled nonlinear spacecraft and in-orbit infrastructure design through the piecewise-linear function approximation. It also provided an insight into the significant reduction in the initial mass in low Earth orbit

(IMLEO) through a campaign-level design rather than a mission-level design. Although these existing mission planning formulations consider the deployment and operation of the in-orbit infrastructures concurrently, they have significant limitations in time dimension scalability, and thus cannot be applied to long-term space transportation design. In addition, these formulations are not suitable to find a sequence of repeating space transportation missions.

On the other hand, time-expanded networks (TENs) have been widely used in different fields, including vehicle and crew scheduling [18], airline fleet assignment [19-21], and ground transportation [22]. Among the literature, a fully periodic TEN was proposed to solve long-term repeating mission planning problems. It has been used in truck fleet sizing problems [22] and airline fleet assignment problems [19-21]. However, to take advantage of space resources and reduce space exploration mission cost, a space infrastructure deployment setup phase is required before the mission entering the repeating transportation phase [17]. Therefore, fully periodic TENs cannot be used in the campaign-level space mission design directly. A similar problem to the setup phase in space missions can be found in the literature on airline schedule recovery problems [23, 24], in which a TEN was used to consider a period of irregular mission planning and then switching to a periodic repeating phase. However, the airline schedule recovery problems mainly focused on the recovery period and did not consider the subsequent schedule optimization in the periodic phase simultaneously.

In response to this background, an interplanetary transportation system mission planning optimization framework is proposed in Chapter 4 by constructing a partially periodic TEN. The model is constructed based on the network-based space logistics optimization framework proposed in Chapter 3, and it has been reformulated to incorporate the scalability of the regular transportation missions to make the mission planning formulation computationally efficient. This new mission planning framework can also find

repeating transportation solutions, which are preferred in practical missions. Thus, the proposed mission planning framework can provide a practical and computationally efficient method for long-term interplanetary transportation mission planning.

2.3 Multi-Fidelity Mission Planning Framework for Infrastructure Design and Resource Logistics

After proposing efficient space logistics optimization frameworks considering both transportation planning and space system design concurrently in Chapters 3 and 4, now we switch our focus to the design and deployment of space infrastructure systems. They are critical elements to support space resource utilization, on-orbit servicing, and interplanetary space transportation. Past space infrastructure design literature has analyzed the system performance of in-situ resource utilization (ISRU) systems, propellant depots, on-orbit servicing platforms, etc. For example, the technical and economic feasibility of commercial propellant production by ISRU systems has been examined and demonstrated by industry, government, and academic experts [25]. Multiple studies have focused on the chemical processes of ISRU reactor and system productivity, such as the hydrogen reduction reaction testbeds by NASA [26] and Lockheed Martin [27], the integrated carbothermic regolith reduction system by Orbitec Inc. and the Kennedy Space Center [28], the integrated molten regolith electrolysis (MRE) reactor modeling method by Schreiner [7], and the Mars oxygen ISRU experiment (MOXIE) by Meyen [29]. Besides ISRU, on-orbit servicing technologies have also been developed in recent years [30,31], its commercial potentials and operations have been analyzed in the literature [32-34]. However, all these referenced studies mainly analyzed the feasibility and performance of the space infrastructure elements, and did not take into account the complex logistics to deploy and support those infrastructure systems.

On the other hand, multiple studies focused on space transportation analysis and considered space infrastructure design, such as ISRU systems, together with space transportation system design. United Launch Alliance proposed the Cislunar-1000 project to build a sustainable space economy by taking advantage of lunar water ISRU plants to produce oxygen and hydrogen [35]. A series of network-based space logistics optimization methods were proposed by Ishimatsu [1], Ho [2], and Chen [17] to solve mission planning, space infrastructure design, and spacecraft design problems concurrently. Their results showed the long-term benefits of ISRU systems and propellant depots to space exploration campaigns. However, in these space logistics optimization methods, referred to as the prefixed space infrastructure optimization formulation, the space infrastructure was considered as a black box, and the subsystem interactions and mass ratios were determined before taking into account space logistics optimization [1,2,36,37]. They ignored the interaction between infrastructure subsystems and space transportation mission planning.

Due to the inadequate consideration in the connection between space infrastructure design and space transportation planning, conventional prefixed space mission planning and infrastructure design have only explored a limited design space. For example, considering the ISRU system as a black box model would miss the tradeoff between the frequency of logistics missions and its impact on ISRU storage system size. Namely, frequent transportation missions require smaller storage subsystems but higher operation cost and complexity; whereas infrequent transportation missions require larger storage subsystems, which can also lead to higher infrastructure deployment cost. The consideration of this tradeoff requires the modeling of ISRU infrastructure subsystems and its coupling with logistics planning. Furthermore, prefixing the space infrastructure design for architecture design can also miss the synergistic effect of space infrastructure technologies and the combination of subsystems to achieve a hybrid system design, particularly when different infrastructure technologies have common supporting

subsystems. An example is an ISRU plant based on the reverse water gas shift reaction (RWGS) and Sabatier reaction (SR). The RWGS process can be used concurrently with SR to produce sufficient oxygen so that the generated O_2 and CH_4 can be used together as propellants optimally. (The oxygen/methane bipropellant has been widely considered as a propellant option to support future robotic and human missions in conjunction with ISRU systems [38,39].) Because of the similar reactants and reaction environment, the RWGS process and the SR process can share the same acquisition subsystem (for CO_2), liquefaction & storage subsystem (for O_2), and power subsystem. Thus, the SR ISRU and the RWGS ISRU need to be designed together for optimal performance, and this design solution depends on the mission scenarios and the logistics planning (e.g., launch frequency, vehicle type/size, available resources from the ground or other sources). To resolve this challenge effectively, a general design optimization framework and its methods need to be developed to handle the synergistic effect of space infrastructure subsystems and the logistics system.

To effectively evaluate the impacts of the space infrastructure design to space missions with higher fidelity (i.e., considering both system-level and subsystem-level tradeoffs), an interdisciplinary space infrastructure optimization framework and its optimization methods are proposed in Chapter 5, leveraging network-based space logistics modeling. The proposed framework enables an integrated architecture trade study for future space infrastructure, considering the coupling between the subsystems design and corresponding logistics planning.

2.4 Flexibility Management for Space Logistics via Decision Rules

The frameworks proposed in Chapters 3, 4, and 5 focus on deterministic mission operation environments. However, uncertainty is another big challenge in mission planning and system design and it cannot be handled effectively leveraging these methods. In

traditional space programs like Apollo, each mission was logistically independent. Thus, the uncertainties in one mission (e.g., spacecraft flight delays/failures and mission demand changes) had a relatively limited impact on subsequent missions, which simplified the evaluation of consequences and solutions to handle uncertainties. More recent studies show that sustainable space exploration needs to be accomplished by a campaign composed of multiple interdependent missions [1,2,17]. Leveraging a campaign enables effective space exploration with a combination of different logistics paradigms such as pre-deployment, carry-along, and resupply. At the same time, however, mission interdependencies also introduce the potential of “cascading failure” behaviors in space exploration, similar to those in the interconnected infrastructures in terrestrial civil infrastructure systems [40]. Particularly, a rocket launch delay in an earlier mission may significantly impact the performance of later missions, such as further launch delays in the future and supply shortages to support mission operations. Therefore, there is a growing need to consider the uncertainties in launch delay in the campaign design.

One example of the impact of complex interdependencies between space missions can be found in the International Space Station (ISS) program. The ISS has encountered three unexpected mission failures in an 8-month span from October 2014, two caused by rocket launch failures (i.e., Orbital Commercial Resupply Service (CRS)-3 and SpaceX CRS-7) and one caused by spacecraft flight failure (i.e., Progress 59) [41]. These failures resulted in an immediate loss in excess of 6,832 kg cargo and supplies including the first of two docking adapters to support the commercial crew program [42-44]. They also led to delays in subsequent space missions to identify the reason for the failures and incorporate the necessary changes to support the return to flight certification for the launch vehicle or spacecraft. The return to flight time was 720 days for the Orbital Antares launch vehicle and 285 days for the SpaceX Falcon launch vehicle [41]. Since the ISS program utilized multiple cargo suppliers and maintained a level of supply to ensure astronaut safety in the

event of an extended disruption, the impact on ISS operations was minimal and there was no risk to astronaut safety [45]. However, future large-scale space campaigns are more complex than ISS. They can include multiple space stations and habitat resupply missions in parallel. To mitigate the impact of the uncertain environment on mission operations, we need a systematic methodology to quantitatively identify the level of safety stock balancing the mission cost and mission performance while ensuring the safety of astronauts under uncertain mission environments.

In the space logistics research field, multiple frameworks have been proposed in the past to perform efficient space mission planning under deterministic environments. These frameworks were established through heuristic methods [3], graph theory [5], simulations [15], and multi-commodity network flow models [1,2,17]. However, deterministic methods tend to give overly optimistic designs and bias anticipated mission performance. Space mission operations following the mission planning results optimized under deterministic environments may end up with failure or significant mission cost increase if any uncertain event occurs during the space campaign such as spacecraft flight delays.

The research for design under uncertainty in the space field mainly focused on analyzing the impact of uncertainty on space missions, but little work has addressed how to counter these uncertainties in the mission planning phase. For example, Shull [46] discussed the impact of campaign-level risks, such as flight delay and cancellation, in a human lunar exploration architecture. Added flexibility was integrated with the format of pre-positioning stockpile and evaluated through sensitivity analysis. Moreover, the threat of uncertainty for future human Mars missions was studied by Stromgren et al. [47] using the Exploration Maintainability Analysis Tool (EMAT). However, these studies cannot generate directly implementable decision strategies for decision-makers to follow in response to uncertain events.

Beyond the space research area, various studies have considered the flexibility in design from different perspectives, including taxonomy [48], empirical evaluation [49], and stochastic programming with real options analysis [50] or decision rules [51]. However, these proposed methods cannot be applied directly to our problem of space logistics planning under uncertainties in launch delays. First, mathematically, the transportation of additional safety stock needs to be taken into account during the logistics of other pre-determined mission demands because of the limited time window opportunities (e.g., due to the launch environment and orbital dynamics). The decision rule formulation needs to be integrated into the space logistics optimization problem. Furthermore, there is a conceptual difference between our problem and classical real-option problems in that our problem involves the uncertainties of the time windows, which prevents the decision-makers from responding to the uncertainties in real time. In classical built-in flexibility examples, we typically assume that we can respond to the uncertainties when they are realized (e.g., expanding the building in response to the increasing demand). However, in our problem, the time steps of the decision windows themselves are uncertain. Therefore, when there is a launch delay, the impact appears on the mission performance immediately, but decision-makers cannot react to it until the delayed launch itself (i.e., after the impacts have already occurred). Namely, at the point of decision making, we can only prepare for the future and compensate for the previous uncertain event immediately before it, rather than reacting to the uncertain event in real time.

In response to this background, a decision rule-based flexibility management framework is proposed in Chapter 6, leveraging multi-stage stochastic programming. It aims to add built-in flexibility to space architectures in the phase of early-stage mission planning. Decision rules, also called implementable policies, map the observations of uncertainty data to the decisions directly. Thus, the resulting decision rule can be

implemented as general decision strategies for decision-makers to follow when stochastic events occur.

CHAPTER 3. INTEGRATED SPACE LOGISTICS AND SPACECRAFT DESIGN

The integrated space logistics optimization formulation, aiming to minimize the total cost of the whole multi-mission campaign, is developed based on Ho et al.'s time-expanded generalized multicommodity network flow model [2]. To improve the fidelity of the infrastructure modeling, we take into account a higher-fidelity ISRU model based on Schreiner's system-level ISRU plant sizing analysis [7], a high-fidelity spacecraft model, and new constraints for crew members.

This integrated optimization problem turns out to be a complex mixed-integer nonlinear programming (MINP) problem and cannot be solved using the conventional formulations proposed by Ishimatsu et al. [1] and Ho et al. [2] due to their linear programming natures. The nonconvex nonlinear in-orbit infrastructure design model, which is used to describe ISRU in this research, the complex nonlinear spacecraft design model, and the quadratic terms in both objective function and constraints make it very challenging to solve the problem and find the global optimum directly [3].

To handle this challenge, two methods are proposed in this chapter: First, the mixed-integer nonlinear programming problem is converted into a mixed-integer linear programming problem after approximating the nonlinear model with a piecewise linear function and linearizing quadratic terms. In addition, another optimization framework is provided based on simulated annealing, which separates the spacecraft model from mission planning formulation.

An example mission scenario based on multiple Apollo missions is considered, and the results show a significant improvement in the initial mass in low Earth orbit by campaign-level design as compared with the traditional mission-level design. It is also

shown that the mixed-integer linear programming-based method gives better-quality solutions than the simulated annealing-based method, although the simulated annealing method is more flexible for the extension to a higher-fidelity spacecraft model.

3.1 Methodology

In order to solve the optimization problem efficiently, we developed two different methods.

The first method to solve this problem is converting the whole problem into a MILP problem. The nonlinear ISRU and spacecraft models are approximated by piecewise linear functions, to then be converted into a binary mixed-integer programming formulation. The remaining quadratic terms in the mission planning formulation are linearized. This MILP formulation can always find the approximated global optimum. The detail of this MILP optimization method is introduced in Sec. 3.1.2.2.

Another developed method solves mission planning and spacecraft model separately using simulated annealing (SA). Since the spacecraft model is separated from mission planning, no quadratic term exists in the formulation. Only the ISRU model needs to be approximated by a piecewise linear function. This SA-based method cannot guarantee its global optimality, but it can potentially provide a solution to the problem with a more realistic and complex spacecraft model. The detail of this SA-based optimization framework is shown in Sec. 3.1.2.3.

3.1.1 Modeling

This section introduces the space logistics, spacecraft, and ISRU modeling methods. The space logistics model is developed based on Ho et al.'s time-expanded GMCNF [2] while using higher-fidelity spacecraft and ISRU models. The spacecraft model

used in this chapter is developed based on Taylor's integrated transportation system design framework [52]. This is a data-based model where all the data comes from preexisting spacecraft. The ISRU plant considered in this chapter is an oxygen ISRU developed by Schreiner [7] based on their system-level ISRU plant sizing analysis for the molten regolith electrolysis process.

3.1.1.1 Space Logistics Modeling

The space logistics problem can be solved as a multicommodity network flow problem. In the network, nodes correspond to planets, celestial objects, or orbits; and arcs correspond to trajectories. Spacecraft, crew members, scientific instruments, and other kinds of payloads are considered as commodities flowing along arcs. The left-hand side of Figure 2 shows a network graph of the Earth-Moon-Mars-NEO space logistics model [36, 53, 54]. A generalized multicommodity network flow formulation has been developed with this network graph for space logistics optimization [1, 2].

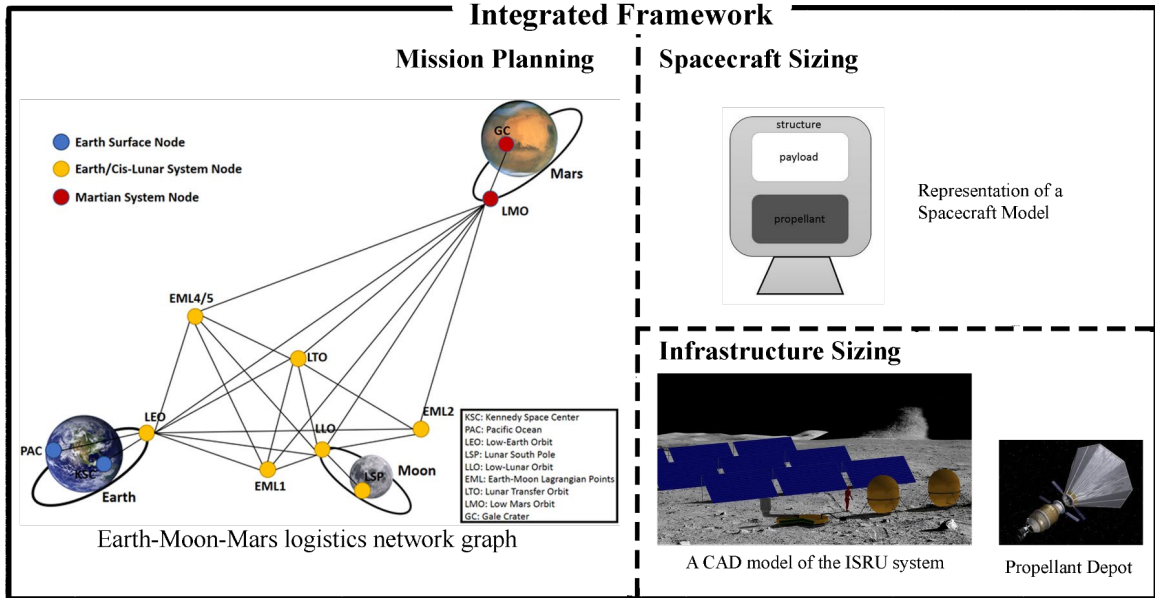


Figure 2 - Integrated optimization framework ([adapted from [7, 52-54]])

The space logistics model in this thesis is developed based on a time-expanded GMCNF formulation. Solutions of the time-expanded GMCNF provide schedules that determine when to transport which commodity from one node to another. In past research, everything that flows over arcs is considered to be one kind of commodity, including crew members, consumables, ISRU plants, spacecraft, etc. [1, 2]. This research separates the spacecraft from other commodities and its model is considered as a separate module so that its nonlinear mixed-integer feature can be included efficiently.

The following shows the mathematical formulation of time-expanded GMCNF. Consider a time-expanded network graph \mathcal{G} that is made up of a set of nodes \mathcal{N} and a set of direct arcs \mathcal{A} , including both transportation arcs that connect different nodes and holdover arcs that connect the node and itself. Each arc has an index (v, i, j) , meaning that spacecraft v flies from node i to node j . We assume that the spacecraft set is \mathcal{V} . Commodities flow over arcs are split into the outflow \mathbf{x}_{vijt}^+ and inflow \mathbf{x}_{vijt}^- , where t is the time step. There are also cost coefficients \mathbf{c}_{vijt}^+ assigned to outflows that enable us to

consider analytic metrics in the optimization. For mission performance evaluations based on non-analytic metrics, such as robustness, postprocessing is required after the mission planning optimization. Note that, if we assume there are p types of commodities delivered in spacecraft, \mathbf{x}_{vijt}^{\pm} and \mathbf{c}_{vijt}^{\pm} are all $p \times 1$ vectors, where each component shows the flows and costs of the corresponding commodity. Therefore, all flows \mathbf{x}_{vijt}^{\pm} are nonnegative. Most of the commodities in \mathbf{x}_{vijt}^{\pm} are continuous variables, except for crew members, which form a discrete (i.e., integer) variable. Moreover, \mathbf{x}_{vijt}^{\pm} represents those commodities delivered by spacecraft. The spacecraft itself is also one kind of commodity denoted by y_{vijt}^{\pm} , which is a discrete (i.e., integer) variable.

Each node i has a demand vector \mathbf{d}_{it} , which is the demand or supply of each commodity at time step t . In the demand vector, demand is shown by a negative value, whereas supply is shown by a positive value. Figure 3 shows an example of a full-time expanded network. For instance, the commodity in node k can take one of three paths:

- 1) Stay at node k over the holdover arc until $t+4$;
- 2) Be transported to node j at time t , and stay at node j until $t+4$;
- 3) Be transported to node j at time t , and then to node i at time $t+2$, and stay at node i until $t+4$.

The optimizer will choose the optimal path of these three.

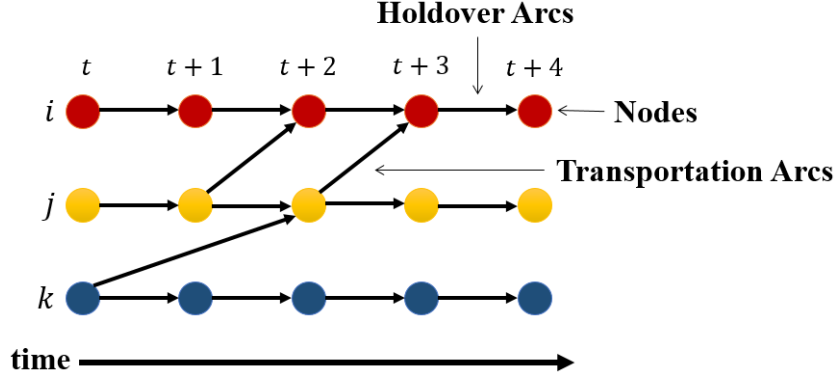


Figure 3 - Full time-expanded network [53]

For each arc from node i to node j , a positive transit time Δt_{ij} is defined. Besides transit time, another important parameter of time-expanded GMCNF is the possible departure time $W_{ij} \subseteq [0, T)$, which corresponds to the time windows of arc i to j . T denotes the maximum time horizon of the campaign-level sequence of space missions. The concept of the time window defines whether it allows commodity flows at a specified time step.

According to the aforementioned notations, the time-expanded GMCNF can be expressed by the following formulation:

Minimize:

$$J = \sum_{t \in \{0 \dots T-1\}} \sum_{(v,i,j) \in \mathcal{A}} (c_{vijt}^+ x_{vijt}^+ + c_{vijt}' s_v y_{vijt}^+) \quad (1)$$

Subject to:

$$\sum_{(v,j):(v,i,j) \in \mathcal{A}} x_{vijt}^+ - \sum_{(v,j):(v,j,i) \in \mathcal{A}} x_{vji(t-\Delta t_{ji})}^- \leq d_{it} \quad \forall i \in \mathcal{N} \quad \forall t \in \{0 \dots T-1\} \quad (2)$$

$$\sum_{j:(v,i,j) \in \mathcal{A}} y_{vijt}^+ - \sum_{j:(v,j,i) \in \mathcal{A}} y_{vji(t-\Delta t_{ji})}^- \leq d_{ivt}^l \quad \forall i \in \mathcal{N} \quad \forall v \in \mathcal{V} \quad \forall t \in \{0 \dots T-1\} \quad (3)$$

$$Q_{vij} \begin{bmatrix} \mathbf{x}_{vijt}^+ \\ s_v y_{vijt}^+ \end{bmatrix} = \begin{bmatrix} \mathbf{x}_{vijt}^- \\ s_v y_{vijt}^- \end{bmatrix} \quad \forall (v, i, j) \in \mathcal{A} \quad \forall t \in \{0 \dots T-1\} \quad (4)$$

$$H_{vij} \mathbf{x}_{vijt}^+ \leq \mathbf{e}_v y_{vijt}^+ \quad \forall (v, i, j) \in \mathcal{A} \quad \forall t \in \{0 \dots T-1\} \quad (5)$$

$$\begin{cases} \mathbf{x}_{vijt}^\pm \geq \mathbf{0}_{p \times 1} & \text{if } t \in W_{ij} \\ \mathbf{x}_{vijt}^\pm = \mathbf{0}_{p \times 1} & \text{otherwise} \end{cases} \quad \forall (v, i, j) \in \mathcal{A} \quad \forall t \in \{0 \dots T-1\} \quad (6)$$

$$s_v = \mathcal{F}(\mathbf{e}_v, f_v) \quad \forall v \in \mathcal{V} \quad (7)$$

$$\mathbf{x}_{vijt}^\pm = \begin{bmatrix} x_1 \\ x_2 \\ \vdots \\ x_p \end{bmatrix}_{vijt}^\pm \quad \text{where } x_1 \in \mathbb{Z}_{\geq 0}, \quad x_2, \dots, x_p \in \mathbb{R}_{\geq 0} \quad \forall (v, i, j) \in \mathcal{A} \quad \forall t \in \{0 \dots T-1\}$$

$$y_{vijt}^\pm \in \mathbb{Z}_{\geq 0} \quad \forall (v, i, j) \in \mathcal{A} \quad \forall t \in \{0 \dots T-1\}$$

$$s_v \in \mathbb{R}_{\geq 0}, \quad \mathbf{e}_v \in \mathbb{R}_{\geq 0}^l, \quad f_v \in \mathbb{Z}_{\geq 0} \quad \forall v \in \mathcal{V}$$

Table 1 - Definition of indices, variables, and parameters.

Name	Definition (dimension)
<i>Index</i>	
v	Spacecraft index
i, j	Node
t	Time step
p	Commodity index
l	Concurrency constraint index
<i>Variables</i>	
x_{vijt}^{\pm}	Commodity outflows/inflows. Commodities in x_{vijt}^{\pm} are considered as integer or continuous variables based on the commodity type. For example, the number of crew members is an integer variable, which is x_1 , whereas other commodities (such as propellant, payload, and human consumables) are considered as continuous variables, which are x_2, \dots, x_p . ($p \times 1$)
y_{vijt}^{\pm}	Number of spacecraft v flying along arc i to j . Integer variable. (scalar)
s_v	Structure mass of spacecraft v . Continuous variable. (scalar)
e_v	Spacecraft design parameters, including payload capacity and propellant capacity. Continuous variables. ($l \times 1$)
f_v	Spacecraft fuel type. Integer variable. (scalar)
<i>Parameters</i>	
c_{vijt}^+	Commodity cost coefficient. ($p \times 1$)
c'_{vijt}^+	Spacecraft cost coefficient. (scalar)
d_{it}	Demands or supplies of different commodities at each node. ($p \times 1$)
d'_{it}	Demand or supply of spacecraft v at each node. (scalar)
Q_{vij}	Commodity transformation matrix. ($(p + 1) \times (p + 1)$)
H_{vij}	Concurrency constraint matrix. ($l \times p$)
W_{ij}	Time window vector. ($1 \times n$, where n is the number of time windows. It is dependent on space missions)

Table 1 lists the definitions of indices, variables, and parameters. The detailed descriptions of the objective function and constraints are as follows.

Equation 1 is the objective function. It gives the value of the initial mass in low Earth orbit (IMLEO), which is the cost metric for space logistics in this chapter.

Equations 2 and 3 are mass balance constraints that limit commodity flows to satisfy the demands of all nodes.

Equation 4 shows the transformation of commodity flows, such as propellant burning, propellant boiloff, ISRU production, and crew consumables. For example, impulsive propellant consumption can be expressed as follows:

$$\begin{bmatrix} 1 & 0 & 0 \\ -\phi & 1 - \phi & -\phi \\ 0 & 0 & 1 \end{bmatrix}_{vij} \begin{bmatrix} \text{payload} \\ \text{propellant} \\ \text{structure mass} \end{bmatrix}_{vijt}^+ = \begin{bmatrix} \text{payload} \\ \text{propellant} \\ \text{structure mass} \end{bmatrix}_{vijt}^- \quad (8)$$

In equation 8, ϕ is the propellant mass fraction which is defined by the rocket equation, $\phi = 1 - \exp\left(-\frac{\Delta V}{I_{sp}g_0}\right)$, where ΔV is the change in the vehicle's velocity along the arc, I_{sp} is the specific impulse, and g_0 is the standard gravity. Another example about propellant production from ISRU can be expressed as follows:

$$\begin{bmatrix} 1 & F_{\text{ISRU}}(\text{ISRU plant mass}) \\ 0 & 1 \end{bmatrix} \begin{bmatrix} \text{propellant} \\ \text{ISRU plant mass} \end{bmatrix}_{vijt}^+ = \begin{bmatrix} \text{propellant} \\ \text{ISRU plant mass} \end{bmatrix}_{vijt}^- \quad (9)$$

In equation 9, $F_{\text{ISRU}}(\text{ISRU plant mass})$ is the ISRU production rate. It is a function of ISRU plant mass, which is introduced in detail in Sec. 3.1.1.3.

Equation 5 is a spacecraft concurrency constraint, which corresponds to the upper bound of commodity flows limited by spacecraft propellant capacity or payload capacity.

In this research, we only consider spacecraft payload and propellant mass capacities as concurrency constraints. Therefore, the number of concurrency constraints is equal to two, which is indexed by l . For example, the concurrency constraints about payload and propellant can be expressed as follows:

$$\begin{bmatrix} 1 & 1 & 1 & 0 \\ 0 & 0 & 0 & 1 \end{bmatrix}_{ij} \begin{bmatrix} \text{payload} \\ \text{crew} \\ \text{consumables} \\ \text{propellant} \end{bmatrix}_{vijt}^+ \leq \begin{bmatrix} C_v \\ M_v \end{bmatrix} y_{vijt}^+ \quad (10)$$

where C_v and M_v are the payload and propellant capacity of spacecraft v . In past literature, Equation 5 could also work as a linear spacecraft model through an inert mass fraction [2]. Note that there is an underlying assumption in this formulation that the spacecraft capabilities of the components can be additively combined. In reality, the interoperability between spacecraft can be significantly more complex.

Equation 6 is the time window of missions defined by the time window matrix W_{ij} .

Equation 7 is the spacecraft design model. It is introduced in detail next, in Sec. 3.1.1.2.

The time index of this model is inspired by a biscale time-expanded network by Ho et al. [2]. In a biscale network model, nodes are partitioned into clusters such that transportation across the same pair of clusters has a common time window [2]. The word “biscale” means a larger time-step scale is used among clusters and a smaller time-step scale is used at the intracluster level.

In this research, based on the biscale time-expanded network, nonuniform time steps are used within clusters. If there are time windows within clusters, the time step length of the holdover arc is determined by the intervals among the time windows. For example,

we have a network defined as shown in Figure 4. Because the time windows of node k only open at time t , $t+2$, and $t+8$, there are only two holdover arcs for node k . The first one starts from time t and ends at $t+2$; the second one starts from time $t+2$ and ends at $t+8$. The time-step lengths of these holdover arcs are two and six in this example for node k . Nonuniform time steps can eliminate redundant time steps and increase computational efficiency.

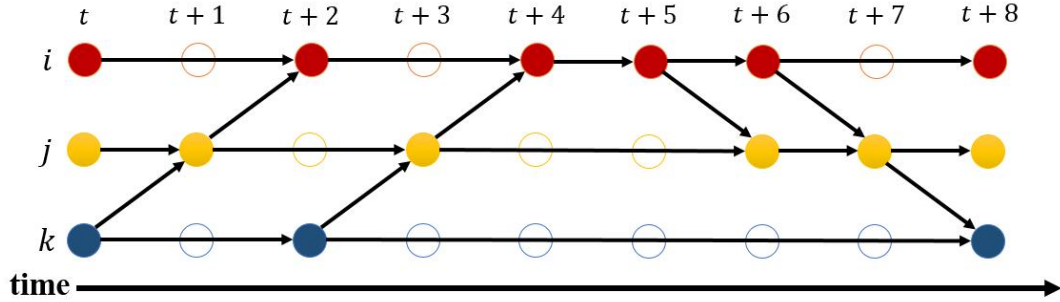


Figure 4 - Nonuniform time-step time-expanded network.

3.1.1.2 Vehicle model

This chapter uses a data-based spacecraft model developed by Taylor in an integrated transportation system [52]. This is a nonlinear regression function based on preexisting spacecraft. The relationship among structure mass and the three design variables is as follows [52]:

$$s^* = 2.3931 * C + \alpha(f) * M * \left(1 - \frac{0.2 * M}{M_{UB}}\right) + \frac{0.4189 \left(\frac{M * I_{sp}(f) * g_0}{t_b}\right)^{0.7764}}{g_0} \quad (11)$$

where s^* is structure mass (or dry mass); C is the spacecraft payload capacity; M is the propellant capacity; f is the fuel type; g_0 is the gravitational acceleration on Earth, 9.8 m/s^2 ; t_b is the spacecraft impulsive burn time that is set as 120 s; M_{UB} is the upper bound allowed for the propellant tank capacity, which is assumed as 500,000 kg; α and I_{sp} are the

structural fraction and specific impulse that are determined by fuel type f . Note that α is the structure fraction of the spacecraft propellant tank defined in [52]. In this chapter, only one kind of propellant liquid oxygen (LOX)/kerosene is considered in the spacecraft model. This is because, compared with other propellants, liquid oxygen (LOX)/liquid hydrogen (LH2), LOX/kerosene, and Monomethylhydrazine (MMH)/Nitrogen tetroxide (N2O4) have relatively high specific impulse I_{sp} with a relatively low structural fraction α (see Table A1). Considering the abundant availability of oxygen on the moon from ISRU and the large boiloff of hydrogen over the long campaign, LOX/kerosene is chosen.

Table 2 - Spacecraft sizing comparison.

Spacecraft	Payload Capacity C , kg	Propellant Capacity M , kg	Propellant	Actual Structure Mass s , kg	Nonlinear Regression s^* , kg	Photographic scaling [5] s , kg
Centaur	0	20,830	LOX/LH2	2,462 [55]	3,131	3,215
S-IVB	0	107,725	LOX/LH2	12,014 [52]	13,513	16,625
HTV	6,000	2,000	MMH/N2O4	10,500 [56]	15,001	15,197
ATV	5,500	2,613	MMH/N2O4	10,300 [57]	13,986	14,257
Apollo LM DS	500	8,804	N2O4/UDMH	2,770 [52]	2,505	2,566
Apollo LM AS	250	2358	N2O4/UDMH	1,719 [52]	1,005	687
Apollo CM	524	0	N2O4/UDMH	4,841 [52]	1,254	1,150
Apollo SM	60	18413	N2O4/UDMH	6,053 [52]	2,682	5,367

The spacecraft data used to develop this spacecraft model is listed in Appendix A. A comparison of this spacecraft model with a conventional sizing method is shown in Table 2 [15, 55-57]. We can find that, as a nonlinear regression model, this spacecraft sizing model has a higher fidelity compared with a conventional method such as photographic scaling [5] when evaluating some historic spacecraft. However, limited by the accuracy of the spacecraft model, this nonlinear spacecraft model output can also diverge from historic spacecraft, such as the Apollo lunar module (LM) absent stage (AS), the Apollo command

module (CM), and Apollo service module (SM), as shown in Table 2. Note that this research does not intend to develop an accurate spacecraft model; instead, this chapter proposes the methods for space logistics optimization with a nonlinear spacecraft model as an input. The aforementioned spacecraft model is chosen from the literature as an example to demonstrate our space logistics optimization method.

3.1.1.3 ISRU (oxygen) model

Only oxygen ISRU is considered in this chapter because oxidizer is a major component of spacecraft mass. Studies have shown that oxygen can be produced at a lower cost as compared with being delivered directly from Earth [58]. The integrated ISRU system developed by Schreiner used a molten regolith electrolysis model and balanced the tradeoff between optimal reactor performance and optimal excavator design. The ISRU system plant includes the reactor, Yttria-Stabilized Zirconia (YSZ) separator, excavator, hopper and feed system, oxygen liquefaction and storage system, and power system. For a detailed description of these systems, please see [7, 59]. Because a separate cooler is designed to reliquefy oxygen that has boiled off in the storage system [7], the boiloff effect of oxygen produced by ISRU is not considered. According to Schreiner's research [7], the ISRU production rate is increasing with the ISRU plant mass. The relationship is shown in Figure 5.

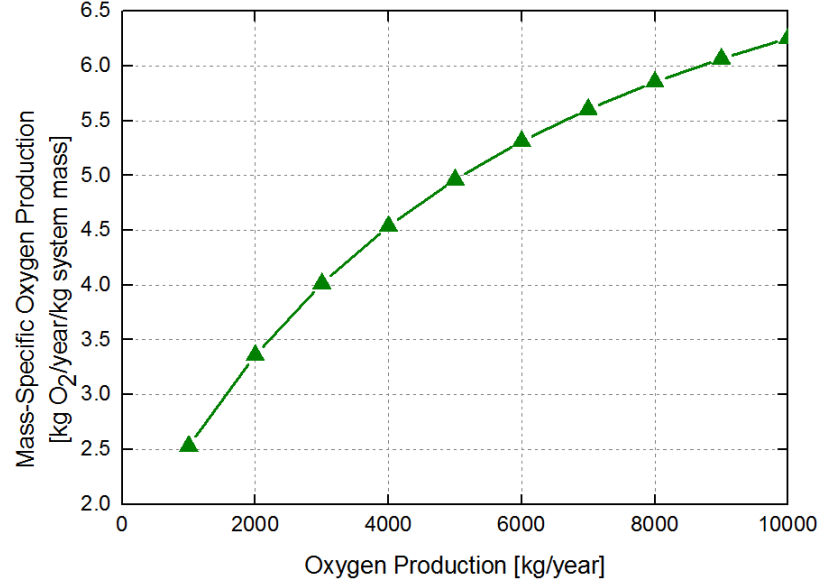


Figure 5 - The oxygen production level normalized by ISRU system mass [7].

It can be expressed as the following function [7]:

$$N_M = 8.8 \exp\left(-\frac{4241}{2405 + N_o}\right) \quad (12)$$

where N_M is the oxygen production rate in kilograms of oxygen (O_2) per year per kilogram system mass and N_o is the oxygen production per year. If we assume ISRU plant mass as M_o , then

$$N_M = N_o / M_o \quad (13)$$

Equation 12 is a regression equation that has a horizontal asymptote as $N_o \rightarrow \infty$. Based on equation 12 and the data from Schreiner [7], we build another regression equation to get $N_M = F_{ISRU}(M_o)$, which is shown as follows:

$$N_M = \begin{cases} 0 & \text{if } M_o \in [0, 400) \\ -0.438 + 6.9623 \left(1 - \exp\left(-\frac{M_o}{812.1563}\right)\right) + 2.0173 \left(1 - \exp\left(-\frac{M_o}{3967.2644}\right)\right) & \text{if } M_o \in [400, 10000) \end{cases} \quad (14)$$

The comparison between the regression equation [equation 14] and Schreiner's model [7] is shown in Figure 6. It is the relationship between the ISRU system plant mass M_o and the oxygen production rate N_M . Figure 6 shows that equation 14 fits the data of Schreiner's model well. It is used to calculate oxygen production in our space logistics model.

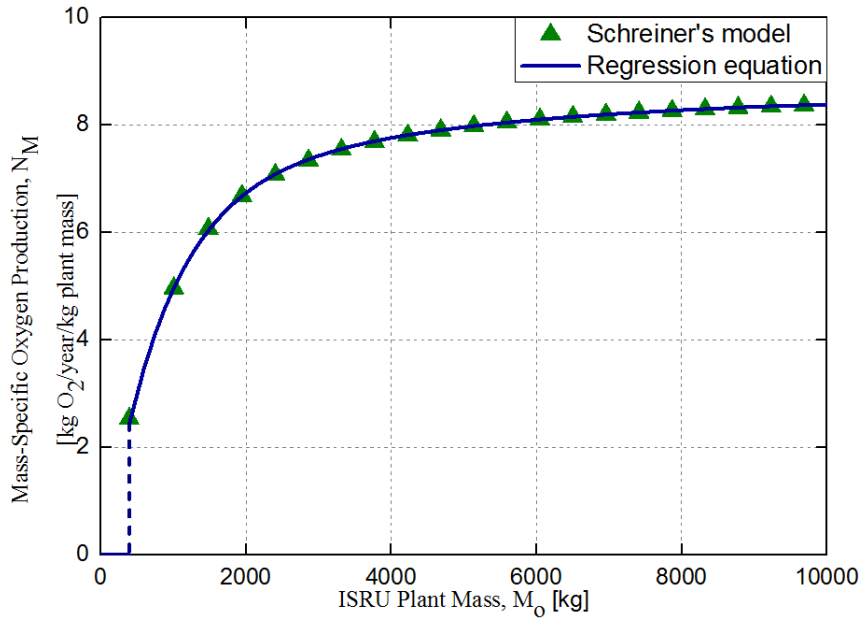


Figure 6 - The oxygen production normalized by ISRU system mass.

Equation 14 is a piecewise nonlinear function. When $M_o < 400$, ISRU does not function. Because the ISRU system includes the reactor, excavator, storage system, power system, etc., if the total mass of the ISRU plant is too low, the integrated ISRU system does not contain enough components to start functioning as a unit. The domain of the ISRU plant mass M_o in this equation is from 0 to 10,000 kg. From equations 13 and 14, we can

get the relationship between the oxygen production every year and the total mass of the ISRU plant deployed, which is $N_O = M_O * F_{ISRU}(M_O)$.

3.1.2 Optimization Methods

The campaign-level space logistics problem considering nonlinear spacecraft and ISRU model is a mixed-integer nonlinear programming (MINP) problem. This section introduces the piecewise function approximation method that linearizes the nonlinear ISRU and spacecraft models, and then converts them into binary mixed-integer programming formulations. Two approaches to solve this MINP problem are proposed. Both methods use the piecewise function approximation method for approximating the ISRU model. The difference between the two methods lies in how to deal with the nonlinear spacecraft model. The first approach converts the whole problem into a MILP formulation, which is expected to solve this problem more efficiently. The second approach is developed based on simulated annealing. It separates the spacecraft design from the mission planning part, which is intended to create the ability to consider higher-fidelity spacecraft models if necessary.

3.1.2.1 Piecewise function approximation method

The following shows the method to approximate a single variable nonlinear function by a piecewise linear function, and then convert it into a binary mixed-integer programming formulation. Considering a nonlinear function, a proper number of breakpoints inside the function domain is selected and then connected linearly, as shown in Figure 7. This single variable nonlinear function is approximated by a piecewise linear function, which can be described as follows:

$$f(x) := \begin{cases} k_1x + c_1, & x \in [u_1, u_2] \\ k_2x + c_2, & x \in [u_2, u_3] \\ \vdots & \\ k_{N-1}x + c_{N-1}, & x \in [u_{N-1}, u_N] \end{cases} \quad (15)$$

for some $N \in \mathbb{Z}_{\geq 0}$: $\{k_i\}_{i=1}^{N-1} \subset \mathbb{R}$, $\{c_i\}_{i=1}^{N-1} \subset \mathbb{R}$, and $\{u_i\}_{i=1}^{N-1} \subset \mathbb{R}$, where u_i is a breakpoint.

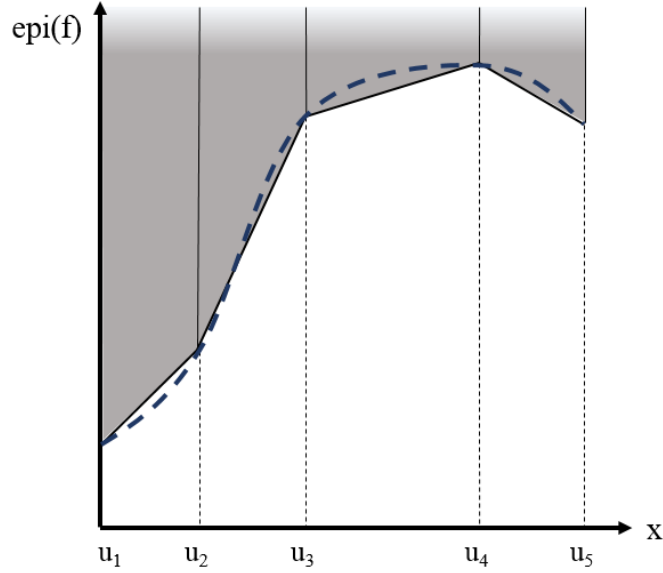


Figure 7 - Piecewise function and its epigraph as the union of polyhedra.

To solve this piecewise function in our mixed-integer linear programming model, the next step is modeling the piecewise function $f: D \subset \mathbb{R} \rightarrow \mathbb{R}$ as a binary mixed-integer programming formulation, where D is the domain of x . An appropriate approach to do it is to model its epigraph

$$epi(f) = \{(x, z) : x \in D, z \in \mathbb{R}, f(x) \leq z\}$$

as shown in Figure 7. The epigraph of a piecewise function can be considered as a union of polyhedra \mathcal{P} . Each polyhedron P corresponds to an interval $[u_i, u_{i+1}]$. Therefore, we can rewrite the piecewise function f as follows:

$$f(x) := \{k_P x + c_P, x \in P, \forall P \in \mathcal{P}\} \quad (16)$$

Vielma et al. [60] reviewed and introduced several ways to convert a union of polyhedra \mathcal{P} into a binary mixed-integer programming formulation, including a convex combination model, logarithmic branching convex combination (referred to as log) model, a multiple-choice model, an incremental method, etc. As one of the most performant formulations, the log model is chosen for the piecewise linear approximation of spacecraft and ISRU models in this research.

Following the theory described by Vielma et al. [60], $(x, z) \in \text{epi}(f)$ can be represented as the convex combination of points $(ve, f(ve))$ for $ve \in V(P)$, where V denotes the set of vertices (i.e., breakpoints) of polyhedron P , plus a ray in $C_1^+ := \{(0, z) \in \mathbb{R} \times \mathbb{R}: z \geq 0\}$. Then a continuous variable λ is assumed for each vertex $ve \in V(P)$ and for each $P \in \mathcal{P}$. As a result, a point $(x, z) \in \text{epi}(f)$ can be represented as

$$(x, z) = r + \sum_{P \in \mathcal{P}} \sum_{ve \in V(P)} \lambda_{P,ve} (ve, f(ve))$$

for $r \in C_1^+$ and

$$\{\lambda_{P,ve}\}_{P \in \mathcal{P}, ve \in V(P)} \subset \mathbb{R}_{\geq 0}$$

such that

$$\sum_{P \in \mathcal{P}} \sum_{ve \in V(P)} \lambda_{P,ve} = 1$$

Moreover, we can further reduce the number of continuous variable λ and constraints of the formulation by identifying a binary branching scheme. As a result, we

only need to define λ variables associated with the vertices (i.e., breakpoints) in the union of polyhedra \mathcal{P} , rather than for each vertex in each polyhedron P . This can reduce the number of λ variables significantly because two adjacent polyhedra share the same vertex (i.e., breakpoint).

Finally, the resulting formulation is given by

$$\sum_{ve \in \mathcal{V}(\mathcal{P})} \lambda_{ve} ve = x, \quad \sum_{ve \in \mathcal{V}(\mathcal{P})} \lambda_{ve} (k_P ve + c_P) \leq z \quad (17)$$

$$\lambda_{ve} \geq 0 \quad \forall ve \in \mathcal{V}(\mathcal{P}), \quad \sum_{ve \in \mathcal{V}(\mathcal{P})} \lambda_{ve} = 1 \quad (18)$$

$$\sum_{ve \in L_u} \lambda_{ve} \leq y_u, \quad \sum_{ve \in R_u} \lambda_{ve} \leq (1 - y_u), \quad y_u \in \{0,1\} \quad \forall u \in U \quad (19)$$

where $\{L_u, R_u\}_{u \in U}$ is a family of dichotomies, which is a branching scheme of λ variables. This formulation is called the logarithmic branching convex combination model. The branching scheme is introduced by Vielma and Nemhauser [61], and the details of the log method can be found in [60]. Using the aforementioned method, an example of building a log formulation is shown in the following.

For example, the nonlinear function in Figure 7 can be approximated by a piecewise function using five breakpoints, given by

$$f(x) := \begin{cases} k_1 x + c_1, & x \in [u_1, u_2] \\ k_2 x + c_2, & x \in [u_2, u_3] \\ k_3 x + c_3, & x \in [u_3, u_4] \\ k_4 x + c_4, & x \in [u_4, u_5] \end{cases} \quad (20)$$

Then, a point (x, z) in this piecewise function can be expressed as a binary mixed-integer programming formulation using the log formulation given by

$$u_1\lambda_1 + u_2\lambda_2 + u_3\lambda_3 + u_4\lambda_4 + u_5\lambda_5 = x \quad (21)$$

$$f(u_1)\lambda_1 + f(u_2)\lambda_2 + f(u_3)\lambda_3 + f(u_4)\lambda_4 + f(u_5)\lambda_5 \leq z \quad (22)$$

$$\lambda_1 + \lambda_2 + \lambda_3 + \lambda_4 + \lambda_5 = 1 \quad \forall \lambda_i \geq 0, i \in \{1, \dots, 5\} \quad (23)$$

$$\lambda_1 + \lambda_5 \leq y_1, \lambda_3 \leq 1 - y_1, \lambda_1 + \lambda_2 \leq y_2, \lambda_4 + \lambda_5 \leq 1 - y_2, y_1, y_2 \in \{0, 1\} \quad (24)$$

3.1.2.2 Mixed-Integer Linear Programming Optimization Framework

From the MILP formulation [equations 1-7], we can see that, if the spacecraft model is considered together with mission planning, even though it is approximated using a piecewise function and then converted into a binary mixed-integer programming formulation, there are still quadratic terms. These quadratic terms exist in an objective function [equation 1], a commodity transformation constraint [equation 4], and a concurrency constraint [equation 5]. The reason is that spacecraft design variables, s_v , C_v , and M_v , are also variables in the MILP formulation. These quadratic terms are the products of discrete and continuous variables. Because the coefficient matrix of quadratic terms is not positive semidefinite, to solve this model, linearizing quadratic terms is a better choice.

Consider a nonlinear equation $z_{vijkt} = e_v b_{vijkt}$, where e_v is a continuous variable representing the dry mass s_v , payload capacity C_v , or propellant capacity M_v of spacecraft v . b_{vijkt} is a binary variable representing whether the k^{th} spacecraft is flying along the arc from i to j at time t . Note that v represents the type of spacecraft, and there are multiple spacecraft for the same type. Also, k is the index of spacecraft of the same type. Assuming the maximum number of spacecraft v can be used is n , we have

$$y_{vijt} = \sum_{k=1}^n b_{vijkt} \quad (25)$$

Therefore, using the big- \mathcal{M} method, product $z_{vijkt} = e_v b_{vijkt}$ can be linearized as follows:

$$z_{vijkt} \leq \mathcal{M} b_{vijkt} \quad (26)$$

$$z_{vijkt} \leq e_v \quad (27)$$

$$z_{vijkt} \geq e_v - (1 - b_{vijkt})\mathcal{M} \quad (28)$$

$$z_{vijkt} \geq 0 \quad (29)$$

where \mathcal{M} is a large constant.

As a result, after approximating the nonlinear model of ISRU and spacecraft by piecewise function approximation method and linearizing quadratic terms in concurrency constraints, all nonlinear terms are converted into linear constraints. The campaign-level space logistics optimization problem considering nonlinear spacecraft and ISRU production models finally becomes a mixed-integer linear programming problem.

3.1.2.3 Simulated Annealing (SA) Optimization Framework

SA is a conventional heuristic optimization method that cannot guarantee or certify its global optimality. Typically, it takes a long time to achieve an acceptable solution. This SA-based method is inspired by the optimization framework developed by Taylor [52]. However, Taylor's approach cannot take into account infrastructure such as ISRU because the mission planning part of the framework uses a shortest-path-based approach. This

section improves this method by using an arc-based formulation and solves it as a multicommodity network flow.

The only difference between the MILP-based method and the SA-based method is how to deal with the nonlinear spacecraft model. The SA-based approach separates the spacecraft model from mission planning. As a result, the spacecraft design variables C_v and M_v are constant inside the MILP formulation. They are only variables in the separated spacecraft model. In other words, the quadratic terms in the MILP formulation disappear. The nonlinear ISRU model is still designed concurrently with the mission planning part. It is converted into a binary mixed-integer programming formulation through piecewise linear approximation.

Because the spacecraft model is separated, the advantage of the SA approach is that it provides the possibility of extending the spacecraft model in an easier manner when compared to the method of MILP formulation.

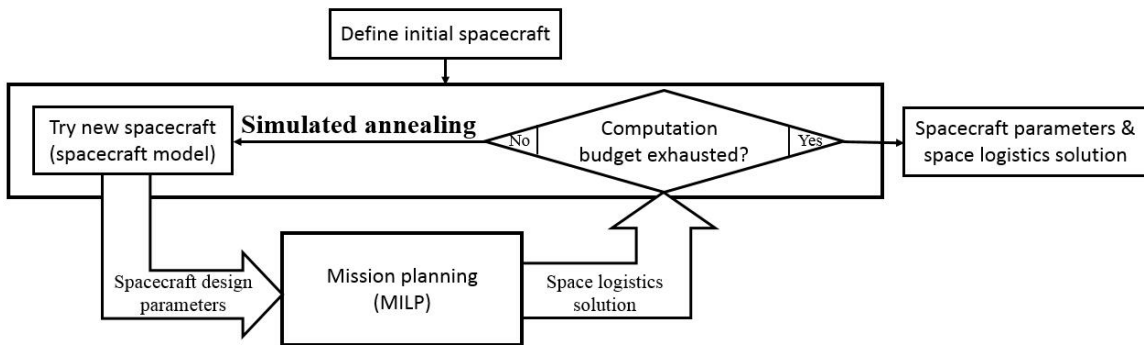


Figure 8 - Flow chart of SA-based approach.

A flow chart of SA is shown in Figure 8. The mission planning section is actually the evaluation step of simulated annealing. After selecting random neighbors in the spacecraft model, the performances of the spacecraft are evaluated by a space logistics mission planning optimization utilizing these spacecraft. The best space logistics solution

is recorded. The optimization algorithm repeats until a stopping criteria (e.g., convergence, computation budget) and then optimal spacecraft parameters and space logistics solutions are output.

3.2 Results and Analysis

3.2.1 Model Validation

This section validates the network model using the Apollo 17 mission as an example, where no ISRU and spacecraft design models are considered. Instead, the original spacecraft in the Apollo mission is used in mission planning. The Apollo 17 mission can be modeled as a four-node network as shown in Figure 9, including the Pacific Ocean (PAC), low Earth orbit (LEO), low lunar orbit (LLO), and lunar surface (LS). The time of flight (TOF) and ΔV for each transportation arc are also shown in Figure 9. We assume that one day is one time step.

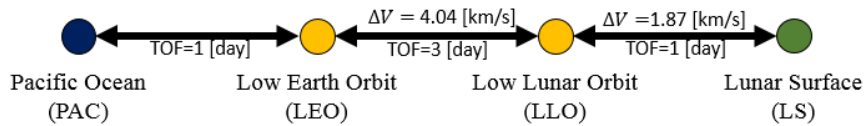


Figure 9 - Apollo 17 network model.

Note that the propellant cost for transportation from Earth to LEO is not considered because the IMLEO is minimized in this research. For a transportation system, the IMLEO is a widely accepted measure of the mission cost [1, 3]. In some literature, the financial cost is also used as a metric [5]. However, this chapter focuses on limited resource utilization and the interaction between mission planning and spacecraft design. To simplify the problem, the IMLEO is used as a metric for mission cost in this chapter.

Table 3 lists all spacecraft used in Apollo 17, and Table 4 lists the demand and supply of the Apollo 17 mission. In this example, two astronauts, along with the scientific

experiment equipment, are sent to the lunar surface, and stay there for one day; whereas a third astronaut stays in lunar orbit for three days. Then, all three astronauts come back with 110 kg of lunar samples. For this Apollo 17 mission, the time window is always open.

Table 3 - Spacecraft used in Apollo 17.

Spacecraft	Propellant capacity M , kg	I_{sp} , s	Payload capacity C , kg	Structure mass s , kg
Saturn V second stage	452,045	421	0	38,415
Saturn V third stage	107,725	421	0	12,014
Command module	0	0	524	4,841
Service module	18,413	314	60	6,053
LM descent stage	8,804	311	500	2,770
LM ascent stage	2,358	311	250	1,719

Table 4 - Demand and supply of Apollo 17 mission.

Payload Type	Node	Demand Time, day	Supply
Crew, ^a no.	Lunar surface	5	-2
Crew, ^a no.	Lunar orbit	4	-1
Crew Return, ^a no.	Lunar surface	6	2
Crew Return, ^a no.	Lunar orbit	7	1
Crew Return, ^a no.	Earth	11	-3
Equipment, ^b kg	Lunar surface	5	-420
Sample, ^c kg	Earth	11	-110
Crew, Equipment, ^b kg	Earth	0-11	$+\infty$
Sample, ^c kg	Lunar surface	0-11	$+\infty$

^aCrew and Crew Returning are separated in order to ensure that the crew shall reach the moon before returning to Earth.

^bEquipment denotes all scientific experiment equipment for lunar surface activities, including a Lunar Roving Vehicle (LRV);

‘Sample denotes all the things we want to bring back from another planet, typically for scientific research.

The optimized solution using the GMCNF model for this example is depicted in Figure 10. All commodities are delivered together from LEO. Notice that crew members fly back to the Earth by LM descent stage (LMDS) instead of the Apollo command/service module (CSM) in the original mission. This is a feasible solution since the payload capacity of LMDS is large enough to contain three crew members and 110 kg of lunar samples. The size of the propellant tank is also sufficient to support the return directly from lunar orbit. This is also an optimal solution because one important function of the CSM is to bring crew members and lunar samples back to the Earth. If the LMDS can complete this work, the service module would not be used because LMDS has a smaller structure mass which means less propellant cost. A similar result is observed in Taylor et al.’s study [3]. Saturn V’s third stage performs as a propellant depot after reaching the lunar orbit. The detailed mass flows are shown in Figure 11. The consumables in Figure 11 include water, oxygen, and food for the crew.

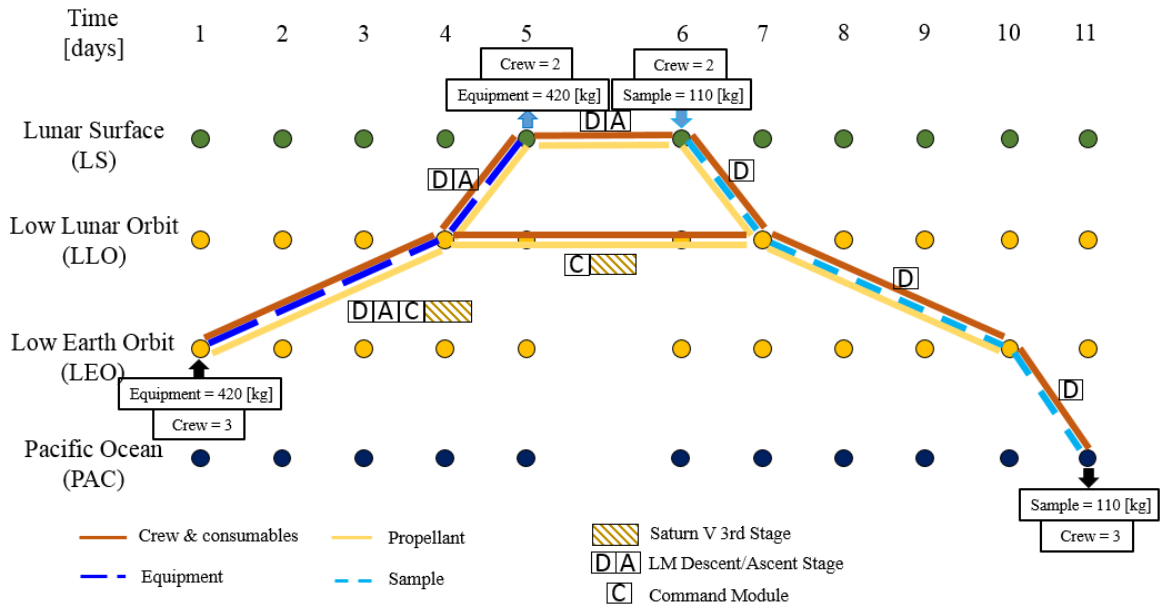


Figure 10 - Apollo 17 example.

From	LEO	LLO	LLO	LS	LS	LLO	LEO
To	LLO	LS	LLO	LS	LLO	LEO	PAC
Time, days	1-4	4-5	4-9	5-8	8-9	9-12	12-13
Saturn V third stage, no.	1	---	1	---	---	---	---
Command module, no.	1	---	1	---	---	---	---
LM descent stage, no.	1	1	---	1	1	1	1
LM ascent stage, no.	1	1	---	1	---	---	---
Crew, no.	3	2	1	2	2	3	3
Consumables, kg	124	26	51	17	9	51	13
Equipment, kg	420	420	---	---	---	---	---
Sample, kg	---	---	---	---	110	110	110
Propellant, kg	83,562	8,940	8,656	2,531	2,531	8,656	---
Total Flow, kg	105,750	14,075	25,662	7,237	5,620	11,887	3,193

Figure 11 - Commodity flows in the optimal solution.

Table 5 compares the differences of payload and propellant at Earth orbit insertion between the optimized Apollo 17 mission and the original mission [62]. Notice that no spacecraft design model is considered in this example. The optimized Apollo mission uses the same vehicles as the original mission.

Table 5 - Mass differences comparison at Earth orbit insertion.

Spacecraft	Class of mass	Original	Optimized
		Apollo 17, kg	Apollo 17, kg
Saturn V third stage	Propellant	96,204	74,758
	Structure mass	12,014	12,014
Command module	Crew member	3*100	— —
	Consumables	124	— —
	Equipment	— —	420
	Structure mass	4,841	4,841
Service module	Propellant	18,413	— —
	Structure mass	6,110	— —
LM descent stage	Crew member	— —	3*100
	Consumables	— —	124
	Equipment	420	— —
	Propellant	8,804	8804
LM ascent stage	Structure mass	2,770	2,770
	Propellant	2,358	— —
	Structure mass	1,719	1,719
All spacecraft	Total mass	154,077	105,750

The GMCNF model actually selects a better solution for the Apollo 17 mission. For validation purposes, we can manually track what has changed as compared with the original mission. Starting from the original Apollo 17 mission, we remove the service module, the propellant in LM ascent stage (LMAS), and the propellant to transport these commodities to lunar orbit. Then, we add the propellant for the LMDS to support its return to Earth. Finally, the initial mass in LEO becomes 105,614 kg. The optimal solution by the GMCNF model is 105,750 kg, which is only a 0.1% difference from our manual validation results. Thus, we can conclude that the time-expanded GMCNF could find an optimal solution and has sufficient accuracy to optimize the space logistic problem.

3.2.2 Campaign-level Space Logistics Design

This section evaluates and analyzes the performance of the space logistics optimization framework for mission planning and spacecraft design. Both ISRU and spacecraft design models are taken into account. Moreover, maintenance costs and the oxygen boiloff are also considered in this case. This is a MILP problem solved in Python by a Gurobi 6.5 solver on an Intel Core i7-4700MQ, quad-core 3.4GHz platform. All the following numerical experiments in this chapter are solved on this platform. The piecewise linear approximations for nonlinear ISRU and spacecraft models are done through a Python-based open-source optimization package named Pyomo.

In this section, we first perform optimization for a single space mission as the baseline solution. Then, we optimize a campaign, which contains multiple space missions, and compare its result with the baseline solution to study the effect of campaign-level space logistics design. These space mission optimizations are all completed through the MILP-based method. Next, we compare the performance of the MILP-based method with the SA-based method. Finally, we perform sensitivity analyses of ISRU productivity and spacecraft design.

3.2.2.1 Single mission Design with MILP

In this part, we optimize a single space mission as the baseline solution. It is used to demonstrate the effect of campaign-level space logistics design in the next section. Based on the Apollo 17 mission, a new large-scale lunar mission is designed as an example for optimization. The demand and supply are shown in Table 6. In this case, 12 crews are delivered to the Moon with 4200 kg of equipment and come back with 500 kg samples. The assumptions are listed in Table 7 [63, 64]. For this single mission example, the time window is always open.

Table 6 - Demand and supply of lunar mission.

Payload Type	Node	Demand Time, day	Supply
Crew, no.	Lunar Surface	5	-12
Crew Return, no.	Lunar Surface	8	12
Crew Return, no.	Earth	13	-12
Equipment, kg	Lunar Surface	5	-4200
Sample, kg	Earth	13	-500
Crew, Equipment, kg	Earth	0-13	+∞
Sample, kg	Lunar Surface	0-13	+∞

Table 7 - Summary of parameters and assumptions.

Parameter	Assumed value
Percentage of oxygen in propellant	71.91% LOX/kerosene
Oxygen boil-off rate	0.016%/day
Food consumption rate [63, 64]	1.015 kg/day/crew
water consumption rate [64]	6.37 kg/day/crew
oxygen consumption rate [64]	1.18 kg/day/crew
Crew mass (including space suit)	100 kg/crew
ISRU maintenance	10%/year
Spacecraft maintenance	1%/flight

The percentage of oxygen in propellant in Table 7 is used to consider the production of oxygen ISRU plant and the boiloff effect. Note that the oxygen consumed by crew members is very low as compared with the oxidizer in propellant (LOX/kerosene). To simplify the problem, the oxygen produced by the ISRU plant is only used for propellant oxidizer.

The maintenance of ISRU is performed every mission, and the amount of ISRU maintenance mass is determined by the ISRU plant mass. In addition, the maintenance of

spacecraft is performed in every flight and the amount of needed maintenance mass is related to the spacecraft structure mass.

The solution of the single mission optimization is listed as follows. Two types of spacecraft are considered, and two spacecraft can be used for each type.

Table 8 - Spacecraft design of a single mission design.

Spacecraft Type	Payload Capacity, C, kg	Propellant Capacity, M, kg	Structure Mass, S, kg
1	2,020	166,481	17,996
2	2,262	23,891	7,342

Table 8 lists the spacecraft design in this case, and the mission planning solution is depicted in Figure 12. Because the mission only lasts for 13 days, no ISRU plant is deployed on the moon. This solution is also an optimal solution of the conventional carry-along strategy. All propellant and consumables used in the mission come from the Earth. The spacecraft size is also shown in Figure 12, corresponding to the structure mass in Table 8. Even though the spacecraft are designed to be multiuse without specific functions assigned for each type, they still perform different roles in the mission. Spacecraft 1, which is relatively larger, is mainly used to deliver equipment. Spacecraft 2, which is smaller, is mainly used to deliver crews and samples back from the moon. The detailed mass flows are shown in Figure 13, and we can see that the IMLEO of this mission is 439,375 kg.

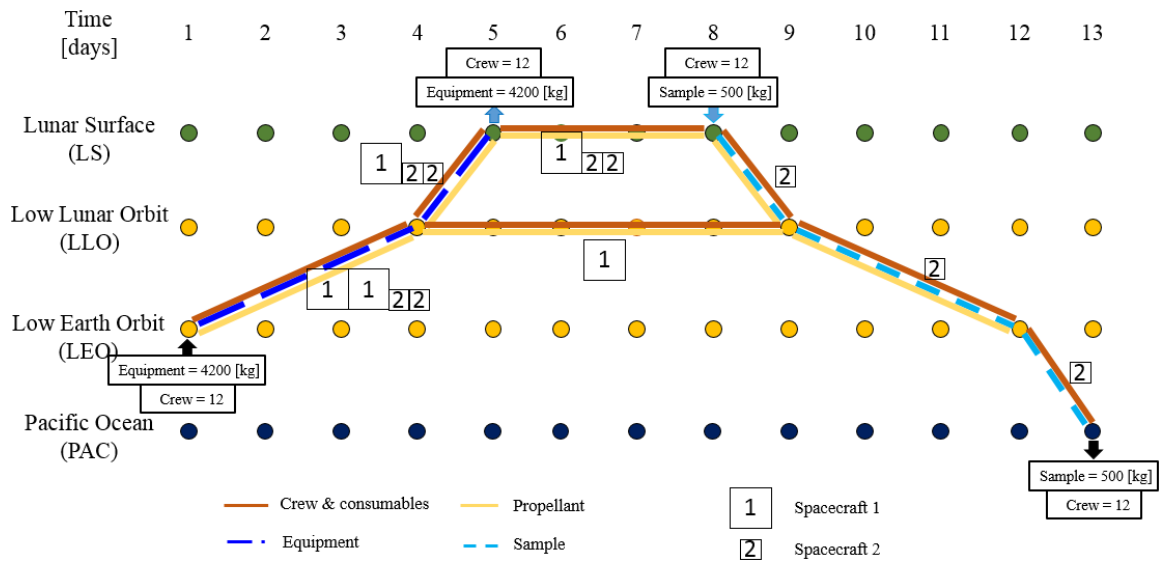


Figure 12 - Single lunar mission solution.

From	LEO	LLO	LLO	LS	LS	LLO	LEO
To	LLO	LS	LLO	LS	LLO	LEO	PAC
Time, days	1-4	4-5	4-9	5-8	8-9	9-12	12-13
Spacecraft 1, no.	2	1	1	1	---	---	---
Spacecraft 2, no.	2	2	---	2	1	1	1
Crew, no.	12	12	---	---	12	12	12
Consumables, kg	1,247	513	415	415	104	415	104
Maintenance, kg	1,307	474	327	147	73	147	73
Equipment, kg	4,200	4,200	---	---	---	---	---
Sample, kg	---	---	---	---	500	500	500
Oxidizer, kg	273,795	31,251	17,183	5,191	5,190	17,180	---
Kerosene, kg	106,950	12,207	6,711	2,027	2,027	6,711	---
Total Flow, kg	439,375	82,525	42,632	40,460	16,436	33,495	9,219

Figure 13 - Commodity flows of single lunar mission.

3.2.2.2 Campaign-Level Mission Design with MILP

This section studies the effect of campaign-level space logistics mission design. Three lunar missions are combined together into a campaign. In each mission, 12 crews are delivered to the moon with 4200 kg of equipment and come back to Earth with 500 kg of lunar samples. All the assumptions remain the same as before. For a multi-mission campaign, the time windows are open at the start of each mission, which are determined by the mission intervals. It takes about 2000 s to optimize this problem. The solution of

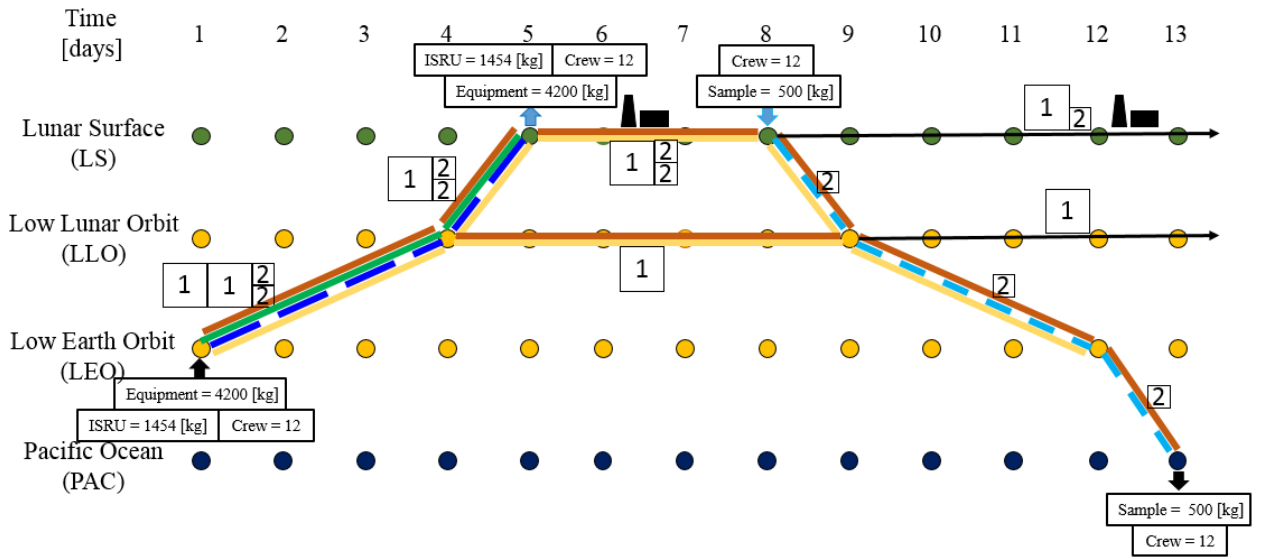
campaign-level mission optimization with one year mission intervals is shown in the following.

Table 9 - Spacecraft design of the multi-mission campaign design solution (interval: one year).

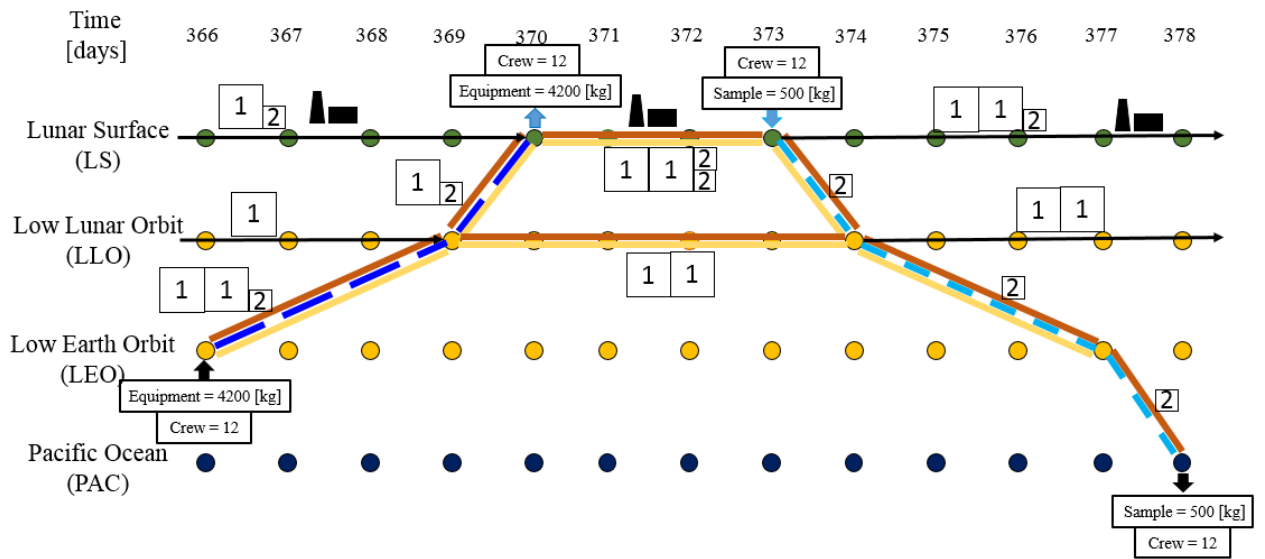
Spacecraft Type	Payload Capacity, C, kg	Propellant Capacity, M, kg	Structure Mass, S, kg
1	3,978	198,580	24,745
2	2,262	23,891	7,342

Table 9 lists the spacecraft design of this case. The mission planning of this campaign is depicted in Figure 14. We can see that the size of spacecraft 2 is the same as it in the single mission case, as shown in Table 8. The reason is that, like the single mission case, spacecraft 2 is mainly used to deliver crews and samples. Because the demands of crews and samples do not change, the size of spacecraft 2 does not change. However, the size of spacecraft 1 is larger because, in a multi-mission campaign, spacecraft 1 is used to deliver not only the equipment but also ISRU plants.

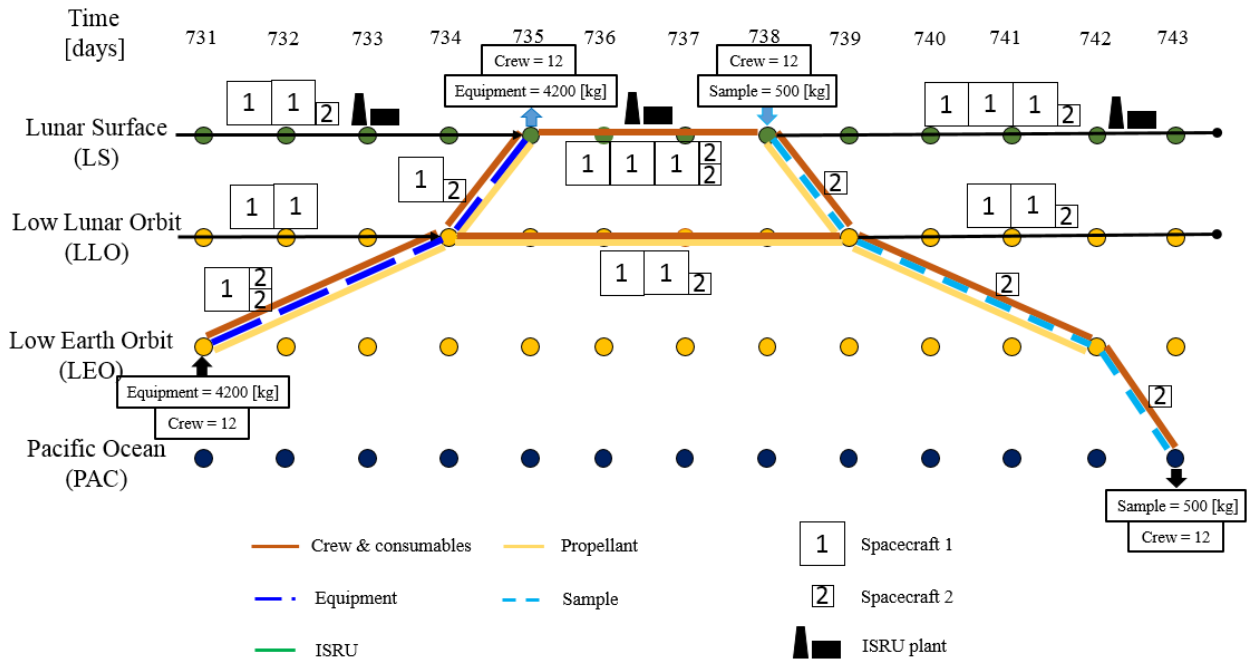
The detailed mass flows are listed in Figure 15. From Figure 15, we can see that the IMLEO for each mission is decreasing. The first mission has the highest IMLEO because the ISRU plant is deployed in this mission. Starting from the second mission, the oxidizer used in the spacecraft flying out of the moon is produced by the ISRU plant. It relies less on the Earth resource for propellant oxidizer, which is expensive to deliver from Earth. As a result, the total IMLEO of this multi-mission campaign is lower than three single missions, as can be seen by comparing Figure 13 and Figure 15. If this mission is repeated in the fourth year, because there is no need to deploy ISRU plants again, the mission cost is still lower than a single lunar mission.



a) Mission-I



b) Mission-II



c) Mission-III

Figure 14 - Multi-mission lunar campaign solution (interval: one year).

From	LEO	LLO	LLO	LS	LS	LLO	LEO
To	LLO	LS	LLO	LS	LLO	LEO	PAC
<i>Mission-I</i>							
Time, days	1-4	4-5	4-9	5-8	8-9	9-12	12-13
Spacecraft 1, no.	2	1	1	1	—	—	—
Spacecraft 2, no.	2	2	—	2	1	1	1
Crew, no.	12	12	—	12	12	12	12
Consumables, kg	1,247	519	415	415	104	415	104
Maintenance, kg	2,165	1,129	394	735	73	147	73
ISRU, kg	1,454	1,454	—	1,454	—	—	—
Equipment, kg	4,200	4,200	—	4,200	—	—	—
Sample, kg	—	—	—	—	500	500	500
Oxidizer, kg	319,854	36,273	17,183	5,165	5,165+25	1,7180	—
Kerosene, kg	125,087	14,315	6,711	2,163	2,027	6,711	—
Total Flow, kg	519,381	98,519	49,448	54,761	16,436	33,495	9,219
<i>Mission-II</i>							
Time, days	366-369	369-370	369-374	370-373	373-374	374-377	377-378
Spacecraft 1, no.	2	1	2	2	—	—	—
Spacecraft 2, no.	1	1	—	2	1	1	1
Crew, no.	12	12	—	12	12	12	12
Consumables, kg	1,246	519	415	415	104	415	104
Maintenance, kg	2,072	320	1,183	440	73	147	73
ISRU, kg	—	—	—	1,454	—	—	—
Equipment, kg	4,200	4,200	—	8,400	—	—	—
Sample, kg	—	—	—	—	500	500	500
Oxidizer, kg	287,032	22,995	14,453	9,432	9,456	14,395+2,785	—
Kerosene, kg	134,018	11,501	25,023	2,654	2,628	6,711	—
Total Flow, kg	486,600	72,822	90,564	88,169	21,303	33,495	9,219
<i>Mission-III</i>							
Time, days	731-734	734-735	734-739	735-738	738-739	739-742	742-743
Spacecraft 1, no.	1	1	2	3	—	—	—
Spacecraft 2, no.	2	1	1	2	1	1	1
Crew, no.	12	12	—	12	12	12	12
Consumables, kg	1,247	519	415	415	104	415	104
Maintenance, kg	394	320	220	147	73	147	73
ISRU, kg	—	—	—	1,454	—	—	—
Equipment, kg	4,200	4,200	—	12,600	—	—	—
Sample, kg	—	—	—	—	500	500	500
Oxidizer, kg	187,691	23,041	14,453	9,432	9,456	14,395+2,785	—
Kerosene, kg	58,671	11,601	6,711	2,628	2,628	6,711	—
Total Flow, kg	292,832	72,968	78,631	116,795	21,303	33,495	9,219

“ ”: this part of propellant oxidizer is produced by ISRU plant

**Figure 15 - Commodity flows of the multi-mission lunar campaign solution
(interval: one year).**

The mission time intervals determine the total working time of the ISRU plant during the campaign. To study the effect of mission interval, the spacecraft structure mass and mission planning results with respect to the mission interval are depicted in Figure 16.

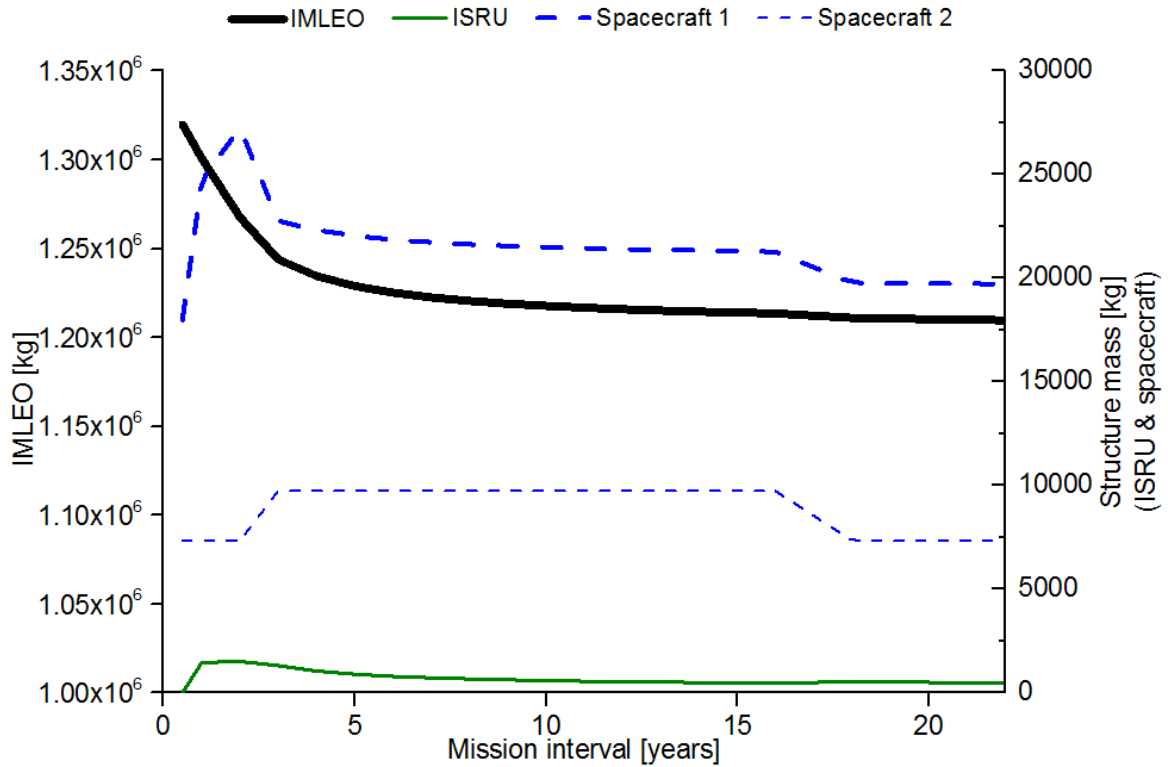


Figure 16 - Results of multi-mission lunar campaign design with respect to mission interval.

As shown in Figure 16, the IMLEO first decreases quickly because the mission obtains lots of benefits from the oxygen ISRU plant with a longer mission interval. However, after the mission interval is longer than 10 years, the IMLEO starts to decrease very slowly with the increase of mission interval because the oxygen ISRU can only produce propellant oxidizer. No matter how much oxidizer can be produced by the ISRU plant, we still need kerosene delivered from Earth. When the mission interval is long enough, the benefit from the oxygen ISRU plant diminishes.

Furthermore, two types of spacecraft are considered. There is a direct relationship between the size of large spacecraft (e.g. spacecraft 1) and the mass of the ISRU plant deployed. In Figure 16, the variation pattern of the structure mass of spacecraft 1 matches the variation pattern of the ISRU plant mass. Similar to the results in campaign-level

mission design, the large spacecraft is mainly used to deliver equipment and the ISRU plants. Because the demand for equipment is constant in each mission, the size of large spacecraft is mainly determined by the ISRU plants; however, the small spacecraft is mainly used to deliver samples and crew members. Even if all spacecraft are designed in a general way (i.e., no specified function identified at the start of spacecraft design), the solver identifies the functions for each type of spacecraft.

3.2.2.3 Optimization Method Comparison

As discussed in the Methodology section (Sec. 3.1), there are two optimization methods proposed in this chapter: the MILP method and the SA optimization framework. This section studies the influences of different optimization methods. These methods are used to solve the same campaign-level mission design problem defined previously.

In the previous section, the nonlinear ISRU model and nonlinear spacecraft model are finally converted into a binary mix-integer programming formulation through piecewise functions. However, these models can initially be assumed as linear to simplify the problem. For the linear ISRU model, we assume that the oxygen production rate is 7.5 kg of O_2 per year per kilogram of ISRU system mass. The linear spacecraft model is a linear simplification of equation 11, which is assumed as

$$S = 2.3931C + 0.09M \quad (30)$$

The comparison of different optimization methods is shown in Table 10.

Table 10 - Comparison of different optimization methods (interval: one year).

Optimization method				
	ISRU model	Spacecraft model	IMLEO, kg	Optimization Time, s
MILP	Nonlinear	Nonlinear	1,298,813	2,000
	Nonlinear	Linear	1,424,484	1,705
	Linear	Nonlinear	1,296,999	2,566
	Linear	Linear	1,424,484	1,360
Simulated annealing			≈1,407,000	≈4,000

The IMLEO of the problem with the linear spacecraft model is much higher when compared with the normal case (i.e., all nonlinear). This is because, in the nonlinear spacecraft model, the structure mass ratio of a large spacecraft is lower than a small spacecraft. The structure mass increases linearly with the spacecraft size in equation 30, which is developed based on small spacecraft; thus, the structure mass of a large spacecraft based on equation 30 is larger than reality. More propellant is consumed due to the large structure mass. On the contrary, the problem with the linear ISRU model has a lower IMLEO compared with a nominal scenario. The reason is the production rate of ISRU is increasing with the ISRU plant mass. As shown in Figure 6, the ISRU would not work before the system mass reaches 400 kg. Then, the production rate is only 2.5 kg of O_2 per year per kilogram of ISRU system mass, with a 400 kg ISRU plant and 5 kg of O_2 per year per kilogram of ISRU system mass with a 1,000 kg plant. To achieve a production rate of 7.5 kg of O_2 per year per kilogram of ISRU system mass, more than 3,000 kg ISRU plant should be deployed. Thus, the ISRU production rate of a linear ISRU model is typically higher than the actual case.

The optimization time cost listed in Table 10 is the running time Gurobi solver, ignoring the model input time, which is typically 1 or 2 min. Because a MILP problem is

generally solved by a linear-programming-based branch-and-bound algorithm, the calculation time is influenced by multiple factors, such as mission interval and ISRU or spacecraft model. For this four-node network in the space logistics model, considering a campaign including three lunar missions, there are approximately 100,000 constraints, 1,500 integer variables and 5,400 continuous variables. In Table 10, the optimization time of all linear MILP methods is 1360 s when the mission intervals are one year. In fact, it may take a longer time when the mission intervals change. When we compare this all-linear MILP method with our method based on a piecewise linear function and MILP, we can find that our methods solve the space logistics problem including nonlinear ISRU and spacecraft models without much deterioration of computational efficiency. Our method may bring in several binary variables and constraints, but most of the constraints and variables come from the mission planning part, which is a GMCNF model. These constraints and variables are not influenced by which ISRU or spacecraft model considered. Therefore, no matter which ISRU or spacecraft model is considered, the optimization time cost of this campaign-level mission solved by the MILP method is at the same order of magnitude of approximately 1,500-2,500 s.

The same problem is also solved by the SA-based method. It cannot guarantee an optimal solution, but it is a good method if the precise global optimum is less important and an acceptable local optimum is wanted in a given time horizon. The biggest advantage of SA in this problem is that the spacecraft model is separated from the mission planning part. As a result, higher-fidelity spacecraft models can easily be considered, such as considering the fuel types. Moreover, different spacecraft can easily be assigned different functions initially in a separate spacecraft model.

The solution of SA is influenced significantly by the cooling strategy and the initial value of the problem (e.g., initial spacecraft). The start temperature is set as 10,000 and the algorithm will stop after the temperature reaches 0.1. The annealing schedule is an

exponential cooling scheme with a cooling rate assumed as 0.985. Thus, there are 762 iterations in total. The initial spacecraft in this chapter is generated by the spacecraft model randomly. Therefore, the final solution of the SA method may vary even for the same scenario.

The comparison of IMLEO between the MILP method and the SA method in different mission intervals is shown in Figure 17. Because finding the optimal strategy to minimize IMLEO in space logistics is a minimization problem and the SA method always achieves a feasible (and suboptimal) solution, we can observe that the results from SA are typically 8-15% higher than the results of the MILP method. The gap is dependent on the candidate spacecraft generation method and cooling strategy.

We can improve the performance of the SA method by starting from a better initial solution with heuristics or optimizing the cooling strategy. Because the spacecraft model is separated from the mission planning part, SA is a better choice if a higher-fidelity spacecraft model needs to be considered and the precise global optimum is less important than finding an acceptable local optimum within the given time.

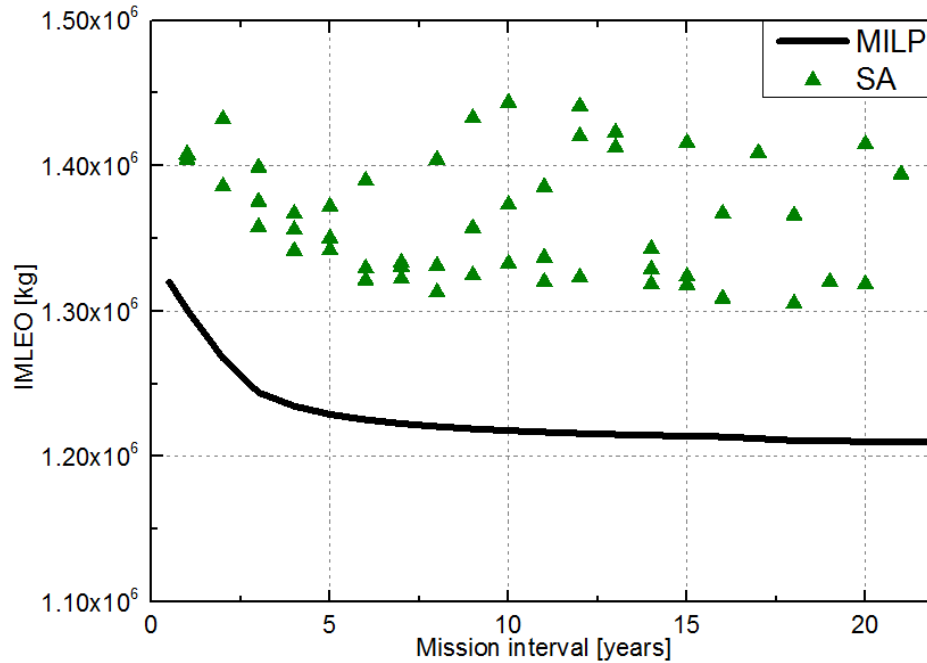


Figure 17 - Comparison of IMLEO results by MILP and SA method.

3.2.2.4 Sensitivity Analysis

With the development of technology, ISRU could have a higher production rate and the spacecraft could have a lighter structure while maintaining sufficient strength at the same time. On the other side, some uncertainty factors may prevent the ISRU system from working properly or the spacecraft may be assigned extra structure mass. This section studies the sensitivity of this campaign-level mission design to the ISRU productivity and the spacecraft structure mass using the MILP method.

The considered problem is the campaign-level mission design with three lunar missions under the same assumptions as before. The mission interval is one year. The IMLEO with respect to ISRU productivity is shown in Figure 18. The baseline is the normal ISRU production rate in equation 14.

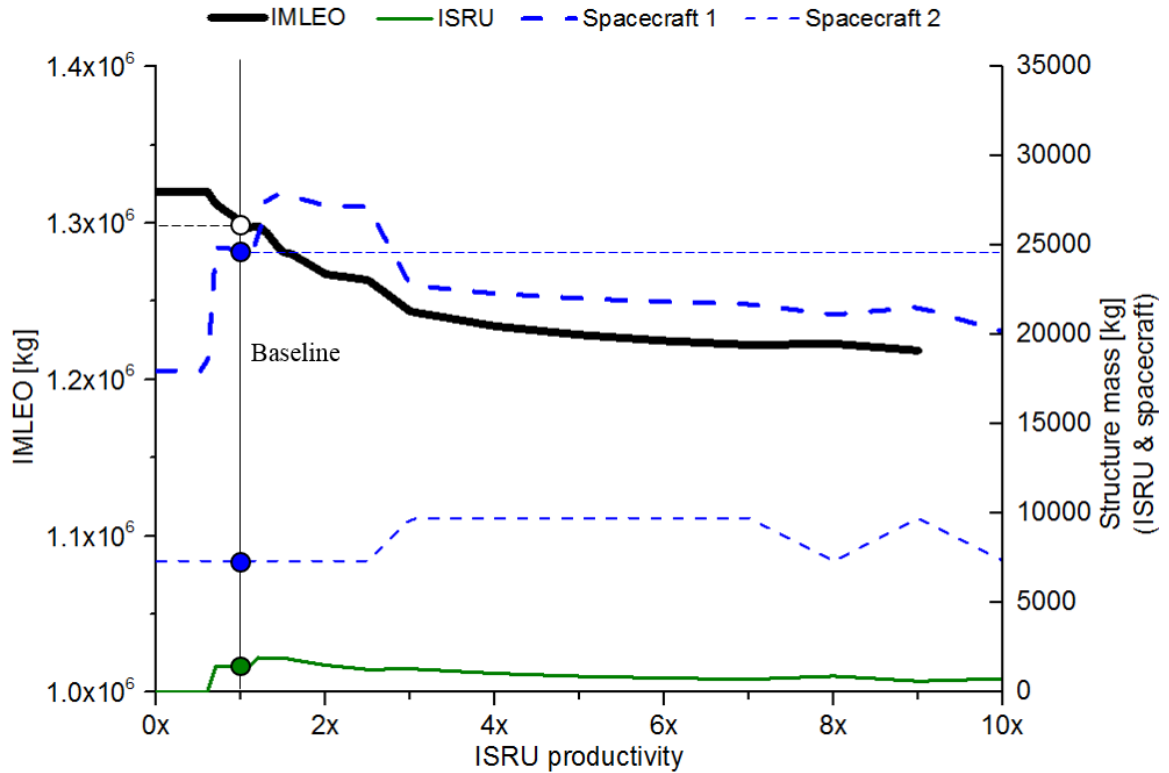


Figure 18 - Results of multi-mission lunar campaign design with respect to ISRU productivity (interval: one year).

As shown in Figure 18, with the increase of ISRU productivity, the IMLEO of space mission is decreasing. When the oxygen ISRU productivity is less than 80% of the normal rate, no ISRU plant is deployed. The IMLEO and spacecraft design stay constant until the productivity reach 80%. Then, with the increase of ISRU productivity, the IMLEO of the whole mission decreases monotonically. When the ISRU productivity reaches 150% of the normal production rate, the mass of ISRU plant deployed starts to decrease slowly. The structure mass of the large spacecraft (i.e., spacecraft 1) still matches the variation pattern of the ISRU plant mass deployed in this case. Although the structure mass of the small spacecraft (i.e., spacecraft 2) varies in a certain range. One important note is that the increase of ISRU production does not reduce IMLEO unlimitedly. When the ISRU productivity is high enough, the mission cost sensitivity to ISRU productivity is very low.

With the increase of ISRU productivity, the total IMLEO is decreasing slowly. The reason is that the oxygen ISRU plant only produces oxidizer for this mission. The transportation still needs kerosene supplied from Earth.

If we fix the ISRU productivity at the normal rate, the sensitivity of the IMLEO with respect to the spacecraft structure mass is shown in Figure 19.

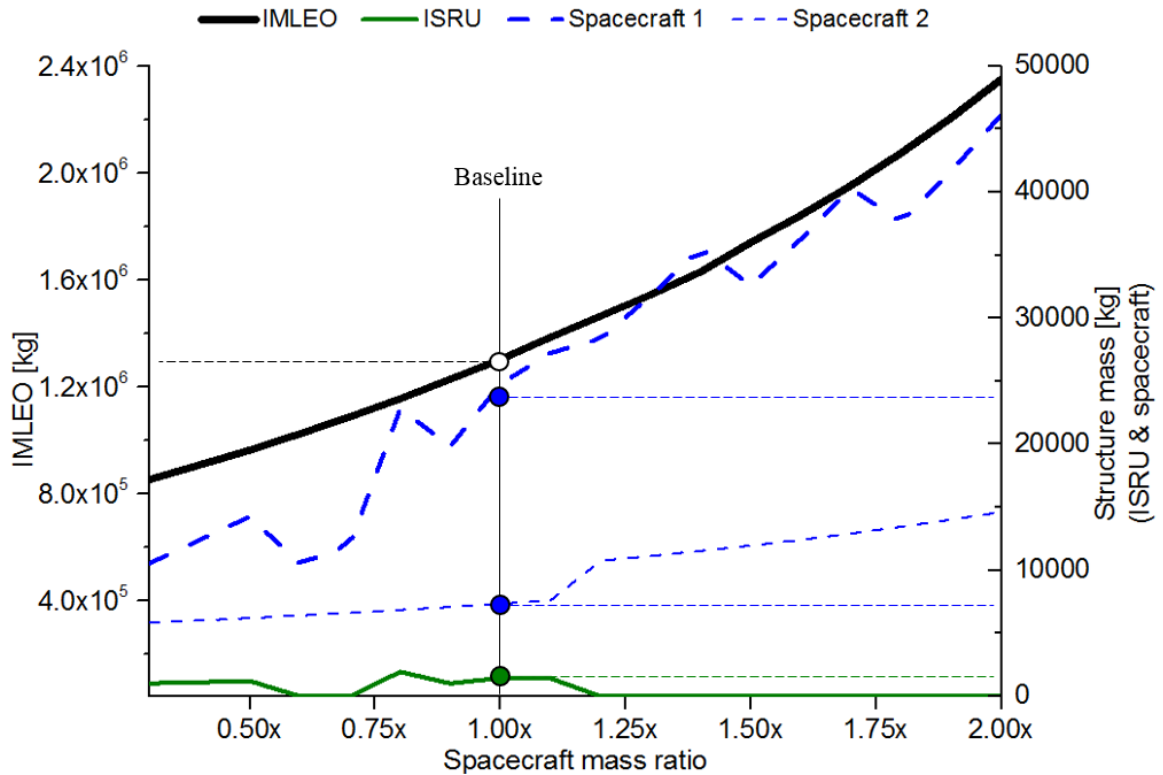


Figure 19 - Results of multi-mission lunar campaign design with respect to spacecraft structure mass (interval: one year).

The spacecraft mass ratio shown in Figure 19 is the spacecraft structure mass divided by the structure mass in baseline [i.e., equation 11]. Because the spacecraft structure mass influences the propellant cost directly, with the increase of spacecraft structure mass, the total IMLEO increases significantly. When the spacecraft structure mass is low, there is a tradeoff between enlarging the spacecraft for ISRU deployment and using small spacecraft without ISRU. When the spacecraft is more than 20% heavier than

normal, it is not worth building a large spacecraft for ISRU deployment. As a result, the structure mass of small spacecraft starts to increase and the division of roles between two types of spacecraft becomes less clear. Both types of spacecraft start to deliver crews, equipment and samples. Note that we can still observe that the structure mass of spacecraft 1 matches the variation pattern of ISRU plant mass if ISRU is deployed in the mission, even though the structure mass is also increasing at the same time.

3.3 Chapter Summary

This chapter proposes two optimization methods to solve the space logistics problem considering nonlinear spacecraft and nonlinear ISRU models. First, the MILP optimization framework is developed based on the GMCNF model. Piecewise functions are used to approximate the nonlinear spacecraft and ISRU models as well as to convert the models into binary mixed-integer programming formulations. After linearizing the remaining quadratic terms, the whole problem is converted into a MILP problem. This MILP-based optimization framework can always find the global optimum of the problem with approximated nonlinear models. The second method is the SA-based optimization framework, which is developed with the concern that a higher-fidelity spacecraft model may be considered. In this method, the spacecraft model is separated from the mission planning part. This SA-based optimization framework can never guarantee or certify its global optimality.

To illustrate the effect of both optimization methods, a campaign-level mission including three lunar missions is optimized.

For the MILP method, the influences of mission interval are studied. The IMLEO of the space logistics system first decreases with the increase of mission interval until ISRU production cannot provide further benefits to the space logistics system. Moreover, even though the spacecraft are all designed as multiuse without specific functions identified

initially, they are all assigned specific functions in the result. The large spacecraft are typically used to deliver equipment and ISRU plants, whereas the small ones are used to deliver crews and samples. Thus, the size of the large spacecraft is directly influenced by the mass of ISRU plant deployed in the mission (see Figure 16, Figure 18, and Figure 19).

The influences of ISRU and spacecraft model fidelities are also studied, as shown in Table 10. A linear ISRU or spacecraft model would not improve the computational efficiency because the nonlinear models can be linearized into binary mixed-integer programming formulations and most of the variables and constraints come from the mission planning part, which is a GMCNF model. Therefore, the MILP method developed in this chapter solves the space logistics problem, including nonlinear ISRU and spacecraft models without much deterioration of computational efficiency.

Besides the MILP method, a heuristic optimization algorithm based on SA is also proposed. Compared with the MILP method, the SA method cannot guarantee an optimal solution and the quality of the results is strongly dependent on the initial settings. For the problem considering a medium-fidelity spacecraft model, the MILP method is always a better choice. However, the separated spacecraft model in the SA optimization framework makes it easier to consider a higher-fidelity spacecraft model, such as considering fuel types and specifically predefined functions of each type of spacecraft.

The ISRU productivity and spacecraft structure mass sensitivity are also studied. The IMLEO decreases monotonously with the increase of ISRU productivity. The spacecraft structure mass is also an important factor in determining the space logistics strategy. With the increase of spacecraft structure mass, the IMLEO of the system increases significantly. When the spacecraft structure mass is too large, as compared with the normal condition, it is too expensive to build a large spacecraft for ISRU deployment and the specified functions of different types of spacecraft also become less clear.

CHAPTER 4. REGULAR INTERPLANETARY MISSION

This chapter proposes a periodic time-expanded network (TEN) to conduct space transportation system design and mission planning for regular interplanetary missions. The proposed periodic TEN resolves the computational scalability issue in the time dimension for the framework proposed in Chapter 3 for long-term human space exploration. The generated mission planning results are also shown to be practically preferred. Properties of the proposed partially periodic time-expanded network are analyzed, and a case study reveals that the total initial mass in the low Earth orbit of regular missions approaches the theoretical lower bound as the number of transportation missions increases.

The rest of this chapter is organized as follows: Sec. 4.1 introduces the partially periodic GMCNF model and its properties. Section 4.2 evaluates the performance of the partially periodic GMCNF using a long-term Earth-Mars transportation mission case study and compares it with the static and the fully time-expanded GMCNF models. Section 4.3 discusses the contribution and the conclusion of this chapter.

4.1 Methodology

4.1.1 *Generalized Multicommodity Network Flow*

As introduced in Chapter 3, the GMCNF model enables the consideration of the interdependency among space missions in a long-term space exploration campaign [1]. The GMCNF model was first proposed leveraging a static network, which considered spacecraft design and space infrastructure design linearly. Following exactly the same definition of notations as Chapter 3, but removing the time dimension, we can write the static GMCNF formulation as follows.

Minimize:

$$\mathcal{J} = \sum_{(v,i,j) \in \mathcal{A}} (\mathbf{c}_{vij}^{+T} \mathbf{x}_{vij}^+ + c'_{vij} s_v y_{vij}^+) \quad (31)$$

Subject to:

$$\sum_{(v,j):(v,i,j) \in \mathcal{A}} \mathbf{x}_{vij}^+ - \sum_{(v,j):(v,j,i) \in \mathcal{A}} \mathbf{x}_{vji}^- \leq \mathbf{d}_i \quad \forall i \in \mathcal{N} \quad (32)$$

$$\sum_{j:(v,i,j) \in \mathcal{A}} y_{vij}^+ - \sum_{j:(v,j,i) \in \mathcal{A}} y_{vji}^- \leq d'_{iv} \quad \forall i \in \mathcal{N} \quad \forall v \in \mathcal{V} \quad (33)$$

$$Q_{vij} \begin{bmatrix} \mathbf{x}_{vij}^+ \\ s_v y_{vij}^+ \end{bmatrix} = \begin{bmatrix} \mathbf{x}_{vij}^- \\ s_v y_{vij}^- \end{bmatrix} \quad \forall (v, i, j) \in \mathcal{A} \quad (34)$$

$$H_{vij} \mathbf{x}_{vij}^+ \leq \mathbf{e}_v y_{vij}^+ \quad \forall (v, i, j) \in \mathcal{A} \quad (35)$$

$$s_v = \mathcal{F}(\mathbf{e}_v, f_v) \quad \forall v \in \mathcal{V} \quad (36)$$

$$\mathbf{x}_{vij}^\pm = \begin{bmatrix} x_1 \\ x_2 \\ \vdots \\ x_p \end{bmatrix}_{vij}^\pm \quad \text{where } x_1 \in \mathbb{Z}_{\geq 0}, \quad x_2, \dots, x_p \in \mathbb{R}_{\geq 0} \quad \forall (v, i, j) \in \mathcal{A}$$

$$y_{vij}^\pm \in \mathbb{Z}_{\geq 0} \quad \forall (v, i, j) \in \mathcal{A}$$

$$s_v \in \mathbb{R}_{\geq 0}, \quad \mathbf{e}_v \in \mathbb{R}_{\geq 0}^l, \quad f_v \in \mathbb{Z}_{\geq 0} \quad \forall v \in \mathcal{V}$$

The static GMCNF model does not consider the time dimension in the problem, which may lead to the ‘‘time paradox’’. For instance, the propellant from an ISRU plant may be used before it is generated [2]. To solve this issue, Ho et al. and Chen et al. proposed a fully time-expanded network [2, 17] to include the time dimension in the static GMCNF model. Using the same notation as the static GMCNF model, a fully time-expanded version

of the static GMCNF model can be written as equations 1-7 as shown in Chapter 3. Compared with the static GMCNF, there is an additional time window constraint in the fully time-expanded GMCNF, which is equation 6. In equation 6, W_{ij} is the time window vector. The commodity flow is permitted only when the time window is open.

The fully time-expanded GMCNF notably improves the space logistics optimization fidelity compared with the static GMCNF model. However, it takes a significantly longer time to solve the problem as compared to the static GMCNF because of the additional time dimension. Numerical experiments in Chapter 3 showed that it takes about 2000 seconds to solve an optimization problem for a campaign-level lunar mission design, containing three Apollo-like short lunar missions, by the Gurobi 6.5 solver on an Intel Core i7-4790 quadcore @3.6 GHz platform. When four lunar missions were considered, it took more than 200 hours to solve the problem. This was the time cost to optimize the mission planning when only considering the transportation missions within the cislunar system. If the subject of interest was the Mars mission, the mission complexity and the time scale would increase much more significantly.

To solve a long-term space transportation mission planning problem efficiently while maintaining the model fidelity, this chapter takes advantage of the regular space transportation concept and develops a partially periodic TEN, which is introduced in detail in the next section.

4.1.2 Partially Periodic TEN

As shown in Figure 20, the proposed logistics network consists of two general phases: an initial setup phase and a periodic steady phase. The initial setup phase of the campaign is a one-time event that is dedicated to the construction and deployment of the in-space infrastructure that will be later used and maintained during the periodic missions. For instance, ISRU systems can provide resources to reduce mission cost and make

transportation sustainable. Propellant depots are in-orbit infrastructure systems that can refuel spacecraft passing by.

After a sufficiently long setup phase, the system enters a periodic steady phase in which the system repeats the same transportation missions regularly. Here, we make the repeating period longer than the longest transportation arc in the network. For example, for Earth-Mars missions, we can consider the repeating period as the launch window cycle to Mars (i.e., ~ 780 days), which is longer than the longest transportation arc in the network (i.e., from Earth to Mars ~ 210 days). Note that this assumption on the length of the repeating period can be relaxed easily if necessary. With this repeating period, we can simplify the TEN into a partially periodic TEN, which only includes the setup phase and one periodic cycle. The idea is to aggregate all the repeating periods into one periodic cycle and constrain the inflow and the outflow of that cycle to be equal to each other. In this way, the mission planning solution for the first regular cycle becomes identical to all the following cycles. As a result, after implementing the partially periodic TEN, we only need to solve the mission planning problem for the setup phase and the first regular cycle. The result obtained is then feasible for all future cycles.

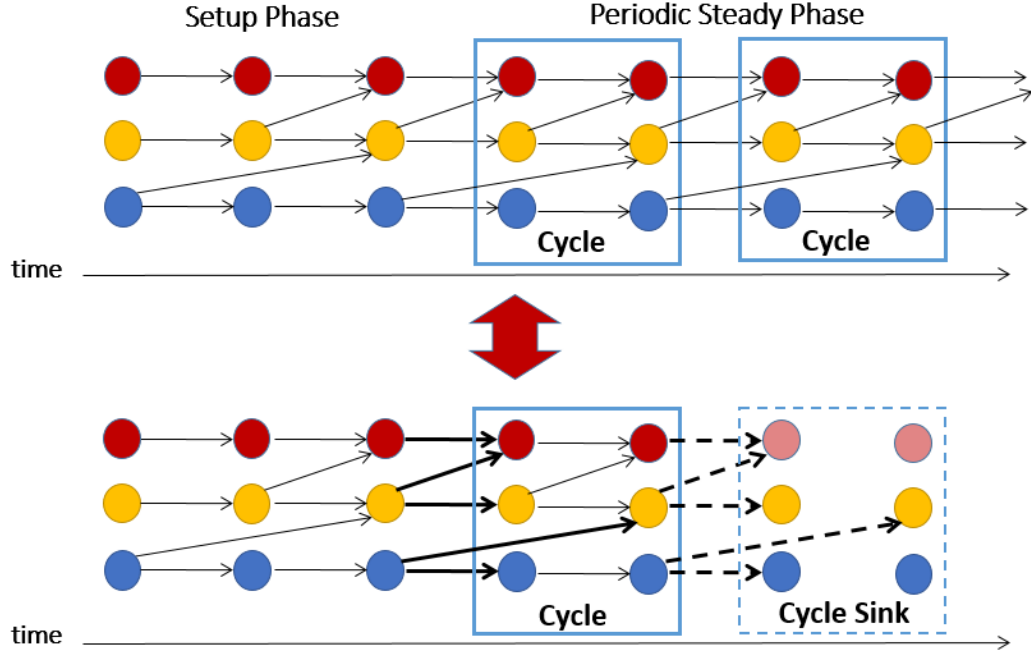


Figure 20 - Partially periodic TEN.

Assume that the objective function of the setup phase is G_s , whereas the objective function of the periodic steady phase is G_r . The total number of regular cycles considered in the optimization is K . The mathematical formulation of this partially periodic GMCNF model is shown as follows:

Minimize:

$$J_r = G_s + K G_r \quad (37)$$

Subject to:

$$G_s = \sum_{t \in \{0 \dots t_0 - 1\}} \sum_{(v,l,j) \in \mathcal{A}} (c_{vij}^+ x_{vijt}^+ + c'_{vij} y_{vijt}^+) \quad (38)$$

$$G_r = \sum_{t \in \{t_0 \dots t_0 + t_p - 1\}} \sum_{(v,i,j) \in \mathcal{A}} (c_{vij}^{+T} x_{vijt}^+ + c_{vij}^{+S} y_{vijt}^+) \quad (39)$$

$$x_{vijt}^\pm = x_{vij(t+t_p)}^\pm \quad \forall t: t < t_0 \text{ and } t + \Delta t_{ij} \geq t_0 \quad (v, i, j) \in \mathcal{A} \quad (40)$$

$$y_{vijt}^\pm = y_{vij(t+t_p)}^\pm \quad \forall t: t < t_0 \text{ and } t + \Delta t_{ij} \geq t_0 \quad (v, i, j) \in \mathcal{A} \quad (41)$$

$$G_s, G_r \in \mathbb{R}_{\geq 0}$$

and

Equations 2-7

where t_0 is the time when the first regular cycle begins and t_p is the length of a regular cycle. Equation 37 is the objective function. It is the sum of the IMLEO of the setup phase and the regular transportation phase, which are calculated in Equations 38 and 39, respectively.

Equations 40 and 41 are periodic flow constraints that constrain all the inflows to a regular cycle are equal to the outflows, thus guaranteeing the repeating nature of the regular cycles. As shown in Figure 20, outflows and inflows are those commodity flows crossing the boundaries of regular cycles. A direct way to constrain cycling is by adding terminal constraints into the TEN:

$$x_{vijt}^\pm = x_{vij(t+t_p)}^\pm \quad \forall t: t < t_0 + (k-1)t_p \text{ and } t + \Delta t_{ij} \geq t_0 + (k-1)t_p \quad (v, i, j) \in \mathcal{A} \quad \forall k \in \{1, 2, 3, \dots, K\} \quad (42)$$

$$\mathbf{y}_{vijt}^{\pm} = \mathbf{y}_{vij(t+t_p)}^{\pm} \quad \forall t: t < t_0 + (k-1)t_p \text{ and } t + \Delta t_{ij} \geq t_0 + (k-1)t_p \quad (v, i, j) \quad (43)$$

$$\in \mathcal{A} \quad \forall k \in \{1, 2, 3, \dots, K\}$$

where k is the index of cycles. If we add equations 42 and 43 into the time-expanded GMCNF problem, we solve the problem shown in the upper half of Figure 20. Equations 42 and 43 are terminal constraints that force the system to repeat the same cycle. We can remove the redundant variables and constraints by solving the problem shown in the lower half of Figure 20 using equations 40 and 41. With equations 40 and 41, we are solving the partially periodic GMCNF problem for the setup phase and the first regular cycle, as the commodity flow results in the first cycle are applicable for all subsequent regular cycles.

Other commodity constraints [i.e., equations 2-7] are the same as the general fully time-expanded GMCNF model.

4.1.3 *Properties of Partially Periodic TEN*

4.1.3.1 Computational complexity

In this section, we discuss the computational complexity of the GMCNF models, which were formulated based on different types of TENs.

Assuming that in a fully time-expanded network model, there are m different types of spacecraft, n nodes, p commodity types, l types of spacecraft concurrency constraints, and T time steps, then the number of nodes and arcs over the fully time-expanded GMCNF model are, at most, nT and mn^2T , respectively. As a result, there are at most $O(mn^2pT)$ variables and, at most, $O(mn^2(p+l)T)$ constraints. If we consider regular space missions, assuming a setup phase over t_0 time steps followed by K transportation mission cycles each of which lasts over t_p time steps, $T = t_0 + Kt_p$; then, for a fully time-expanded

network model, there are, at most, $O(mn^2p(t_0 + Kt_p))$ variables and, at most, $O(mn^2(p + l)(t_0 + Kt_p))$ constraints. Following the same logic and notations, we can get the computational complexity of the static network and the partially periodic network, as shown in Table 11.

Table 11 - Computational complexity comparison.

TEN Type	Variables	Constrains
Static	$O(mn^2p)$	$O(mn^2(p + l))$
Fully time-expanded	$O(mn^2p(t_0 + Kt_p))$	$O(mn^2(p + l)(t_0 + Kt_p))$
Partially periodic	$O(mn^2p(t_0 + t_p))$	$O(mn^2(p + l)(t_0 + t_p))$

Compared with the static network, a caveat of the fully time-expanded network is that it requires a large number of nodes and arcs, generated by the time dimension, which will lead to a large number of variables and constraints. The complexity of the TEN is pseudo-polynomial. For the partially periodic network model proposed in this chapter, as shown in equations 37-41 and 2-7, the computational complexity is much smaller than the fully time-expanded network. With the increase of the number of cycles (i.e., K), the number of variables and constraints in the fully time-expanded network increases linearly (with an offset due to the setup phase). However, the number of variables and constraints in the partially periodic network stays the same as the increase in the number of cycles. Therefore, for large-scale space transportation mission planning optimization problems (e.g., Earth-Mars transportation mission), the partially periodic network has significantly less computational workload, thus greatly increasing the time dimension scalability.

4.1.3.2 Bounds on Optimal Solutions

In this section, we discuss the bounds of the partially periodic network model solution. For the specific minimization problem considered in this research, we discuss the

lower bound of the partially periodic network and the relationship among static, fully time-expanded, and partially periodic network models.

Consider the fully time-expanded GMCNF problem discussed earlier in Chapter 3 [shown in equations 1-7]. The following arguments show that it can be relaxed to a static GMCNF problem by aggregating nodes and arcs.

Because the cost coefficient c_{vij}^+ and c_{vji}^+ are constant over time, equation 1 can be written as

$$\mathcal{J} = \sum_{(v,i,j) \in \mathcal{A}} (c_{vij}^+ \mathbf{X}_{vij}^+ + c_{vji}^+ s_v Y_{vij}^+) \quad (44)$$

where $\mathbf{X}_{vij}^+ = \sum_{t \in \mathcal{T}} \mathbf{x}_{vijt}^+$ and $Y_{vij}^+ = \sum_{t \in \mathcal{T}} y_{vijt}^+$. They are the total commodity flows throughout the time horizon along each arc.

Equations 2 and 3 can be aggregated over the time horizon and be relaxed to the following form:

$$\sum_{(v,j):(v,i,j) \in \mathcal{A}} \mathbf{X}_{vij}^+ - \sum_{(v,j):(v,j,i) \in \mathcal{A}} \mathbf{X}_{vji}^- \leq \mathbf{D}_i \quad \forall i \in \mathcal{N} \quad (45)$$

$$\sum_{j:(v,i,j) \in \mathcal{A}} Y_{vij}^+ - \sum_{j:(v,j,i) \in \mathcal{A}} Y_{vji}^- \leq D'_{iv} \quad \forall i \in \mathcal{N} \quad \forall v \in \mathcal{V} \quad (46)$$

where $\mathbf{D}_i = \sum_{t \in \mathcal{T}} \mathbf{d}_{it}$ and $D'_{iv} = \sum_{t \in \mathcal{T}} d'_{ivt}$. They are the total commodity demand or supply throughout the time horizon at each node.

Similarly, equations 4 and 5 can be relaxed as follows:

$$Q_{vij} \begin{bmatrix} \mathbf{X}_{vij}^+ \\ S_v Y_{vij}^+ \end{bmatrix} = \begin{bmatrix} \mathbf{X}_{vij}^- \\ S_v Y_{vij}^- \end{bmatrix} \quad \forall (v, i, j) \in \mathcal{A} \quad (47)$$

$$H_{vij} \mathbf{X}_{vij}^+ \leq \mathbf{e}_v Y_{vij}^+ \quad \forall (v, i, j) \in \mathcal{A} \quad (48)$$

The time window constraint [equation 6] is relaxed and eliminated through the aggregation of commodity flows throughout the time horizon, thus eliminating the information about time windows.

The resulting formulation [equation 44] with constraints in equations 45-48 and the spacecraft design model [equation 7] leads to a static GMCNF problem as a lower (relaxed) bound of the fully time-expanded GMCNF problem if both formulations are feasible and bounded. This static formulation and the original fully time-expanded GMCNF formulation are defined as the *corresponding* formulations of each other.

From the above derivation, the following important theorem has been proved.

Theorem 1. *A lower bound of the optimal objective of a fully time-expanded GMCNF problem can be found by solving its corresponding aggregated static GMCNF problem if both problems are feasible and bounded.*

A more detailed proof and a generalization of Theorem 1 have been derived by Ho in Ref. [53].

From this theorem, it can be seen that a lower bound of a computationally expensive fully time-expanded GMCNF problem can be found by a computationally cheaper aggregated GMCNF problem if both are feasible and bounded. In other words, $\mathcal{J}_s \leq \mathcal{J}_f$, where \mathcal{J}_s is the optimal solution of a static GMCNF problem and \mathcal{J}_f is the optimal solution

of its corresponding fully time-expanded GMCNF problem, as shown in equations 31 and 1, respectively.

Now, consider a partially periodic GMCNF problem [shown in equations 37-41 and 2-7]. The following arguments show that it can be relaxed to a fully time-expanded GMCNF problem.

First, consider the time-expanded GMCNF formulation with terminal constraints [equations 42 and 43]. It is a cycling time-expanded GMCNF problem shown in the upper half of Figure 20. We can obtain its formulation by adding terminal constraints [i.e., equations 42 and 43] into the fully time-expanded GMCNF problem. Additional terminal constraints reduce the solution space of the optimization problem. Therefore, the fully time-expanded GMCNF problem provides a lower (relaxed) bound of the cycling time-expanded GMCNF problem if both formulations are feasible and bounded.

Moreover, the cycling time-expanded GMCNF problem shown in the upper half of Figure 20 is an equivalent problem to the lower half by replacing the terminal constraints of equations 42 and 43 by equations 40 and 41 and removing the redundant variables and constraints. As a result, the fully time-expanded GMCNF problem is also a lower (relaxed) bound of the partially periodic GMCNF problem [shown in equations 37-41 and 2-7] if both formulations are feasible and bounded. Moreover, the partially periodic GMCNF problems are not necessarily feasible even when the fully time-expanded GMCNF problems are feasible. This partially periodic formulation and the original fully time-expanded GMCNF formulation are defined as the *corresponding* formulations of each other.

From the above derivation, the following theorem has been proved.

Theorem 2. *A lower bound of the optimal objective of a partially periodic GMCNF problem can be found by solving its corresponding relaxed fully time-expanded GMCNF problem if both problems are feasible and bounded.*

In summary, for the optimal solutions of the corresponding static, fully time-expanded, and partially periodic GMCNF problems, expressed by J_s , J_f , and J_r , there is a relationship: $J_s \leq J_f \leq J_r$, if all of them are feasible and bounded.

4.2 Case Study Results and Analysis

This section evaluates the performance of the partially periodic network by solving a long-term Mars space transportation mission planning problem. The results of the partially periodic network are compared with the results from the static and fully time-expanded networks.

4.2.1 Mars Transportation Mission

Our case study considered in this chapter is a Mars exploration with the cislunar transportation system. We model the transportation network as a seven-node network. The ΔV and the time of flight (TOF) are shown in Figure 21. Because the IMLEO is the cost metric used in this research, ΔV and TOF between Earth and low Earth orbit LEO are not considered. Space mission time windows, spacecraft flight ΔV and the TOF are determined by interplanetary transportation trajectories. In this chapter, we use Hohmann transfer orbits as the transportation trajectories and the high-thrust liquid oxygen/ liquid hydrogen (LO₂/LH₂) propulsion system in spacecraft for Mars transportation. The boiloff of liquid oxygen and liquid hydrogen in space is also considered. As shown in Figure 21, the spacecraft flight can take advantage of aerocapture to reduce the propellant cost. The aeroshell and thermal protection system (TPS) can be reused in space. However, after the spacecraft reentry to Earth or Mars, the aeroshell and the TPS cannot be reused again; new

aeroshell/TPS needs to be launched. The mass of aeroshell/TPS is assumed as 40% of the total flight mass according to NASA Design Reference Architecture 5.0 [65].

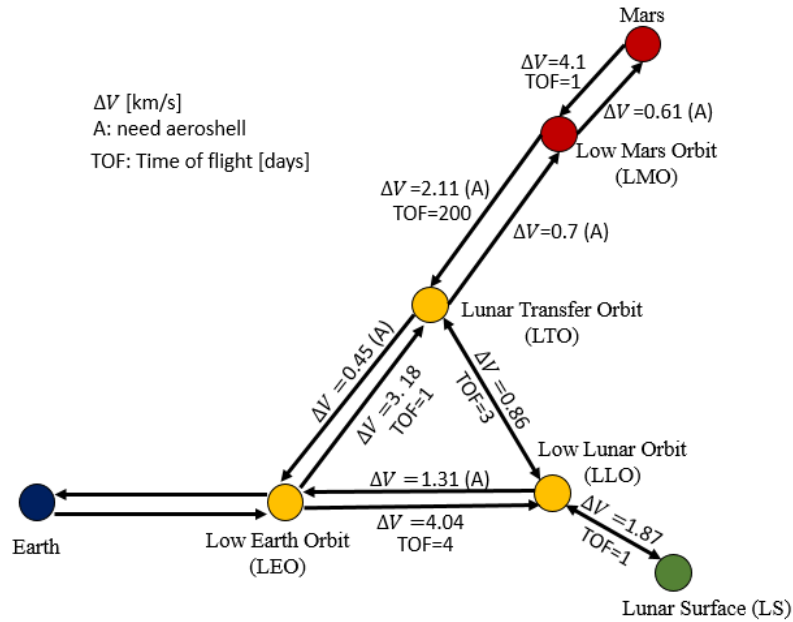


Figure 21 - Earth-moon-Mars transportation network model.

The scenario considers a set of regular missions that transport cargo from Earth to Mars every 780 days when the Earth-Mars system opens its repeating time windows. We consider the first Earth-Mars time window as the setup phase and each of the subsequent time windows as a regular repeating cycle. The mission demand and supply are shown in Table 12.

Table 12 - Demand and supply of Mars transportation mission.

Payload Type	Node	Demand Time, day	Supply, kg
Payload	Mars	780 (repeating every 780 days)	-51,700
Payload, propellant, ISRU, ISRU maintenance spares	Earth	All the time	+∞

The considered ISRU system is a lunar water ISRU for which the productivity is assumed as 5 kg propellant/ year/ kg system. The ISRU plant is supplied from Earth. To use the ISRU system, the transportation system must deploy ISRU plant first on the Moon or Mars. If some ISRU systems are in operation for the mission, the transportation system also needs to supply its maintenance spares. We assume that ISRU maintenance requires the spares equal to 10% of the system total mass every transportation mission (i.e., every 780 days). We also assume that two types of spacecraft propulsive stages are designed and two spacecraft propulsive stages are available to be launched on Earth for each mission. Spacecraft sizing is also part of the trade space and is shown in detail in Sec. 4.2.2. A summary of mission parameters and assumptions is shown in Table 13.

Table 13 - Summary of parameters and assumptions.

Parameter	Assumed value
Propellant	LO2/LH2 [52]
I_{sp}	420 s [52]
Type of spacecraft designed	2 types
Available spacecraft each mission	2 spacecraft each type
Aeroshell	40% of total mass [65]
Oxygen boil-off rate	0.016%/day [2, 17]
Hydrogen boil-off rate	0.127%/day [2]
Earth-Mars time window	780 days [65]
ISRU productivity	5 kg propellant/year/kg system [65]
ISRU maintenance	10%/mission [2, 17]

Moreover, to evaluate the effectiveness of a partially periodic GMCNF model, we need to set a baseline TEN formulation for comparison. A naive fully time-expanded network with uniform time steps (e.g., one day) would be computationally expensive to analyze. In this chapter, we use a cluster-based TEN as the baseline [2]. For the interplanetary exploration mission, the system can be divided into several clusters (e.g., Earth/cislunar cluster and Martian system), in which only the transportation across the

boundary of the clusters involves periodic time windows and long flights. In a cluster-based TEN, we only consider the time window of the space flights between two clusters and assume the short space flights inside each cluster as instantaneous transits. This method is known to give a good approximation of the optimal solution of the naive formulation with a reasonable computational effort [2]. In later analysis cases, both the fully time-expanded GMCNF and the partially periodic GMCNF model are formulated based on this cluster-based TEN formulation, although our theory developed in Sec. 4.1 applies to any other TEN formulation as well.

4.2.2 *Spacecraft design model*

Our space logistics optimization includes spacecraft sizing as part of the trade space. For the sizing model of spacecraft, this chapter uses a nonlinear regression model developed by Taylor [52] based on preexisting spacecraft elements, which is also introduced in Chapter 3 [i.e., equation 11]. Although the original model includes the structure for payload, we do not consider that as a part of the spacecraft design model in this case study. The payload is enclosed in the aeroshell, which is considered separately. We are only designing the propulsive stage using this spacecraft design model. Therefore, in the mission assumptions (shown in Table 13), designing two types of spacecraft means designing two different sizes of propulsive stages. In addition, due to the MILP nature of the proposed optimization method, there is an underlying assumption for the spacecraft flowing across the network: the spacecraft capacities can be additively combined and the propulsive stages designed are modular and reconfigurable. In reality, the interoperability between spacecraft can be significantly more complex.

Denoting the spacecraft propellant capacity as M , spacecraft fuel type as f , and structure mass as s , the spacecraft propulsive stage structure mass is a function of

propellant capacity and spacecraft fuel type [$s = \mathcal{F}(M, f)$], which is shown as follows [52]:

$$s = \alpha(f) * M * \left(1 - \frac{0.2 * M}{M_{UB}}\right) + \frac{0.4189 \left(\frac{M * I_{sp}(f) * g_0}{t_b}\right)^{0.7764}}{g_0} \quad (49)$$

where g_0 is the standard gravitational acceleration on Earth, 9.8 m/s²; t_b is spacecraft impulsive burn time, set as 120 s; M_{UB} is the upper bound of spacecraft propellant capacity, assumed as 500,000 kg, as in Chapter 3, which defines the scope of application of this data-based spacecraft design model; I_{sp} is the specific impulse determined by fuel type f ; α is the spacecraft structural fraction defined in Ref. [52], which is also determined by fuel type f . In this case study, LO2/LH2 is chosen as the spacecraft propellant as an example. As a result, according to Appendix A, I_{sp} is 420 s and α is equal to 0.079.

Although this spacecraft model is nonlinear, We employ the piecewise-linear approximation and big- \mathcal{M} method proposed in Chapter 3 to convert the space mission design problem with the nonlinear spacecraft model into a MILP for efficient mission design optimization.

Note that, this thesis uses the aforementioned nonlinear spacecraft stage design model as an example to illustrate the ability of the proposed space logistics optimization method; our method can accommodate other spacecraft design models if necessary. The focus of this chapter is on the TEN method, and we do not claim the accuracy of the spacecraft design model used.

4.2.3 Comparison of Optimization Formulations

This problem is solved in Python by the Gurobi 7.0 solver on an Intel Core i7-4790, quadcore @3.6 GHz platform. The results of the average IMLEO for each regular space transportation mission (i.e., cycle) based on different network models are shown in Figure 22, and their computational times are shown in Figure 23. The result from the partially periodic GMCNF model is compared with the results from the static and fully time-expanded GMCNF models. The number of missions in Figure 22 and Figure 23 corresponds to the number of regular cycles after the setup phase because each cycle only contains one mission. Note that we only obtain the results for the fully time-expanded GMCNF model when the number of space missions is less than four because the optimization becomes computationally infeasible with our computational resource when the number of missions is large.

The results obtained from static, fully time-expanded, and partially periodic GMCNF models are compared in Figure 22. As the number of regular space transportation missions (i.e., cycles) increases, the average mission IMLEO from both fully time-expanded and partially periodic GMCNF models are approaching to the result from static GMCNF (i.e., lower bound). The result from the fully time-expanded GMCNF model is slightly closer to the static GMCNF model result as compared with the partially periodic GMCNF model. The reason is that the fully time-expanded GMCNF model does not have the periodic and terminal constraints, meaning that each period can have a different mission, whereas the partially periodic GMCNF model assumes that the mission repeats infinitely. This also matches with our analysis in Sec. 4.1 that proves that, for the optimal objective, $J_s \leq J_f \leq J_r$.

The comparison of computational time among three GMCNF models is shown in Figure 23. We can find that, as the number of missions increases, the computational time of the fully time-expanded GMCNF model increases dramatically while the computational times of the partially periodic and the static GMCNF models remain at a low level. This

figure demonstrates that our partially periodic GMCNF model can achieve a better time dimension scalability than the fully time-expanded GMCNF model.

In summary, we can see that the proposed partially periodic GMCNF model can provide a good approximation of the fully time-expanded GMCNF model with a much lower computational cost.

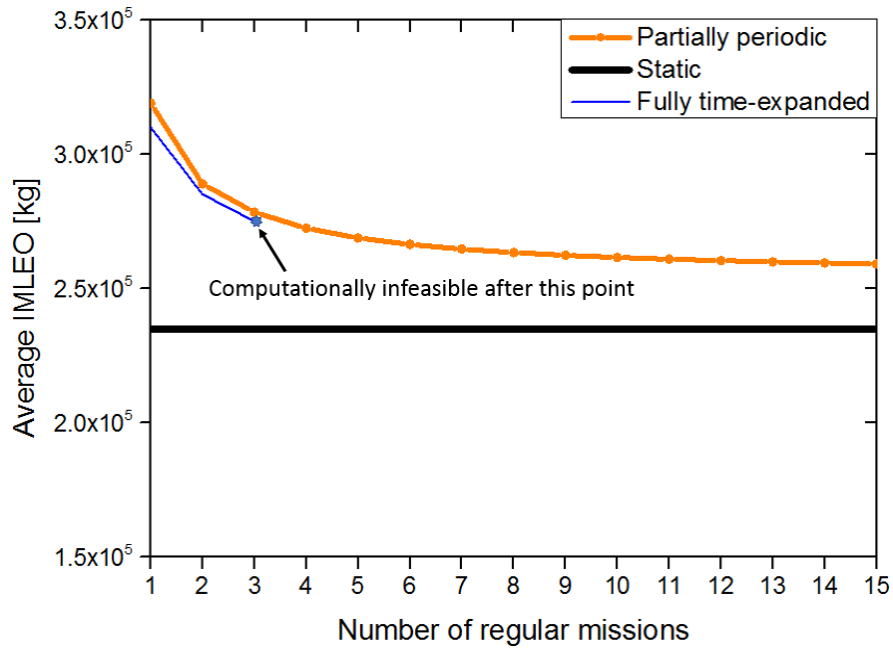


Figure 22 - Mission IMLEO comparison among GMCNF formulations.

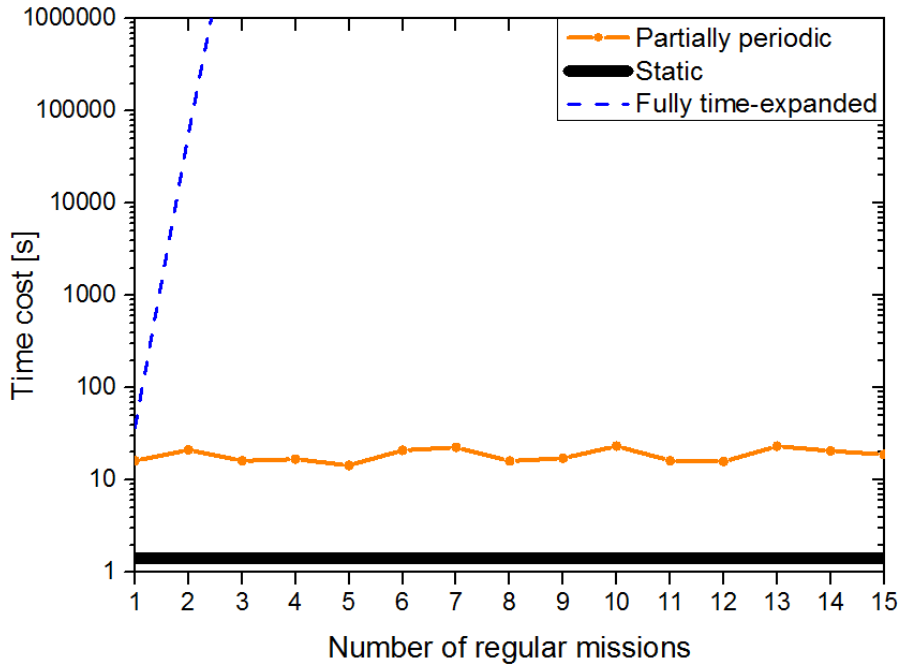


Figure 23 - Problem-solving time cost comparison among GMCNF formulations.

4.2.4 Analysis of Partially Periodic GMCNF Results

With our developed partially periodic TEN formulation, we can analyze the long-term space campaign with regular missions more computationally efficiently than traditional methods. This section analyzes the results from the partially periodic GMCNF model.

The mission planning result of ten regular transportation missions to Mars is shown in Figure 24. In the setup mission phase, the ISRU system is deployed on the Moon. It starts to produce propellant on the Moon to support subsequent space missions. When the second Earth-Mars flight time window is open, all spacecraft launched for the Mars mission fly to the lunar transfer orbit (LTO) first. Then, some spacecraft fly to the moon to transport propellant produced on the moon back to the LTO. The spacecraft used to deploy the ISRU system in the setup mission phase assists this propellant transportation. As a result, the propellant from Earth only needs to support the flights from the LTO to the low

lunar orbit (LLO) in the moon propellant transportation. Other spacecraft flights during this propellant transportation are covered by the propellant generated on the moon. After being refueled by the propellant from the moon, the spacecraft that stay in LTO temporarily during the propellant transportation fly to Mars. This regular space transportation mission is repeated, following the same mission planning and spacecraft design. This resulting solution can be preferred in practical missions to the global optimal solution with no repeating missions due to the simplicity of its repeating mission architecture. The learning curve effect, which is not considered in this chapter, can also be incorporated to further identify the potential benefits of repeating space missions.

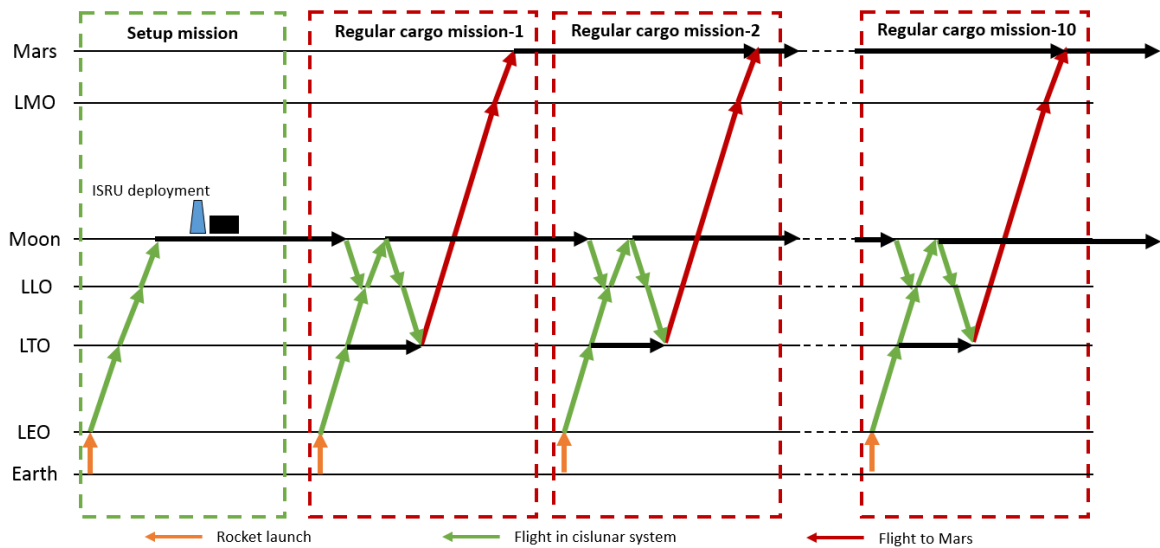


Figure 24 - Mars regular space transportation mission planning (10-mission case).

A sensitivity analysis of the campaign performance against ISRU productivity is shown in Figure 25, which shows the relationship between average mission IMLEO and ISRU productivities for different numbers of missions. It demonstrates that a higher ISRU productivity can always lead to a lower mission cost. Moreover, the performance of low-productivity ISRU is more sensitive to the total number of space missions. In Figure 25, when ISRU productivity is 2 kg/yr/kg system, the average mission IMLEO decreases more than 25% as the total number of transportation missions considered increases from 1 to 15.

However, the average mission IMLEO only decreases by about 14% when the ISRU productivity is high (i.e., 8 kg/yr/kg system). This result shows that the impact of a large number of missions is especially critical when the ISRU productivity is low. This type of analysis is not possible under the previous fully time-expanded network formulation for a long-term space campaign due to the scalability issue but is possible with our newly developed partially periodic TEN method.

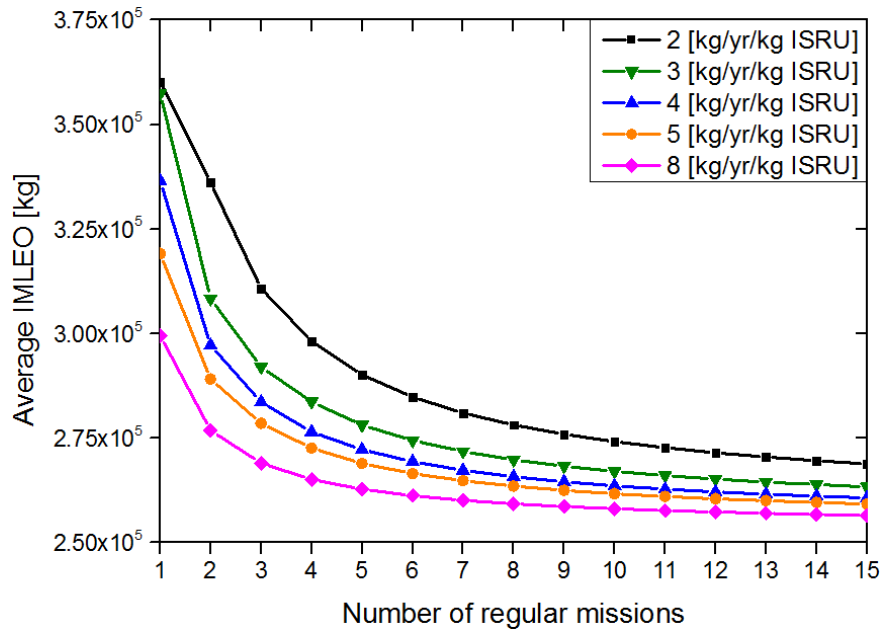


Figure 25 - Relationship between average mission IMLEO and ISRU productivities.

4.3 Chapter Summary

This chapter proposes a computationally efficient interplanetary space transportation mission planning optimization framework by constructing a partially periodic time-expanded network. It takes advantage of the periodic nature of regular space transportation missions, thus resulting in a practical and computationally efficient mission planning method.

The analysis and result comparisons with the traditional static and fully time-expanded GMCNF models show that the partially periodic GMCNF model could solve a long-term interplanetary mission planning problem significantly faster than the previous mission planning frameworks while maintaining a reasonable level of fidelity. This chapter also derives the mathematical properties of the proposed partially static GMCNF formulation and its relationship with the traditional static and fully time-expanded GMCNF formulation.

The proposed work can be useful for future large-scale space transportation campaign design, which contains multiple interplanetary transportation missions. Moreover, the framework improves the mission planning computational efficiency and enables a quick sensitivity analysis on space infrastructures and spacecraft in interplanetary transportation missions. The proposed methodology can be further explored to consider the mixed cargo/human missions to Mars with consideration of life support systems.

CHAPTER 5. INFRASTRUCTURE DESIGN AND RESOURCE LOGISTICS

The goal of this chapter is to develop an effective interdisciplinary space infrastructure optimization framework and its optimization methods, leveraging network-based space logistics modeling. First, a full-size space infrastructure optimization formulation is established to consider all infrastructure subsystems separately throughout the space campaign. Because the full-size version of this proposed problem formulation can be computationally prohibitive, a new multi-fidelity optimization formulation is developed by varying the granularity of the commodity-type definition over the space logistics network; this multi-fidelity formulation can find an approximate solution to the full-size problem computationally efficiently with little sacrifice in the solution quality. The proposed problem formulation and method are applied to the design of in situ resource utilization systems in a multi-mission lunar exploration campaign to demonstrate their values.

The remainder of this chapter is organized as follows. Section 5.1 first introduces the prefixed optimization formulation for space infrastructure design (including the methods proposed in Chapters 3 and 4), where space infrastructure is considered as a black box. Then, Sec. 5.2 discusses the full-size version of the proposed space infrastructure optimization problem formulation, taking into account space infrastructure subsystems tradeoffs together with space mission planning concurrently. In Sec. 5.3, we propose a multi-fidelity optimization formulation and its methods to resolve the computational challenge inherent in the full-size formulation. Section 5.4 demonstrates the proposed optimization formulations through a multi-mission human lunar exploration campaign case study. Finally, Sec. 5.5 summarizes the conclusion of this chapter and discusses future work.

5.1 Prefixed Space Infrastructure Optimization Formulation

The network-based space logistics optimization formulation considers space missions as commodity network flow problems as discussed in Chapters 3 and 4, where nodes represent planets or orbits and arcs represent trajectories. Vehicles, payloads, infrastructure, and crewmembers are all considered as commodities. The inputs of this infrastructure optimization formulation are space mission demands and corresponding available infrastructure systems to be implemented (i.e., mainly representing ISRU systems and their supporting structures in this research). Based on the mission demands and time window constraints, this formulation outputs selected infrastructure systems to be deployed, including system sizing, plant deployment strategy, system operating mechanisms, and further resource logistics processes if mission demands occur at a location different from the infrastructure deployment spot.

In this space infrastructure optimization problem, space logistics mission planning is the main goal for optimization. Space logistics optimization includes space transportation scheduling and space infrastructure deployment strategy optimization. The space infrastructure subsystem interactions are determined in advance before space logistics optimization. The optimizer of this formulation only finds the optimal total mass of the space infrastructure, where the mass ratios between subsystems are fixed.

Let's consider a simplified version of the space logistics optimization framework introduced in Chapter 3 (i.e., equations 1-7) without spacecraft design. We mainly focus on the space infrastructure design in this chapter. As a result, we do not need to define the commodity outflow and inflow independently in the formulation. We only need a commodity outflow variable, defined as the vector \mathbf{x}_{vijt} . Note that this \mathbf{x}_{vijt} is the same as the commodity outflow variable, \mathbf{x}_{vijt}^+ , defined in Chapter 3. Each element of the commodity flow variable vector \mathbf{x}_{vijt} corresponds to one type of commodity, and it can be

either continuous or discrete (i.e., integer) depending on the corresponding commodity; the former commodity set (i.e., continuous commodity set) is defined as \mathcal{C}_c , and the latter commodity set (i.e., discrete commodity set) is defined as \mathcal{C}_d . For example, the number of spacecraft and crew members are integers while the mass of propellant and payload are continuous.

Then, similar to the space logistics optimization formulation as defined in Chapter 3 (i.e., equations 1-7), the formulation of the prefixed space infrastructure optimization formulation can be written as follows.

Minimize:

$$\mathcal{J} = \sum_{t \in \mathcal{T}} \sum_{(v,i,j) \in \mathcal{A}} \mathbf{c}_{vijt}^T \mathbf{x}_{vijt} \quad (50)$$

Subject to:

$$\sum_{(v,j):(v,i,j) \in \mathcal{A}} \mathbf{x}_{vijt} - \sum_{(v,j):(v,j,i) \in \mathcal{A}} Q_{vji} \mathbf{x}_{vji(t-\Delta t_{ji})} \leq \mathbf{d}_{it} \quad \forall i \in \mathcal{N} \quad \forall t \in \mathcal{T} \quad (51)$$

$$H_{vij} \mathbf{x}_{vijt} \leq \mathbf{0}_{l \times 1} \quad \forall (v, i, j) \in \mathcal{A} \quad \forall t \in \mathcal{T} \quad (52)$$

$$\begin{cases} \mathbf{x}_{vijt} \geq \mathbf{0}_{p \times 1} & \text{if } t \in W_{ij} \\ \mathbf{x}_{vijt} = \mathbf{0}_{p \times 1} & \text{otherwise} \end{cases} \quad \forall (v, i, j) \in \mathcal{A} \quad \forall t \in \mathcal{T} \quad (53)$$

$$\mathbf{x}_{vijt} = \begin{bmatrix} x_1 \\ x_2 \\ \vdots \\ x_p \end{bmatrix}_{vijt}, \quad \begin{cases} x_n \in \mathbb{R}_{\geq 0} & \forall n \in \mathcal{C}_c \\ x_n \in \mathbb{Z}_{\geq 0} & \forall n \in \mathcal{C}_d \end{cases} \quad \forall (v, i, j) \in \mathcal{A} \quad \forall t \in \mathcal{T}$$

For the detailed definition of each of the constraints, please refer to the explanation in Chapter 3.

One thing to note is that in this prefixed space infrastructure optimization formulation, space infrastructure systems, specifically focusing on the ISRU systems in this chapter, are considered as integrated systems that cannot be disassembled into different subsystems. We ignore the detailed interactions among ISRU subsystems. In this optimization, we only take into account its nominal productivity as a function of its total structure mass. We use lunar water ISRU as an example. The water ISRU will first extract water from lunar regolith and then electrolyze water to generate O_2 and H_2 . Define the commodity flow variables as

$$\mathbf{x}_{vijt} = \begin{bmatrix} x^{O_2}, \text{kg} \\ x^{H_2}, \text{kg} \\ x^{ISRU}, \text{kg} \end{bmatrix}_{vijt}$$

Then, we can express the ISRU production process for one hour for O_2 and H_2 as follows:

$$\begin{bmatrix} x^{O_2} \\ x^{H_2} \\ x^{ISRU} \end{bmatrix}_{vijt}^{inflow} = \begin{bmatrix} 1 & 0 & \sigma_{ISRU}^{O_2} \\ 0 & 1 & \sigma_{ISRU}^{H_2} \\ 0 & 0 & 1 \end{bmatrix}_{vij} \begin{bmatrix} x^{O_2} \\ x^{H_2} \\ x^{ISRU} \end{bmatrix}_{vijt} \quad (54)$$

In equation 54, there are three constraints. The first two constraints represent the ISRU production for O_2 and H_2 for one hour, where σ is the ISRU plant productivity, representing the amount of resource generation per hour per unit mass of the ISRU plant. The last constraint means the ISRU plant system mass does not change during the production process.

In this simplified formulation, the concurrency constraint also needs to guarantee the non-negativity of the commodity inflow. For the non-negativity of commodity inflow variables, we have,

$$\mathbf{x}_{vijt}^{inflow} \geq \mathbf{0}_{p \times 1}$$

which is equivalent to,

$$-Q_{vij}x_{vijt} \leq \mathbf{0}_{p \times 1}$$

In this constraint, the concurrency constraint matrix H_{vij} corresponds to the negative of the transformation constraint matrix, $-Q_{vij}$. It guarantees the feasibility of commodity transformations during spaceflights or surface system operations.

In this space infrastructure optimization formulation, the infrastructure subsystem designs are determined in advance. Space logistics optimization only identifies the optimal total size of the space infrastructure in space missions and cannot optimize the mass ratio between subsystems. It ignores the interaction between space infrastructure subsystems and space logistics transportation planning. This formulation is not able to perform sufficient trade studies for infrastructure technology selections and identify technology gaps.

5.2 Full-Size Space Infrastructure Optimization Formulation

To increase the space infrastructure design fidelity and take into account the detailed interactions between space infrastructure subsystems and space logistics transportation, this section introduces a newly developed full-size space infrastructure optimization formulation that considers all infrastructure subsystems separately throughout the space campaign. In this section, we first discuss the integrated ISRU system modeling in Sec. 5.2.1. Then, we discuss the implementation of different constraints to enable full-size infrastructure optimization in space logistics in Sec. 5.2.2.

5.2.1 ISRU system modeling

There are six subsystems considered in this ISRU infrastructure model. The first subsystem is reactors, which is the core of ISRU plants. They conduct chemical processes

to transform reactants into valuable products, such as water (H_2O), oxygen (O_2), hydrogen (H_2), and methane (CH_4). The sizing parameter of a reactor is the ISRU resource hourly productivity N , in the unit of kg/hr. The mass and power consumption sizing models of a reactor can be written as equations 55 and 56. Note that, there are some ISRU reactors that use rigid solar concentrators to provide thermal energy to the chemical reactions, such as the integrated carbothermic reduction system [28] developed by Orbitec Inc. and NASA. For those reactors that use a special power source, we consider the power architecture as part of the reactor in the sizing model and the reactor does not require external power input anymore.

$$M_{Re} = F_1(N) \quad (55)$$

$$P_{Re} = G_1(N) \quad (56)$$

To obtain raw materials as ISRU reactants, we need the second subsystem, excavator or acquisition systems, to collect soil/regolith for the soil-based ISRU system or CO_2 for the Martian atmosphere-based ISRU system. We introduce the excavation rate $m_{Soil/Gas}$, in the unit of kg/hr, as an intermediate variable to decouple the excavation schedule and the reactor operating time. It is a function of the ISRU resource productivity N , written as $m_{Soil/Gas} = f(N)$. Based on the excavation rate $m_{Soil/Gas}$, the sizing models for excavator/acquisition subsystems can be written as equations 57 and 58. The excavation complexity, difficulty, and site specificity vary depending on the target raw materials attributes. Using Mars exploration as an example, 95% of the Martian atmosphere is made up of CO_2 . It is everywhere on Mars. Therefore, the reactant excavation of atmosphere-based ISRU is not a constraint for mission landing site selection on Mars. For the Martian soil-based water ISRU system, landing site selection can directly impact the ISRU performance. Granular regolith is a type of garden variety soil, which contains 1-3% water

concentration. It is easy to excavate and is found in most places on Mars [66]. Gypsum/sulfate on Mars has a higher water concentration, 5-10%. However, it is a harder material that may require a rock excavator and crushing. Its locations are also limited to the equatorial region and mid-latitude area [66]. There is also subsurface ice on Mars, which requires drilling devices to collect it. The landing site for Martian icy regolith is highly selective. The design of excavator/acquisition subsystems is determined by the trade-off between the landing site and ISRU technology selections.

$$M_{Ex} = F_2(m_{Soil/Gas}) \quad (57)$$

$$P_{Ex} = G_2(m_{Soil/Gas}) \quad (58)$$

The third subsystem is separators that are used to separate products from the reactor exhaust gas. The performance and sizing of separators are directly relevant to reactor types, exhaust gas components, and operating environments. Therefore, the sizing parameter of a separator is the same as the reactor, which is the ISRU resource productivity N . The mass and power consumption sizing models of separators can be written as equations 59 and 60.

$$M_{Se} = F_3(N) \quad (59)$$

$$P_{Se} = G_3(N) \quad (60)$$

The fourth subsystem is a hopper/feed/secondary subsystem, which is a supporting structure for other ISRU subsystems. Therefore, its sizing is directly determined by other subsystem sizing results. To make the ISRU infrastructure design model consistent, we also use the ISRU resource productivity N as the sizing parameter. Its mass and power consumption sizing models can be written as equations 61 and 62.

$$M_{HF} = F_4(N) \quad (61)$$

$$P_{HF} = G_4(N) \quad (62)$$

After resources are produced, it requires storage subsystems to temporarily store the resources before they are consumed. The capacity of storage subsystems is determined by the maximum amount of produced resources to be stored during space missions. We can define the storage length variable L , in the unit of days, then the storage subsystem capacity should be equal to $Q_I LN$, where Q_I is the daily operating length (hr/day) and N is the ISRU hourly productivity (kg/hr). Note that, L is not the same as the total space mission duration. It is the time between two space resource logistics missions. Frequent logistics missions reduce the value of L , which decreases the capacity requirement on storage subsystems. However, frequent missions also increase the propellant consumption and operation complexity during spaceflights. On the other hand, occasional space missions enlarge the value of L that leads to less propellant consumption in space transportation but requires larger storage subsystems to be deployed. This is a trade-off between the space logistics operation and the ISRU production operation. Based on the storage capacity $Q_I LN$, its mass and power consumption sizing models can be written as equations 63 and 64.

$$M_{St} = F_5(Q_I LN) \quad (63)$$

$$P_{St} = G_5(Q_I LN) \quad (64)$$

The last subsystem is the power subsystem, which is one of the most important subsystems in ISRU trade studies. The design and technology selections of a power subsystem are relevant to landing site choice, space mission planning, ISRU operation mechanism, and ISRU infrastructure sizing. There are two categories of power sources

considered in this research. The first power source is nuclear power, including the fission surface power system (FSPS) and the large-scale radioisotope thermoelectric generator (RTG). This type of power system works continuously regardless of the operating environment. Therefore, it is relatively easier to perform trade studies and system sizing analysis. The second power source is solar power, which mainly includes the photovoltaic (PV) power system whose performance is highly site-sensitive. For example, at the 0-20° N latitude region of Mars, the peak solar irradiance after shadowing is 450 W/ m² and the period of high activity for solar arrays is 6-7 hr/sol [67]. In this region, solar arrays can work throughout the whole year after implementing dust mitigation technologies. In the northern polar area of Mars, the peak solar irradiance after shadowing is 150 W/ m² and the period of high activity for solar arrays is 24.6 hr/sol [67]. However, the exploration mission can only last for about 90 days during summer in this area because of the limited solar source for the rest of the year. Moreover, if the PV power system is the main power source and ISRU systems are planned to work during the night, additional energy storage systems need to be deployed. They can be batteries or fuel cells. Different attributes of power systems and operation environments make the trade studies more complex, especially considering their interaction with space logistics mission planning. In the next section, we will discuss how to integrate power system trade studies into the space mission planning framework. The design parameter of the power subsystem is the total power demand of all other ISRU subsystems. Then, the mass sizing model can be written as equation 65.

$$M_{Power} = F_6(P_{Re} + P_{Ex} + P_{Se} + P_{HF} + P_{St}) \quad (65)$$

Based on the aforementioned ISRU subsystem sizing models and their dependencies, we can combine them together and obtain an integrated ISRU modeling flow chart as shown in Figure 26. The inputs of this integrated model are available ISRU

technologies, potential power sources, and the requirement of ISRU daily productivity N . The outputs are designated ISRU subsystem infrastructure designs and technology selections.

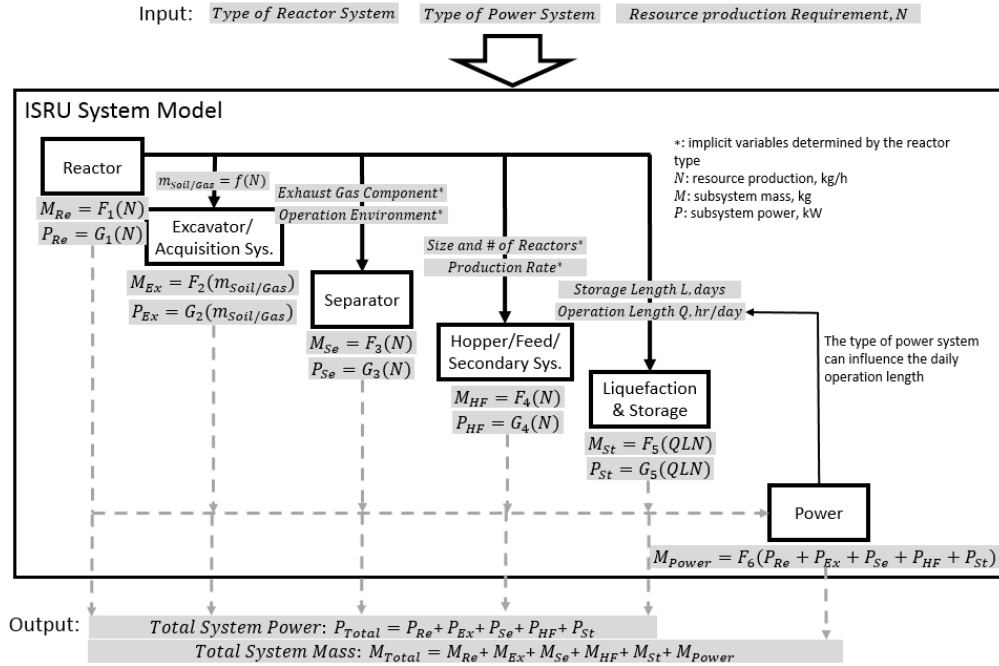


Figure 26 - Integrated ISRU modeling flow chart.

5.2.2 Full-Size Space Logistics Formulation

The integrated ISRU model as shown in Figure 26 can be combined with the network-based space logistics formulation to build a full-size space logistics optimization for space infrastructure design. As shown in Figure 27, there are two main components to be optimized in the full-size space infrastructure optimization formulation. The first component is the same as the prefixed space infrastructure optimization formulation, as shown on the right side of Figure 27. It considers space transportation mission planning, space infrastructure deployment strategy, and resource logistics after production. The second component is the space infrastructure trade studies, as shown on the left side of Figure 27. It considers the internal tradeoffs among space infrastructure subsystems and

their external interactions with space transportation to provide infrastructure subsystem sizing and technology selections. In this chapter, we use ISRU systems as an example of multi-subsystem space infrastructure optimization, although the proposed method can be generally implemented in different types of space infrastructure design trade studies. There are six subsystems considered in the ISRU infrastructure model as introduced in Sec. 5.2.1. There can be multiple different reactors, excavators, etc. depending on the ISRU technologies. These subsystems are all considered as different commodities in space logistics to enable effective analysis of subsystem interactions.

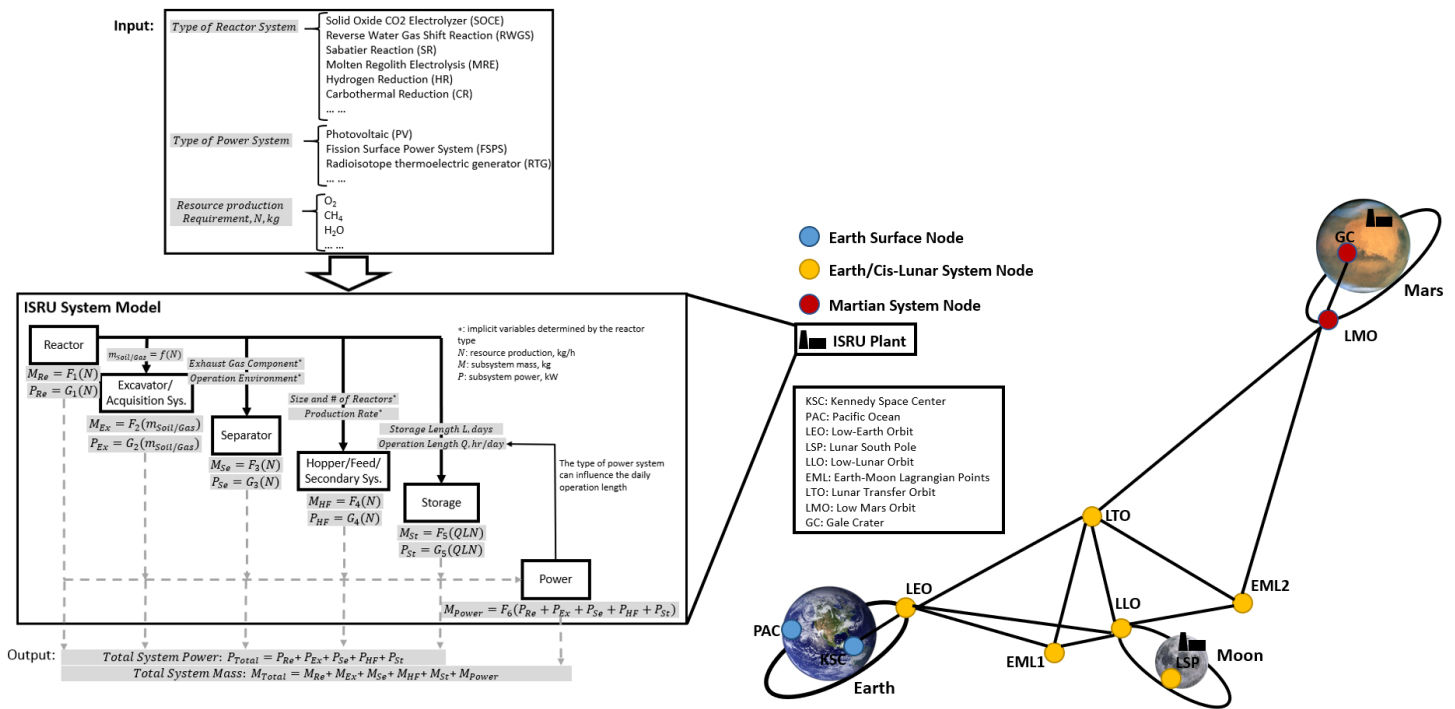


Figure 27 - An example of the full-size space infrastructure optimization formulation.

The formulation of the full-size space infrastructure optimization formulation is the same as the prefixed optimization formulation, as shown in equations 50-53. However, the constraints are interpreted and implemented in a different way because each infrastructure subsystem is considered separately. In the following parts, we show the additional

relationships to be considered to enable system-level space infrastructure trade studies together with space logistics optimization.

5.2.2.1 Objective Function

The objective function (i.e., equation 50) is exactly the same as it is in the prefixed optimization formulation. The only point to note is that a higher fidelity mission performance measurement model is needed in this formulation because each subsystem is considered independently. For example, if a cost model is implemented in the objective function, then the cost model in the full-size optimization formulation should include the detailed cost information for each subsystem and each technology.

5.2.2.2 Mass Balance Constraint

In the mass balance constraint (i.e., equation 51), we need to take into account the ISRU resource production process from the subsystem-level. The same lunar water ISRU example is used to illustrate the differences in the setting of the transformation matrix Q_{vij} . There are multiple technology options to build a lunar water ISRU. In this example, we assume that the lunar water ISRU plant is mainly made up of two reactors: the soil/water extraction (SWE) reactor and the direct water electrolysis (DWE) reactor. The SWE reactor, $x^{reactor_SWE}$, extracts water from lunar or Martian soil. The DWE reactor, $x^{reactor_DWE}$, electrolyzes water produced by the SWE reactor to generate O_2 and H_2 . We can define the commodity flow variables as,

$$x_{vijt} = \begin{bmatrix} x^{O_2}, \text{kg} \\ x^{H_2}, \text{kg} \\ x^{H_2O}, \text{kg} \\ x^{reactor_DWE}, \text{kg} \\ x^{reactor_SWE}, \text{kg} \end{bmatrix}_{vijt}$$

Then, we can express the ISRU production process for one hour for O_2 , H_2 , and H_2O as follows:

$$\begin{bmatrix} x^{O_2} \\ x^{H_2} \\ x^{H_2O} \\ x^{reactor_DWE} \\ x^{reactor_SWE} \end{bmatrix}_{inflow}^{vijt} = \begin{bmatrix} 1 & 0 & 0 & \sigma_{DWE}^{O_2} & 0 \\ 0 & 1 & 0 & \sigma_{DWE}^{H_2} & 0 \\ 0 & 0 & 1 & -\beta_{DWE}^{H_2O} & \sigma_{SWE}^{H_2O} \\ 0 & 0 & 0 & 1 & 0 \\ 0 & 0 & 0 & 0 & 1 \end{bmatrix}_{vij} \begin{bmatrix} x^{O_2} \\ x^{H_2} \\ x^{H_2O} \\ x^{reactor_DWE} \\ x^{reactor_SWE} \end{bmatrix}_{vijt} \quad (66)$$

In equation 66, there are five constraints in total. The first two constraints represent O_2 and H_2 generations by the DWE reactor for one hour, where σ is the reactor productivity. The third constraint illustrates H_2O consumption by the DWE reactor and production by the SWE process for one hour, where β denotes the consumption rate. Both σ and β are nonnegative values. Note that because of the mass balance of chemical reactions, we have $\sigma_{DWE}^{O_2} + \sigma_{DWE}^{H_2} \leq \beta_{DWE}^{H_2O}$. The last two constraints show that the masses of the DWE reactor and the SWE reactor do not change during the resource production processes.

5.2.2.3 Concurrency Constraint

In the concurrency constraint (i.e., equation 52), besides the spacecraft payload and propellant capacities considered during space transportation, the resource storage capacities for infrastructure storage systems, the power supply capacities for power generation systems, and the energy storage capacities for energy storage systems also need to be considered. Among these, the constraint format of resource storage capacities is the same as the constraints for spacecraft payload and propellant capacities.

In the following, we show two examples of the concurrency constraint in the full-size optimization formulation. One example is about space infrastructure power supply

capacities and another is about energy storage capacities. For space infrastructure power supply capacities, we define the commodity flow variables as

$$\mathbf{x}_{vijt} = \begin{bmatrix} x^{I_1}: \text{infrastructure system 1, kg} \\ x^{I_2}: \text{infrastructure system 2, kg} \\ x^{I_3}: \text{infrastructure system 3, kg} \\ x^P: \text{power generation system, kg} \end{bmatrix}_{vijt}$$

Then, we can express the power supply capacity constraint for infrastructure system design as follows,

$$\left[P_{I_1} \left(1 + \frac{Q_{I_1} - Q_p}{\varepsilon Q_p}\right) \quad P_{I_2} \left(1 + \frac{Q_{I_2} - Q_p}{\varepsilon Q_p}\right) \quad P_{I_3} \left(1 + \frac{Q_{I_3} - Q_p}{\varepsilon Q_p}\right) \quad -P_0 \right]_{vij} \begin{bmatrix} x^{I_1} \\ x^{I_2} \\ x^{I_3} \\ x^P \end{bmatrix}_{vijt} \leq 0 \quad (67)$$

where $P_{I_i}, i \in \{1,2,3\}$ is the infrastructure power demand of system i (in kW/kg); $Q_{I_i}, i \in \{1,2,3\}$ is the infrastructure operating length per solar day, in the unit of hours; P_0 is the power generation system output power per unit mass (in kW/kg); Q_p is the power system working time per solar day. If the power system is a fission surface power system (FSPS) or a radioisotope thermoelectric generator (RTG), it works continuously during the space mission, which means Q_p is equal to the length of a solar day. If the power system is a photovoltaic (PV) system, it only works during the daytime, which means Q_p is equal to the daytime length of a solar day at the destination. If the infrastructure system operating time is longer than the power system working time per solar day, which means $Q_{I_i} > Q_p$, an energy storage system (e.g., battery or fuel cell) is necessary to support the infrastructure systems. There is an energy loss during the power storage process in battery charging/discharging. Therefore, we define an energy storage efficiency parameter, ε .

To identify the size of the energy storage system, a concurrency constraint for energy storage capacities is needed. Define the commodity flow variables as

$$\mathbf{x}_{vijt} = \begin{bmatrix} x^{I_1}: \text{infrastructure system 1, kg} \\ x^{I_2}: \text{infrastructure system 2, kg} \\ x^{I_3}: \text{infrastructure system 3, kg} \\ x^P: \text{power generation system, kg} \\ x^E: \text{energy storage system, kg} \end{bmatrix}_{vijt}$$

Then, we can express the energy storage capacity constraint as follows

$$\begin{bmatrix} -P_{I_1} & -P_{I_2} & -P_{I_3} & P_0 & -\frac{\gamma}{\varepsilon Q_p} \end{bmatrix}_{vij} \begin{bmatrix} x^{I_1} \\ x^{I_2} \\ x^{I_3} \\ x^P \\ x^E \end{bmatrix}_{vijt} \leq 0 \quad (68)$$

where γ is the specific mass of the energy storage system, in the unit of kWh/kg. It shows the ability of energy storage per unit mass.

5.2.2.4 Time Window Constraint

The time window constraint (i.e., equation 53) is the same as in the prefixed optimization formulation. Typically, the time windows for different space infrastructure subsystems are the same.

5.2.3 *Relationship with the Prefixed Formulation*

It is easy to show that the solution from the prefixed formulation J_{prefixed} is an upper bound of that from the full-size formulation $J_{\text{full_size}}$.

$$J_{\text{full_size}} \leq J_{\text{prefixed}}$$

This is because the only difference between the two formulations is that the prefixed formulation fixes the mass ratios of the infrastructure subsystems, whereas the full-size formulation allows the variation of those mass ratios. Thus, the prefixed formulation has

an equal or smaller feasible design space than the full-size formulation, and thus provides an equal or larger solution.

5.2.4 Limitations of the Full-Size Formulation

The full-size space infrastructure optimization formulation considers all infrastructure subsystems as separated commodities during the entire space campaign, and this significantly increases the number of commodities in logistics optimization. Generally, as a mixed-integer linear programming formulation, which is an NP-hard problem, the computational time cost increases exponentially as the problem size increases. Studies showed that even for a short lunar exploration campaign (i.e., including three lunar missions), the concurrent optimization of space mission planning, spacecraft design, and space infrastructure design can make the network-based space logistics optimization formulation computationally prohibitive [17]. This caveat can make the full-size formulation computationally intractable for long-term space mission planning. In the next section, we will propose a new approximate optimization formulation that can achieve a significant computational cost saving with little sacrifice in the solution quality.

5.3 Multi-Fidelity Space Infrastructure Optimization Formulation

In response to the computational challenge of the full-size space infrastructure optimization formulation, we propose a new approximate optimization problem formulation. Our idea is to note the fact that the infrastructure subsystem design trade studies only exist at the destination nodes, where these subsystems are deployed; there may exist redundant commodity variables and constraints in transportation arcs that can be reduced. With this idea, we develop a mechanism to combine the infrastructure subsystem variables into fewer commodity variables during space transportation (“packing” process) and separate these packed commodities after delivery to the destination nodes

(“unpacking” process). Namely, we vary the granularity of the commodity type definition over the network graph, resulting in a multi-fidelity space infrastructure optimization formulation. This formulation can significantly reduce the number of commodity variables and corresponding constraints in space logistics during space transportation and improve computational efficiency.

The multi-fidelity space infrastructure optimization leverages the theory of constraint and variable aggregations for a general mixed-integer linear programming formulation. For large and complex engineering problems, we often need to balance the accuracy of the model with the cost of computation. Constraint and variable aggregation methods have been explicitly or implicitly used in realistic problems, which are typically large and complex, to find surrogate models of the original formulations. Zipkin [68, 69] performed thorough analyses on solution bounds for linear programming through constraint aggregation and variable aggregation, respectively, under certain assumptions about the problem, although their assumptions limit their methods’ applicability to our problem. In the multicommodity network flow context, Evans et al. [70, 71] developed the commodity aggregation for multicommodity capacitated transportation problems to find the lower bound. More recently, Ho [53] also developed a formulation based on constraint aggregation and variable aggregation to enable an efficient way to reduce the size of the time-expanded network for the generalized multicommodity network flow.

In this section, we first discuss the general constraint and variable aggregations in linear programming. Then, we show how to perform a partial constraint and commodity aggregations, referred to as commodity packing based on its physical meaning, over particular space transportation arcs to enable a multi-fidelity optimization. We show that the solution of this multi-fidelity optimization formulation provides a lower bound of that of the full-size optimization formulation. Furthermore, a commodity packing

preprocessing algorithm is also developed to enable an automatic decision on where and when to pack the commodities.

5.3.1 Constraint Aggregation and Variable Packing

The commodity variable packing is processed in two steps: constraint aggregation and variable packing. The first step, constraint aggregation, aggregates the constraints with designated packable commodities into shared constraints through an aggregation matrix. Then, the second step, variable packing, aggregates the packable commodities into shared package commodities. The transportation, transformation, and flow bounds of these commodities are considered together through the package commodities.

5.3.1.1 Constraint Aggregation

Consider a general (full-size) linear programming formulation showed as follows.

Formulation F1 (Full-Size)

Minimize:

$$J = C\mathbf{X} \quad (69)$$

Subject to:

$$A\mathbf{X} \leq \mathbf{b} \quad (70)$$

where

$$\mathbf{X} = \begin{bmatrix} x_1 \\ x_2 \\ \vdots \\ x_n \end{bmatrix}, C = [c_1 \quad c_2 \quad \dots \quad c_n], A = \begin{bmatrix} a_{1,1} & a_{1,2} & \dots & a_{1,n} \\ a_{2,1} & a_{2,2} & \dots & a_{2,n} \\ \vdots & \vdots & \ddots & \vdots \\ a_{m,1} & a_{m,2} & \dots & a_{m,n} \end{bmatrix}, \mathbf{b} = \begin{bmatrix} b_1 \\ b_2 \\ \vdots \\ b_m \end{bmatrix}$$

We define an “aggregation matrix” G and multiply both sides of the constraint equation 70 by G . Then, we can obtain a new formulation as follows,

Formulation F2 (Constraint Aggregation)

Minimize:

$$J = C\mathcal{X} \tag{71}$$

Subject to:

$$GAX \leq Gb \tag{72}$$

where the aggregation matrix G has a size $K \times m$, where m is the number of rows in the A matrix and K is the number of constraints after aggregation ($K \leq m$), and satisfies the following two conditions:

Condition 1: The aggregation matrix G has exactly one nonzero entry per column, and that entry is positive.

Condition 2: The aggregation matrix G has at least one nonzero entry per row, and these entries are all positive.

For these formulations, we show that a lower bound of the optimal objective of **F1** can be found by solving **F2** if both problems are feasible and bounded.

We first rewrite the constraint 72 as,

$$G(A\mathcal{X} - b) \leq \mathbf{0}_{K \times 1}$$

The column indices of the positive entries in each row of the aggregation matrix G define a partition of the corresponding constraints $\{1, \dots, m\}$ into K sets. Denote the partition as $\Omega = \{S_k: k = 1, \dots, K\}$, where S_k is the set of constraint indices in the k -th set. Define $m_k = |S_k|$, which is the number of constraint indices in the k -th set. The partition satisfies

$$\bigcup_{k=1}^K S_k = \{1, \dots, m\} \text{ and } S_k \cap S_{k'} = \emptyset \quad \forall k \neq k'$$

Define $G = \begin{bmatrix} \mathbf{g}_1^T \\ \mathbf{g}_2^T \\ \vdots \\ \mathbf{g}_K^T \end{bmatrix}$, where each row of the aggregation matrix is a $1 \times m$ weighting

vector, \mathbf{g}_k^T , that satisfies

$$\begin{cases} \mathbf{g}_k[j] > 0 & \text{if } j \in S_k \\ \mathbf{g}_k[j] = 0 & \text{if } j \notin S_k \end{cases} \quad \forall k \in \{1, \dots, K\}$$

To aggregate and relax the constraints, we replace each subset of constraints S_k by a single constraint through weighting vectors. As a result, we can write the k -th constraint after aggregation for **F1** as,

$$\mathbf{g}_k^T(A\mathbf{X} - \mathbf{b}) \leq 0$$

This constraint aggregates m_k number of constraints in **F1** with indices $\{j: j \in S_k\}$. Because all non-zero entries in the weighting vectors are positive, these constraints are also relaxed. By applying the weighing vectors to **F1**, we can get a relaxed formulation,

Minimize:

$$\mathcal{J} = C\mathbf{X} \tag{73}$$

Subject to:

$$\begin{bmatrix} \mathbf{g}_1^T \\ \mathbf{g}_2^T \\ \vdots \\ \mathbf{g}_K^T \end{bmatrix} (A\mathbf{x} - \mathbf{b}) \leq \mathbf{0}_{K \times 1} \quad (74)$$

By solving the formulation 73-74, which is equivalent to **F2**, we can get a lower bound of **F1**'s solution.

5.3.1.2 Variable Packing

After the constraint aggregation, we can perform variable packing to further improve computational efficiency by reducing the number of variables. The purpose of this step is to find a formulation equivalent to **F2**, but with fewer variables; this step corresponds to packing the commodities. Note that, in the following discussion, we only consider the aggregation of the continuous commodity flow variables for simplicity.

Consider a variable vector as follows,

$$\mathbf{x} = \begin{bmatrix} x_1 \\ x_2 \\ \vdots \\ x_n \end{bmatrix}$$

Assume that there exists a set of index set $Q = \{Q_u : u = 1, \dots, U\}$, where each set Q_u includes the packable commodity variable indices to be packed into one package commodity $\tilde{x}_u = \sum_{i \in Q_u} x_i$. This index set Q satisfies

$$\bigcup_{u=1}^U Q_u \subseteq \{1, \dots, n\} \text{ and } Q_u \cap Q_{u'} = \emptyset \quad \forall u \neq u'$$

The variable packing operation is defined as replacing the n original variables \mathcal{X} into U new variables $\tilde{\mathcal{X}}$ following the conversion $\tilde{x}_u = \sum_{i \in Q_u} x_i$.

In the following, we show that we can find an equivalent formulation after performing variable packing if coefficients in **F2** satisfy the following two conditions:

Condition 3: For each index set Q_u , there exists a constant c'_u such that $c_i = c'_u$ for all $i \in Q_u$;

Condition 4: For each index set Q_u , there exists a constant vector $R'_u = [r'_1, r'_2, \dots, r'_K]_u^T$ such that $\sum_{j=1}^m g_{k,j} a_{j,i} = r'_k$ for all $i \in Q_u$ and for all $k \in \{1, \dots, K\}$.

Without loss of generality, we consider a case where the last $n - q$ variables are to be packed into one package commodity. This corresponds to the case where $Q = \{q + 1, \dots, n\}$ and $U = 1$. Thus, the expected variable vector after packing is

$$\tilde{\mathcal{X}} = \begin{bmatrix} x_1 \\ \vdots \\ x_q \\ \tilde{x} \end{bmatrix}$$

where the package commodity variable $\tilde{x} = \sum_{i=q+1}^n x_i$. In the objective function of **F2** (i.e., equation 71), we have,

$$C\mathcal{X} = [c_1 \quad c_2 \quad \dots \quad c_n] \begin{bmatrix} x_1 \\ x_2 \\ \vdots \\ x_n \end{bmatrix} = [c_1 \quad \dots \quad c_q \quad c_{q+1} \quad \dots \quad c_n] \begin{bmatrix} x_1 \\ \vdots \\ x_q \\ x_{q+1} \\ \vdots \\ x_n \end{bmatrix}$$

From the first condition, we know that $c_i = c'$ for all $i \in \{q + 1, \dots, n\}$. Therefore, we can get

$$\begin{aligned}
C\mathbf{X} &= [c_1 \quad \dots \quad c_q \quad c' \quad \dots \quad c'] \begin{bmatrix} x_1 \\ \vdots \\ x_q \\ x_{q+1} \\ \vdots \\ x_n \end{bmatrix} = [c_1 \quad \dots \quad c_q \quad c'] \begin{bmatrix} x_1 \\ \vdots \\ x_q \\ \sum_{i=q+1}^n x_i \end{bmatrix} \\
&= [c_1 \quad \dots \quad c_q \quad c'] \begin{bmatrix} x_1 \\ \vdots \\ x_q \\ \tilde{x} \end{bmatrix} = \tilde{C}\tilde{\mathbf{X}}
\end{aligned}$$

Similarly, in the constraint of **F2** (i.e., equation 72), we have

$$GAX = \begin{bmatrix} \sum_{j=1}^m g_{1,j}a_{j,1} & \sum_{j=1}^m g_{1,j}a_{j,2} & \dots & \sum_{j=1}^m g_{1,j}a_{j,n} \\ \sum_{j=1}^m g_{2,j}a_{j,1} & \sum_{j=1}^m g_{2,j}a_{j,2} & \dots & \sum_{j=1}^m g_{2,j}a_{j,n} \\ \vdots & \vdots & \ddots & \vdots \\ \sum_{j=1}^m g_{K,j}a_{j,1} & \sum_{j=1}^m g_{K,j}a_{j,2} & \dots & \sum_{j=1}^m g_{K,j}a_{j,n} \end{bmatrix} \begin{bmatrix} x_1 \\ x_2 \\ \vdots \\ x_n \end{bmatrix}$$

From the second condition, we have $R' = [r'_1, r'_2, \dots, r'_K]$ such that $\sum_{j=1}^m g_{k,j}a_{j,i} = r'_k$ for all $i \in \{q+1, \dots, n\}$ and for all $k \in \{1, \dots, K\}$. Therefore, we can get

$$GAX = \begin{bmatrix} \sum_{j=1}^m g_{1,j}a_{j,1} & \dots & \sum_{j=1}^m g_{1,j}a_{j,q} & r'_1 \\ \sum_{j=1}^m g_{2,j}a_{j,1} & \dots & \sum_{j=1}^m g_{2,j}a_{j,q} & r'_2 \\ \vdots & \ddots & \vdots & \vdots \\ \sum_{j=1}^m g_{K,j}a_{j,1} & \dots & \sum_{j=1}^m g_{K,j}a_{j,q} & r'_K \end{bmatrix} \begin{bmatrix} x_1 \\ \vdots \\ x_q \\ \tilde{x} \end{bmatrix} = \tilde{A}\tilde{\mathbf{X}}$$

By repeating this process, we can pack commodities into multiple package commodities.

As a result, we achieve a new formulation.

Formulation F3 (Variable Packing)

Minimize:

$$J = \tilde{c}\tilde{X} \quad (75)$$

Subject to:

$$\tilde{A}\tilde{X} \leq G\mathbf{b} \quad (76)$$

According to the above analysis, the formulation **F3** is equivalent to **F2**.

In summary, we have shown how to find a lower-bound formulation through constraint aggregation and variable packing for general linear programming problems. It is necessary to first find the aggregation matrix G that satisfies the two defining properties (i.e., conditions 1 and 2). Then, we need to identify the variables whose coefficients satisfy the two variable packing conditions (i.e., conditions 3 and 4). This sequence can be generalized to the commodity packing in the space logistics formulation and formulation **F3** can be generalized to the multi-fidelity formulation. Thus, together with the prefixed formulation discussed before, we have the following relationship:

$$J_{\text{multi_fidelity}} \leq J_{\text{full_size}} \leq J_{\text{prefixed}}$$

Bounding the computationally prohibitive full-size formulation from both the upper and lower sides enables us to find the approximation solution of the computationally prohibitive full-size formulation with the knowledge about the worst possible approximation error.

5.3.2 Preprocessing Algorithm for Automatic Commodity Packing

Although the previous subsection showed an efficient way to pack the commodities in space logistics formulation under certain conditions, we still need a method to identify what commodities are able to be packed in each arc and then find the aggregation matrix

to aggregate corresponding constraints so that all conditions are satisfied. Therefore, this subsection proposes a preprocessing algorithm to compile a multi-fidelity optimization formulation automatically for the full-size space infrastructure optimization problem. The consequent formulation performs constraint and variable aggregations in a subset of network arcs, which achieves a lower bound approximation of the original full-size optimization formulation.

Considering a full-size space infrastructure optimization problem as shown in the formulation 50-53, we can identify the packable commodities leveraging the special structure of this formulation. In the mass balance constraints (i.e., equation 51), each constraint is designated to guarantee the mass balance of one type of commodity. The commodity transformation matrix Q defines the interactions between commodities. To make the commodities packable, they should have the same transformation coefficients with respect to all other commodities. The concurrency constraints (i.e., equation 52) provide the commodity flow upper bound by considering the total weights of different commodities. For example, the total mass of crew, consumables, instruments, and infrastructure elements must be smaller or equal to the spacecraft total payload capacity; this constraint has a set of packable commodity weights. Therefore, the packable commodities should have the same weight coefficients in all concurrency constraints. After identifying the packable commodities, they can be packed directly in the concurrency constraints without an aggregation matrix. The time window constraints (i.e., equation 53) are also defined specifically for each type of commodity. However, by definition, the time window is always the same for different commodities in one specific arc. In summary, according to conditions 3 and 4 in Sec. 5.3.1.2, to pack the packable commodities in space transportation, the associated coefficients must satisfy the following three commodity packing conditions:

- 1) For the objective function, equation 50, the cost coefficients of packable commodities need to be equal;
- 2) For the mass balance constraint, equation 51, the transformation coefficients of packable commodities with respect to all other commodities need to be equal;
- 3) For all concurrency constraints, equation 52, the weight coefficients of packable commodities need to be equal.

Based on the preceding commodity packing conditions, we can propose a preprocessing algorithm to automatically identify the packable commodities and aggregation matrices in the original full-size space infrastructure optimization problem. The pseudo code of the preprocessing is shown as follows. We assume there are p types of commodities in the system. Note that, in this pseudo code, there is a sorting process after identifying packable commodity index sets. The reason for this step is to enable flexible packing decision; if the users prefer to generate fewer package commodities than the number of packable commodity index sets $\mathcal{Q} = \{Q_u: u = 1, \dots, U\}$ for an arc (i.e., only N package commodities, where $N \leq U$), they can generate the N most impactful package commodities in the sorted list, where “most impactful” means it contains the most packable commodities. Fewer package commodities, which means fewer commodities are packed, leads to a tighter lower-bound of the optimization.

To generate the aggregation matrix G for the mass balance constraint and time window constraint, we first need to identify the packable commodity index set, denoted by $\check{\zeta}$ as shown in the preprocessing pseudo code. If we assume that we would like to generate N package commodities, then $N = |\check{\zeta}|$. Each subset in $\check{\zeta}$ represents the corresponding packable commodities that will be packed into one package commodity. Suppose that L

types of commodities are packed into N package commodities, then $L = \sum_{S_t \in \zeta} |S_t|$. Therefore, before the commodity packing, the number of variables over each arc is p , where each variable represents one type of commodity. After the commodity packing, the number of variables is $K = N + p - L$, where the first N variables represent the package commodities, they contain the information of L types of commodities that are packed; the remaining $p - L$ variables represent commodities that are not packed. Note that the mass balance constraints and the time window constraints are defined for each commodity independently. Therefore, before the commodity packing, the number of mass balance constraints or the time window constraints over each arc is also p ; after the commodity packing, the number of these constraints becomes $K = N + p - L$.

Preprocessing for commodity packing pseudo code

For $\forall(v, i, j) \in \mathcal{A} \quad \forall t \in \mathcal{T}$:

Step 1. For the cost matrix in the objective function, c_{vijt} : Let $\Omega_1 = \{S_k: k = 1, \dots, q\}$ be a partition of the commodity indices $\{1, \dots, p\}$ and define $n_k = |S_k|$. The partition satisfies

$$c_{vijt}[l] = c_{vijt}[l'] \quad \forall l, l' \in S_k \quad \forall k$$

$$\bigcup_{k=1}^q S_k = \{1, \dots, p\} \quad \text{and} \quad S_k \cap S_{k'} = \emptyset \quad \forall k \neq k'$$

Step 2. For the transformation matrix in mass balance constraint, F_{vij} : Let $\Omega_2 = \{S_f: f = 1, \dots, q'\}$ be a partition of the commodity indices $\{1, \dots, p\}$ and define $n_f = |S_f|$. The partition satisfies

$$F_{vij}[l, u] = F_{vij}[l', u] \quad \forall l, l' \in S_f, \forall u \in \{1, \dots, p\} \setminus \{l, l'\}, \quad \forall f$$

$$\bigcup_{f=1}^{q'} S_f = \{1, \dots, p\} \quad \text{and} \quad S_f \cap S_{f'} = \emptyset \quad \forall f \neq f'$$

Step 3. For the concurrency matrix in concurrency constraint, H_{vij} : Let $\Omega_3 = \{S_h: h = 1, \dots, q''\}$ be a partition of the commodity indices $\{1, \dots, p\}$ and define $n_h = |S_h|$. The partition satisfies

$$H_{vij}[:, l] = H_{vij}[:, l'] \quad \forall l, l' \in S_h \quad \forall h$$

$$\bigcup_{h=1}^{q''} S_h = \{1, \dots, p\} \quad \text{and} \quad S_h \cap S_{h'} = \emptyset \quad \forall h \neq h'$$

Step 4. Find all intersection sets

$$\zeta = \{S_\tau: \tau = 1, \dots, U \mid S_\tau \neq \emptyset \text{ and } S_\tau = S_k \cap S_f \cap S_h, \forall S_k \in \Omega_1, \forall S_f \in \Omega_2, \forall S_h \in \Omega_3\}$$

Step 5. Identify the packable commodities

Pseudo code (continued)

If $\zeta = \emptyset$:

Step 5.1. There are no packable commodities in this arc. **Screen the next arc:**

Go to Step 1.

Else:

Step 5.2. Define the cardinality $n_\tau = |S_\tau|$.

Step 5.3. Perform sorting in a descending order based on the cardinality for $\forall S_\tau \in \zeta$ and get a new set $\check{\zeta}$.

Step 5.4. Based on the predefined preference, define the number of package commodities as N ($N \leq U$), the packable commodity index set as $\check{\zeta} = \{S_\tau: \tau = 1, \dots, N | S_\tau \in \check{\zeta}\}$.

Step 6. Find the aggregation matrix for the mass balance constraint and time window constraint:

Step 6.1. Get the number of commodities that will be packed: $L = \sum_{S_\tau \in \check{\zeta}} |S_\tau|$.

Step 6.2. Get the number of variables after commodity packing: $K = N + p - L$.

Step 6.3. For this arc, define $G = [\mathbf{g}_1^T \quad \mathbf{g}_2^T \quad \dots \quad \mathbf{g}_K^T]^T$, where each row of the aggregation matrix is a $1 \times p$ weighting vector, \mathbf{g}_k^T , that satisfies

For $\forall k \in \{1, \dots, N\}$ (the first N variables are package commodities):

$$\begin{cases} \mathbf{g}_k[j] = 1 & \text{if } j \in S_k \\ \mathbf{g}_k[j] = 0 & \text{if } j \notin S_k \end{cases} \quad S_k \in \check{\zeta}$$

For $\forall k \in \{N + 1, \dots, K\}$ (the remaining variables are for commodities that are not packed):

$$\begin{cases} \mathbf{g}_k[j] = 1 & \text{if } k = N + j - L \\ \mathbf{g}_k[j] = 0 & \text{if } k \neq N + j - L \end{cases}$$

Step 7. Screen the next arc: Go to Step 1.

5.4 Case Study and Analysis

This section evaluates the performances of the proposed space infrastructure optimization formulations with a case study on a multi-mission human lunar exploration campaign, considering ISRU system designs. The mission scenario, including mission demand, spacecraft design, and ISRU architecture models, is first introduced in Sec. 5.4.1, and then Sec. 5.4.2 evaluates the performance of the formulations. Note that although this chapter introduces the formulations in the order of the prefixed, full-size, multi-fidelity formulations, the later analysis considers the full-size optimization formulation as the baseline and compares the other two formulations against it; this is because the full-size optimization is the most accurate and computationally costly one, and we are interested in the solution quality and the computational cost of the prefixed formulation (i.e., the upper-bound formulation) and the multi-fidelity formulation (i.e., the lower-bound formulation).

5.4.1 Mission Scenario

A simple scenario is considered as a case study where all formulations (including the full-size formulation) can complete their computation within a reasonable time. We consider a cis-lunar transportation system with Earth, low-Earth orbit (LEO), geosynchronous equatorial orbit (GEO), Earth-Moon Lagrangian point 1 (EML1), and the Moon. The five-node transportation network model and the spaceflight ΔV values are shown in Figure 28. Note that we do not consider the propellant cost from Earth to LEO (i.e., the ΔV is considered as zero); instead, Earth is assumed as the main supply node and the arc from Earth to LEO is convenient to calculate the space mission cost. Every year, 5 astronauts fly to the Moon with habitat and equipment. These demands are considered as one type of general payload together with a crew cabin. The total mass of the crew cabin

and lunar equipment is assumed as 30,000 kg, which is estimated based on the Apollo mission [62]. The astronauts stay on the lunar surface for 120 days and then come back with lunar samples and materials. The total mass of crew cabin and lunar samples is assumed as 5,000 kg and they are delivered back to the Earth at the end of the mission. For this mission design, the optimizer needs to decide whether it requires ISRU systems to support the transportation, whether the system needs a propellant depot, and where we should deploy the depot (i.e., LEO, GEO, or EML1) if needed. We assume that a spacecraft can serve as a propellant depot if it stays at a node during the mission [35]. The mission demands and supplies are summarized in Table 14. Note that, the mission demands and supplies are defined at the same time step for each flight to minimize the number of time steps assigned for the transportation.

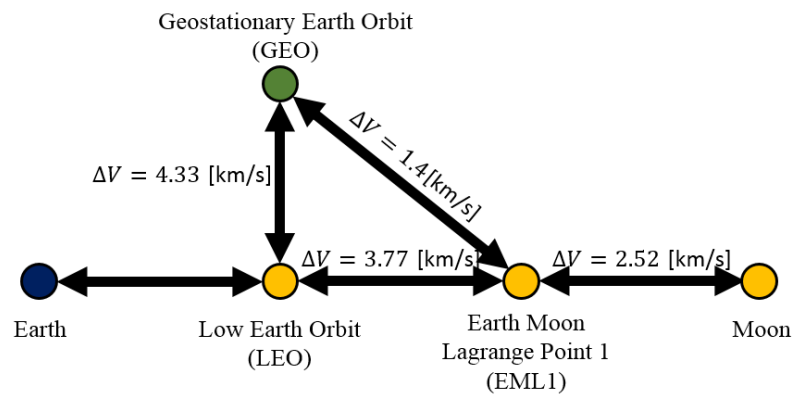


Figure 28 - Cis-lunar transportation network model.

Table 14 - Lunar exploration demands and supplies.

Payload Type	Node	Time, day	Supply
Go to the Moon			
ISRU, propellant & food, kg	Earth	All the time	$+\infty$
Crew cabin & equipment, kg	Earth	240	+30,000 [62]
Crew cabin & equipment, kg	Moon	240	-30,000 [62]
Back to Earth			
Crew cabin & lunar sample, kg	Moon	360	+5,000
Crew cabin & lunar sample, kg	Earth	360	-5,000

We need spacecraft to deliver payloads from Earth to the Moon. To simplify the analysis, the spacecraft design is not considered as part of the trade space in space logistics optimization. Instead, two types of spacecraft with fixed design parameters are considered for space transportation. Spacecraft 1 is modeled based on the Advanced Cryogenic Evolved Stage (ACES) from United Launch Alliance [35]. It uses liquid hydrogen and liquid oxygen (LH2/LOX) as the propellant. The spacecraft structure mass is 5,917 kg and the propellant tank capacity is 68,040 kg [35]. Because of the implementation of long-duration storage technologies in ACES propellant tanks, the LH2/LOX propellant boiloff rate is considered as zero during space transportation. Spacecraft 2 is modeled based on the lunar surface access module (LSAM) descent stage pressure-fed design from the green propellants study. The design parameters are found in the SpaceNet database [72]. It uses liquid methane and liquid oxygen (LCH4/LOX) as the propellant. The spacecraft design assumptions are listed in Table 15. For simplicity, we assume that both spacecraft can be used for all trajectories in the transportation network, including lunar landing and ascending. Also, they are considered as single-stage transportation vehicles, but they can be combined to form a larger transportation vehicle.

Table 15 - Spacecraft design parameters.

Parameter	Assumed value
Spacecraft 1	
Propellant type	LH2/LOX
Propellant capacity, kg	68,040 [35]
Structure mass, kg	5,917 [35]
Propellant I_{sp} , s	420
Propellant component mass ratio	$O_2:H_2=5.5:1$
Spacecraft 2	
Propellant type	LCH4/LOX
Propellant capacity, kg	40,737 [72]
Structure mass, kg	6,560 [72]
Propellant I_{sp} , s	350
Propellant component mass ratio	$O_2:CH_4=3.5:1$

The ISRU infrastructure design model is another essential part of the space infrastructure optimization case study. For the lunar exploration campaign considered in this chapter, the ISRU architecture design models are listed in Table 16. These models are extrapolated from historical ISRU infrastructure design concept literature and prototypes by Chen et al. [73].

In Table 16, the reference product is used to size the ISRU subsystems. For reactors and excavators, the specific power and specific mass mean the power demand and the system mass needed to reach 1 kg/hr productivity of the reference product. For storage systems and power systems, the specific power and specific mass mean the necessary system size to store 1 kg resource, 1 kWh energy or to supply 1 kW power. The soil/water extraction process and the excavator are classified based on different soil types, soil @3% H_2O and soil @8% H_2O . Note that the regolith water concentration values assumed here are extrapolated from the literature relating to Martian surface soil [73]. They are used as example values only here. Because of the difference in lunar regolith composition, the

hydrogen reduction process also has different productivity in different regions. Moreover, according to the ISRU infrastructure design prototype, we assume that rigid solar concentrators provide thermal energy to the HR and CR reactors [28]. They are considered as part of the reactors. Therefore, the nominal power demands of the HR and CR reactors are zero. In this case, we only consider ISRU systems for O_2 and H_2 generation during the mission. It is up to the optimizer's choice whether to use Spacecraft 1 and leverage ISRU systems or to use Spacecraft 2 and deliver all necessary propellant from Earth.

Besides the ISRU infrastructure sizing models, mission operation management is also critical to be considered in space logistics optimization. It includes rocket launch frequency, ISRU system maintenance [2, 17], power system working environment, degradation, and energy storage efficiencies [67, 74-77]. The mission operation assumptions are listed in Table 17. The rocket launch interval determines the frequency of mission operation. We define that the mission operation time windows are open for a few time steps after each rocket launch opportunity. When the mission operation time windows are closed, space flights are not permitted. The ISRU maintenance rate means that every year, the mass of maintenance spare demand is equivalent to 10% of the ISRU system total mass [2, 17].

Table 16 - ISRU infrastructure design models. [73]

System	Chemistry reactions	Reference product	Specific power, kW	Specific mass, kg
Reactor				
Soil/Water extraction (SWE)	$Soil \rightarrow H_2O$	H_2O , kg/hr	@3%: 13.7 @8%: 7	@3%: 357 @8%: 195
Direct water electrolysis (DWE)	$2H_2O \rightarrow 2H_2 + O_2$	O_2 , kg/hr	5.83	83.3
Molten regolith electrolysis (MRE)	$Soil \rightarrow O_2$	O_2 , kg/hr	26.94	197.58
Hydrogen reduction (HR)	$Soil + H_2 \rightarrow H_2O$	H_2O , kg/hr	0	@equator: 228 @pole: 482
Carbothermal reduction (CR)	$Soil + 2CH_4 + 2H_2 \rightarrow 2CH_4 + 2H_2O$	H_2O , kg/hr	0	520.5
Soil extraction system				
Excavator for soil @3% H_2O	— —	Soil, kg/hr	0.004	0.38
Excavator for soil @8% H_2O	— —	Soil, kg/hr	0.027	23
Storage system				
O_2 storage	— —	O_2 , kg	0.0088	5.15
H_2 storage	— —	H_2 , kg	0.0267	3.33
H_2O storage	— —	H_2O , kg	0	40
CH_4 storage	— —	CH_4 , kg	0.0073	1.67
Power system				
Photovoltaic (PV) power system	— —	Power, kW	— —	6.8 (@ 1 AU)
Energy storage system: battery	— —	Energy, kWh	— —	4
Energy storage system: fuel cell	— —	Energy, kWh	— —	2
Fission surface power system (FSPS)	— —	Power, kW	— —	150
Radioisotope power system (RPS)	— —	Power, kW	— —	124

Table 17 - Mission operation parameters and assumptions.

Parameter	Assumed value
Rocket launch interval, day	120
ISRU maintenance, system mass/yr	10% [2, 17]
Solar irradiance (@ 1 AU), kW/m ²	1.36 [67]
PV radiation degradation, /sol	0.014% [74]
Battery charging efficiency	95% [75]
Fuel cell energy efficiency	60% [76]
RPS degradation rate, /yr	1.9% [77]

The problem is solved using the Gurobi 8.1 solver through Python on an i9-9900k, 3.6GHz platform with 32GB RAM. The detailed analysis and discussion of this human lunar exploration campaign case study are shown in the next section.

5.4.2 Comparison of Optimization Formulations

This section compares the solution and computational cost of the prefixed infrastructure optimization formulation (i.e., the upper-bound formulation), the full-size infrastructure optimization formulation (i.e., the baseline formulation), and the proposed multi-fidelity optimization formulation (i.e., the lower-bound formulation). We consider a lunar exploration campaign with multiple consecutive lunar missions, with a mission operation frequency of 120 days. The lunar landing area is in the equatorial region with lunar regolith @3% H_2O . The initial mass in low-Earth orbit (IMLEO) is used as the mission cost metric. It is a widely used mission cost measurement in past space logistics optimization literature [1, 2, 17]. As a baseline mission scenario, the FSPS is selected as the stationary power supply system on the lunar surface. The PV power system and energy storage system are considered as candidate power sources in space.

By fixing the number of human lunar missions to three and changing other mission scenario parameters, we can evaluate the performance of three optimization formulations

under different settings. The ISRU infrastructure design models shown in Table 16 are relatively conservative models. With the development of technology and material science, ISRU systems can have higher productivity and lower system structure mass. Table 18 compares the infrastructure optimization formulation performances with respect to ISRU productivity. It shows the results when the ISRU productivities are 100%, 125%, and 150% of the original design models. The mission cost errors illustrate the mission cost difference of solutions with respect to the results of the baseline full-size optimization formulation.

In Table 18, we can find that multi-fidelity optimization can provide a very accurate approximation of the full-size formulation at a significant computational cost reduction. The computation time reduction was more than 60%, whereas the performance loss is within 2.5%. This is enabled by packing commodity variables and eliminating infrastructure subsystem tradeoffs during space flights. The (small) solution difference between the multi-fidelity and full-size formulations is caused by the inability of the multi-fidelity formulation to distinguish different commodity types when they are packed together; for example, when two commodities are packed and then unpacked later on, we lose the information about the original mass ratio between these two commodities, which can lead to an overoptimistic solution.

On the other hand, the upper-bound solutions provided by the prefixed optimization formulation are much larger than optimal solutions. The physical meaning of the prefixed infrastructure optimization is that it ignores the infrastructure subsystem trade studies and their interactions with space mission planning. It considers the infrastructure as an integrated system. We can still size the infrastructure; however, the mass ratios between infrastructure subsystems are fixed in advance before considering space logistics. Therefore, it can provide an upper-bound, feasible solution, which is significantly larger than the optimal solution. It is also the fastest method among three infrastructure

optimization formulations because it has the least variables and constraints and explores the smallest design space.

Table 18 - Comparison of formulation performances w.r.t. ISRU productivity.

ISRU productivity index	Optimization formulation	Mission cost (IMLEO), kg	Mission cost errors	Computation time, s	Computation time reduction
100% (default)	Prefixed (Upper Bound)	565,622.9	33.7%	110.9	-89.6%
	Full-size (Baseline)	422,930.7	— —	1,062.3	— —
	Multi-fidelity (Lower Bound)	414,393.7	-2.0%	92.5	-91.3%
125%	Prefixed (Upper Bound)	528,563.7	33.6%	91.1	-92.0%
	Full-size (Baseline)	395,422.6	— —	1,135.7	— —
	Multi-fidelity (Lower Bound)	394,302.7	-0.3%	301.9	-73.4%
150%	Prefixed (Upper Bound)	513,612.6	37.1%	25.7	-95.7%
	Full-size (Baseline)	374,732.9	— —	592.2	— —
	Multi-fidelity (Lower Bound)	366,229.3	-2.3%	246.8	-58.3%

We can vary the problem complexity by changing the number of human lunar missions or the rocket launch frequency. If we fix the ISRU productivity as normal and

increase the number of human lunar missions from 3 to 4 and 5, the mission planning results are shown in Table 19. It shows that the mission cost errors of the multi-fidelity optimization with respect to the full-size optimization are within 2%. Both the multi-fidelity optimization and the prefixed optimization formulations are significantly faster than the full-size optimization formulation (i.e., >90% computation time reduction).

Table 19 - Optimization formulation performance comparison.

Number of human lunar missions	Optimization formulation	Mission cost (IMLEO), kg	Mission cost errors	Computation time, s	Computation time reduction
3 (default)	Prefixed (Upper Bound)	565,622.9	33.7%	110.9	-89.6%
	Full-size (Baseline)	422,930.7	— —	1,062.3	— —
	Multi-fidelity (Lower Bound)	414,393.7	-2.0%	92.5	-91.3%
4	Prefixed (Upper Bound)	671,716.3	31.3%	321.3	-96.7%
	Full-size (Baseline)	511,476.6	— —	9,607.4	— —
	Multi-fidelity (Lower Bound)	509,792.9	-0.3%	439.8	-95.4%
5	Prefixed (Upper Bound)	774,626.1	29.7%	693.8	-98.4%
	Full-size (Baseline)	597,300.8	— —	42,675.8	— —
	Multi-fidelity (Lower Bound)	596,347.8	-0.2%	2,074.1	-95.1%

We can also fix the number of human lunar missions to three and the ISRU productivity as normal, then change the launch frequency to evaluate its impact on ISRU infrastructure design, especially the storage system design. As there is a 120-day long human lunar exploration at the end of each year, the human lunar mission begins on day 240 in each year. By varying the rocket launch frequency interval to 60, 120 (default), or 240 days, there are 3, 1, or 0 extra cargo mission opportunities before each human lunar mission. The formulation performance comparison under different launch frequencies is shown in Table 20.

Table 20 shows that the performance of the multi-fidelity optimization formulation is stable. The mission cost errors are always within 2% compared with the optimal solutions from the full-size optimization formulation. If we observe the computation times in Table 19 and Table 20, we can analyze a general trend in the computational time saving by the multi-fidelity formulation. In Table 19, as the number of human lunar missions increases, the computation time reduction of the multi-fidelity formulation increases slightly from 91% to 95%. In Table 20, as the rocket launch opportunity interval decreases (i.e., from 240 to 60), the time steps considered in the optimization increase significantly, and the computation time reduction of the multi-fidelity formulation increases from 70% to more than 95%. These observations show that the proposed multi-fidelity optimization formulation achieves a large computational time saving compared with the full-size formulation for complex space mission design problems.

Table 20 - Comparison of formulation performances w.r.t. the launch frequency.

Launch frequency, day	Optimization formulation	Mission cost (IMLEO), kg	Mission cost errors	Computation time, s	Computation time reduction
240	Prefixed (Upper Bound)	697,800.9	65.0%	7.1	-94.8%
	Full-size (Baseline)	422,930.7	— —	135.9	— —
	Multi-fidelity (Lower Bound)	414,393.7	-2.0%	39.9	-70.6%
120 (default)	Prefixed (Upper Bound)	565,622.9	33.7%	110.9	-89.6%
	Full-size (Baseline)	422,930.7	— —	1,062.3	— —
	Multi-fidelity (Lower Bound)	414,393.7	-2.0%	92.5	-91.3%
60	Prefixed (Upper Bound)	480,705.3	13.7%	604.9	-98.2%
	Full-size (Baseline)	422,926.5	— —	33,383.0	— —
	Multi-fidelity (Lower Bound)	414,388.1	-2.0%	1,581.9	-95.3%

Moreover, the results also show that the launch frequency and the sizing of infrastructure storage systems need to be considered concurrently to find the optimal infrastructure design. With a higher launch frequency, a smaller storage system is needed because resources produced by the infrastructure can be delivered to other destinations

through spacecraft when mission time windows are open. Keeping this intuition in mind, the storage system design in the prefixed optimization formulation is pre-set to be able to store the exact amount of resources produced between two mission time windows. For example, if the launch frequency is 240 days, then the storage system in the prefixed optimization formulation is exactly able to store the resources produced in 240 days. In Table 20, the mission cost results by the full-size and the multi-fidelity optimization formulations show that the launch frequency has a limited influence on mission costs for this mission scenario. However, the mission cost from the prefixed optimization formulation decreases significantly as the launch frequency increases, which leads to a decrease in infrastructure storage system size. This result shows that this mission scenario may prefer small infrastructure storage systems.

To confirm this hypothesis, we conduct a sensitivity analysis on the ISRU storage system sizing under the default launch frequency (i.e., 120 days). The results are shown in Table 21. We find that as we decrease the storage system size, the mission costs obtained through the prefixed optimization formulation decrease dramatically until the storage system is too small to make the mission feasible. Note that our full-size formulation's solution is still much better than any of the prefixed formulations tested here. This result shows that our proposed interdisciplinary space infrastructure optimization methods can optimize the ISRU storage size as well as any other ISRU subsystems by concurrently capturing the detailed interactions between each infrastructure subsystem and space transportation mission planning in an optimal way. The optimal subsystem designs cannot be achieved by considering space infrastructure design independently in advance and treating it as a black box in space logistics.

Table 21 - Sensitivity analysis of ISRU storage system sizing.

Optimization formulation	ISRU storage system size	Mission cost (IMLEO), kg	Mission cost errors	Computation time, s	Computation time reduction
Prefixed (Upper Bound)	100%	565,622.9	33.7%	110.9	-89.6%
	80%	524,412.9	24.0%	41.5	-96.1%
	60%	494,243.2	16.9%	37.2	-96.5%
	40%	467,241.3	10.5%	59.4	-94.4%
	20%	444,414.1	5.1%	151.2	-85.8%
	0%	<i>infeasible</i>	— —	— —	— —
Full-size (Baseline)	— —	422,930.7	— —	1,062.3	— —
Multi-fidelity (Lower Bound)	— —	414,393.7	-2.0%	92.5	-91.3%

5.5 Chapter Summary

This chapter proposes a system-level space infrastructure and logistics mission design optimization framework to perform architecture trade studies. A new space infrastructure logistics optimization problem formulation is proposed that considers infrastructure subsystems' internal interactions and their external synergistic effects with space logistics simultaneously. A natural implementation of this formulation is referred to as the full-size formulation, which explores a larger trade space and thus provides the same or a better (i.e., lower-cost) solution than the prefixed formulation. However, the inherent limitation of this full-size formulation is its prohibitive computational cost for complex systems. In response to this challenge, another new multi-fidelity optimization formulation is developed by varying the granularity of the commodity type definition over the network graph. The developed multi-fidelity formulation can find an approximation lower-bound

solution to the full-size problem computationally efficiently with little sacrifice in the solution quality.

A multi-mission human lunar exploration campaign case study shows the consistent improvement of the multi-fidelity optimization formulation in computational efficiency. For the tested cases, the multi-fidelity optimization formulation found solutions that are within 2-3% of those of the full-size optimization formulation with a significant computational time reduction (>90% for the majority of the tested cases). The sensitivity analysis of launch frequency demonstrates the value of the proposed interdisciplinary infrastructure optimization method.

CHAPTER 6. FLEXIBILITY MANAGEMENT VIA DECISION RULES

The space logistics mission planning frameworks proposed in Chapters 3, 4, and 5 mainly focus on the transportation operation and system performance under deterministic environments. These methods tend to give overly optimistic designs and bias anticipated mission performances under stochastic mission operation environments. To handle this issue, this chapter proposes a flexibility management framework for space logistics leveraging decision rules and multi-stage stochastic programming. In this research, decision rules are formulated focusing on the uncertainties of rocket launch delays. However, the proposed decision rule formulation can also be easily extended to integrate with other space logistics optimization methods and handling different types of uncertainty sources. A case study on crewed space station resupply missions is established to demonstrate how flexible space mission designs achieve greater mission performance under uncertainty as compared to mission concepts developed under deterministic assumptions.

The remainder of this chapter is organized as follows. Section 6.1 first introduces the problem setting and proposes the formulation of decision rules for space logistics mission planning problems. The performance of the proposed flexibility management framework is then demonstrated in Sec. 6.2 through a space station resupply mission example. Finally, Sec. 6.3 concludes the chapter.

6.1 Methodology

6.1.1 Problem Setting

In this chapter, we consider a problem of space logistics mission planning under uncertain rocket launch delay. The logistics requirement is to support persistent scientific missions/experiments on space stations by regular rocket launches. However, the rocket launch may delay, which would impact the operation of space missions. We assume that the space missions/experiments to be supplied are time-sensitive so that the supply shortage influences the operating time of these missions within the planned mission period. The total length of the mission period is fixed regardless of the launch delay, which means the mission duration cannot be extended even if it is temporarily paused due to the shortage of scientific instruments and maintenance spares. Thus, a temporary supply shortage reduces the time that astronauts can spend on the experiments or maintenance, resulting in less available operating time to support the mission performance. Note that this assumption is not always true for any space missions. For space missions with a specific time window, the mission can be non-extendable; whereas some space experiments may be extended with no or little penalty, such as educational activities. In reality, the penalty may also be in the format of extra cost instead of the operating time loss. In this chapter, we presume this assumption to simplify the analysis process of the mission planning and the structure of decision rules.

To mitigate such operating time loss, we can launch more supplies in earlier launches and maintain them as safety stocks for later missions. These safety stocks are buffers to temporarily support space activities. Launching more safety stocks can decrease the operating time loss but increase mission costs in earlier space missions. Therefore, the decision maker's goal is a tradeoff between the mission cost and performance (i.e., operating time loss)¹. The amount of safety stock for each rocket launch is the outcome of decisions. Note that the focus of this research is on the scientific experiment cost and

¹ Crew time also has been used as a metric of space missions in some previous literature such as SpaceNet [15].

performance; the crew consumables or other mandatory supplies are assumed to be sufficiently stocked on the stations and thus are not considered as part of the tradeoff.

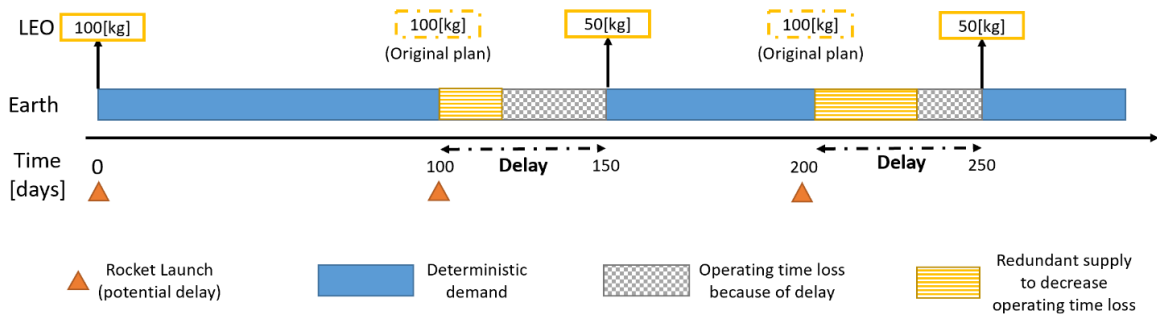


Figure 29 - How delay and safety stock influence space missions (an example).

Figure 29 shows one example of how the rocket launch delay and safety stock influence space missions in our problem. Consider a case where there is a rocket launch every 100 days to ISS. For this example, we assume ISS needs materials to support an in-space experiment that is consumed at a rate of 1 kg/day. If all supply missions are launched as planned, each rocket will deliver 100 kg of material to ISS, which is enough to support a 100-day duration space mission. If there is a 50-day delay in the second and the third launches as shown in Figure 29, we only need to launch 50 kg of material to support the rest space experiment in each launch. However, because of the shortage of material on ISS, the space experiment is paused during the 50-day delays. If there is no safety stock on ISS, two 50-day delays result in the suspension of the space experiment for 100 days due to the lack of supply. Our space mission is still terminated on the originally scheduled end date. As a result, the actual time for the experiment, which is originally planned as 300 days long, only runs for 200 days because of the shortage of materials. This results in 100 days of operating time loss due to the crew not having the material available to run the science experiment for the full 300 days duration. If we launched more material in the first and the second rocket launches, the safety stock can partially support the space experiments and decrease the operating time loss when a rocket launch delay occurs in subsequent missions.

However, the mission costs for the first and the second rocket launch increase to launch these additional safety stock materials.

6.1.2 Scenario Generation Model

The scenario generation model provides launch dates for the cargo and crew to support mission requirements as uncertainty inputs. The launch delay model is prescribed as a continuous cumulative probability function created from available data. To limit the number of possible mission outcomes to a computationally manageable number, we perform inverse transform sampling to generate uncertainty mission scenarios based on the continuous launch delay probability function. In the later case study, we consider the case where each launch delay is independent, but the approach can be applied to dependent launch delays as well. Because we conduct a random sampling method, the probability of realization for each possible outcome is equivalent. If there are n scenarios in total, then the probability is $1/n$ for each mission scenario.

6.1.3 Flexibility Management Background and Overview

To manage space mission operations under complex uncertain mission scenarios, we need to incorporate uncertainty mitigation methods in space logistics optimization. Multiple analytical tools have been introduced in past literature to deal with uncertainties in engineering fields, such as the backward induction and dynamic programming by Buurman et al. [78], the optimization-based hybrid real options analysis by Jiao [79], and the simulation-based decision analysis by de Neufville et al. [80]. However, these methods provide decisions as outcomes of the model. There is no general decision strategy for managers to follow when a different scenario appears throughout the system life cycle. On the other hand, the decision rule, also called implementable policy, maps the observations of uncertainty data to the decisions. Cardin et al. [51] showed that for a highly structured

problem, optimization based on decision rules can provide a good approximation of optimal solution that is typically found by real option analysis techniques, while the solutions of decision rule were more practical and intuitive for decision-makers to use in practical applications. Numerical experiments on waste-to-energy systems in past literature showed that decision rules-based methods can find a very close solution to traditional uncertainty analysis methods with a significantly reduced computational time required [51]. These results also showed that decision rules are suitable to analyze complex systems with multiple sources of uncertainties. Multiple decision strategies can also be considered concurrently.

The decision rule is a gradient-free direct policy search method. Compared with the value-based method in reinforcement learning, direct policy search solves the problem by searching the policy space directly without the value estimation of states or state-action pairs. For certain problems, including the space logistics problem considered in this research, where we have a clear idea about what the nature of policy representations might look like, constructing good policies is often easier than modeling good state functions. Another benefit of the decision rule method is that it does not rely on gradient information. It can be explicitly integrated with the space logistics mission planning framework through mixed-integer linear programming, where a global optimum can be achieved. Compared with other stochastic sequential decision-making approaches, considering uncertainties via decision rules also avoids the dramatic increase of computational complexity.

There are multiple types of decision rules that are suitable for different uncertainty problems. Four classes of decision rules were identified and studied by Garstka and Wets via case examples [81], including zero-order, linear, safety-first, and conditional-go decision rules. A detailed introduction about decision rules is provided in Ref. [51] and [81]. The conditional-go decision rule has been used in generation expansion planning problems [82]; whereas the linear decision rule has been used in electrical reserve operation

problems [83]. In this research, we focus on the uncertainty from rocket launch delays, which is contrary to traditional uncertainty in other engineering fields [51, 81-83]. When a rocket launch delay occurs, we have already missed the opportunity to respond to this situation. We have to make decisions in previous launches to counter the uncertainty before we observe the delay.

To identify the influence of launch delay on mission objectives and determine the amount of safety stock for each launch, the decision rule in rocket launch delay problems is formulated based on a combination of the conditional-go decision rule and the linear decision rule through integer programming (IP). The amount of safety stock is the decision variable. The conditional-go decision rule identifies whether previous safety stock on board is enough to counter the launch delay and the penalty of launch delay to the mission performance. The linear decision rule finds the additional supply needed to be launched in the upcoming mission. The developed decision rule can also be used in other uncertainties in space logistics problems, such as spacecraft flight or docking delay and demand change in space missions.

To balance mission cost and mission performance for flexibility management, we consider a multi-objective optimization solved through the weighted sum method. The initial mass in low-Earth orbit (IMLEO) and crew operating time loss are used as the metrics for mission cost and mission performance. IMLEO is widely used as a space logistics mission cost metric in previous studies, such as space logistics mission planning frameworks [1, 2, 17] and the Mars mission design reference architecture by NASA [65]. The crew operating time loss, as discussed earlier, is used to represent space mission performance. More specifically, the operating time loss is calculated as the summation of the crew time loss for each commodity, representing its dependence on both the length of launch delays and the crew time task assignment. For example, astronauts may spend a different length of time on scientific experiments and maintenance. The consumption rate

of scientific instruments and maintenance spares may also be different. Therefore, for the same length of supply shortage, the lack of scientific instruments or maintenance spares can cause different lengths of operating time loss.

The flexibility management framework can be expressed as the following optimization problem.

Minimize:

$$\sum_{\xi \in \mathcal{K}} q_{\xi} \mathcal{J}_{\xi}(\mathbf{x}_{\xi}) + \varphi \sum_{\xi \in \mathcal{K}} q_{\xi} \mathcal{Z}_{\xi}(\mathbf{R}) \quad (77)$$

Subject to:

$$f(\mathbf{x}_{\xi}, \mathbf{R}, \mathbf{y}) \leq 0 \quad (78)$$

$$g(\mathbf{x}_{\xi}, \mathbf{R}, \mathbf{y}) = 0 \quad (79)$$

where \mathcal{J}_{ξ} is the mission cost function for mission scenario ξ from the space logistics problem; \mathcal{Z}_{ξ} represents the operating time loss for mission scenario ξ due to the lack of supplies determined from the decision rule formulation. The decision variables \mathbf{x}_{ξ} and \mathbf{R} denotes the space transportation commodity flow and the safety stock for space logistics and decision rule, respectively. Note that \mathbf{x}_{ξ} and \mathbf{R} are dependent on each other through the constraints, and so need to be optimized concurrently. In the constraints, \mathbf{y} represents other variables in mission planning that do not directly impact the value of objectives. In this problem, the mission cost \mathcal{J}_{ξ} , space logistics decision variable \mathbf{x}_{ξ} , and the mission performance \mathcal{Z}_{ξ} all depend on the mission scenario ξ , while the decision rule variable \mathbf{R} is independent of mission scenarios as it is a general implementable policy that can be applied

to any scenario. We define a mission scenario set \mathcal{K} , then the probability for each scenario is $q_{\xi} = 1/|\mathcal{K}|$.

In equation 77, φ is the weighting coefficient to determine how important the mission performance is compared with the mission cost. If φ is infinity, decision-makers will prepare for the worse scenario, where safety stock levels reach maximum for each launch. By changing the weighting coefficient φ , we can get Pareto front solutions between the expected IMLEO \mathcal{J} and the expected operating time loss \mathcal{Z} based on different strategies. Note that we claim the solutions as the Pareto front since all the decision rule solutions obtained by the weighted sum method are all on the Pareto-optimal front. However, the weighted sum method cannot guarantee to find all Pareto-optimal solutions, particularly in the case of a nonconvex objective space. We use the weighted sum method because the objective function keeps linear that guarantees a global optimum of the optimization. Moreover, it also avoids extra constraints to ensure computational efficiency. The constraints equations 78 and 79 are general constraint expressions for space logistics and decision rules that will be introduced in detail in the following sections.

In the following sections, we first introduce the space logistics optimization model to calculate \mathcal{J} based on mission demands and decision rules. Then, we introduce the proposed decision rule method to determine \mathcal{Z} based on the stochastic mission operation environment. Finally, we integrate decision rules into space logistics mission planning through the optimization problem equation 77 and establish the flexibility management framework.

6.1.4 Mission Cost Evaluation through Space Logistics

This section introduces the space logistics model to calculate the mission cost (i.e., IMLEO) \mathcal{J} . The space logistics section in the flexibility management framework is

developed based on network-based multi-commodity flow models as introduced in Chapters 3, 4, and 5. In this chapter, we follow the same definitions of notations in the space logistics optimization formulation. In addition, we also need to define a set of scenarios \mathcal{K} (index ξ), where each scenario ξ has a probability of q_ξ (i.e., $\sum_{\xi \in \mathcal{K}} q_\xi = 1$) to occur. The decision variable for space logistics optimization is the commodity flow variable $\mathbf{x}_{\xi v i j t}$, representing the commodity flow from node i to node j using spacecraft v at time t in the scenario ξ . For each scenario ξ , we need a demand parameter $\mathbf{d}_{\xi i t}$, representing demands or supplies of different commodities in node i at time t .

Besides the pre-planned mission demands and supplies defined in $\mathbf{d}_{\xi i t}$, we also need another demand variable $\mathbf{u}_{\xi i t}$, representing additional commodities required to be delivered to maintain the level of required safety stocks for each rocket launch. It is an interface variable to connect space logistics optimization and decision rules. The value of this variable is positive only at the node of space stations. We define a subset of the node set \mathcal{N} for space stations, $\widehat{\mathcal{N}}$. Therefore, we have

$$\mathbf{u}_{\xi i t} = \begin{cases} \mathbf{0}_{p \times 1} & \text{if } i \in \mathcal{N} \setminus \widehat{\mathcal{N}} \\ \mathbf{u}_{\xi i t}, & \text{otherwise} \end{cases}$$

where the value of $\mathbf{u}_{\xi i t}$, when $i \in \widehat{\mathcal{N}}$, is determined by the decision rule for each space station.

Then, the formulation for space logistics optimization under uncertainties is shown as follows.

Minimize:

$$\sum_{\xi \in \mathcal{K}} q_\xi \mathcal{J}_\xi = \sum_{\xi \in \mathcal{K}} q_\xi \left(\sum_{t \in \mathcal{T}} \sum_{(v, i, j) \in \mathcal{A}} \mathbf{c}_{v i j t}^T \mathbf{x}_{\xi v i j t} \right) \quad (80)$$

Subject to:

$$\sum_{(v,j):(v,i,j) \in \mathcal{A}} \mathbf{x}_{\xi v i j t} - \sum_{(v,j):(v,j,i) \in \mathcal{A}} Q_{v j i} \mathbf{x}_{\xi v j i (t - \Delta t_{j i})} \leq \mathbf{d}_{\xi i t} - \mathbf{u}_{\xi i t} \quad \forall i \in \mathcal{N} \quad \forall t \in \mathcal{T} \quad \forall \xi \in \mathcal{K} \quad (81)$$

$$H_{v i j} \mathbf{x}_{\xi v i j t} \leq \mathbf{0}_{l \times 1} \quad \forall (v, i, j) \in \mathcal{A} \quad \forall t \in \mathcal{T} \quad \forall \xi \in \mathcal{K} \quad (82)$$

$$\begin{cases} \mathbf{x}_{\xi v i j t} \geq \mathbf{0}_{p \times 1} & \text{if } t \in W_{\xi i j} \\ \mathbf{x}_{\xi v i j t} = \mathbf{0}_{p \times 1} & \text{otherwise} \end{cases} \quad \forall (v, i, j) \in \mathcal{A} \quad \forall t \in \mathcal{T} \quad \forall \xi \in \mathcal{K} \quad (83)$$

$$\mathbf{x}_{\xi v i j t} \in \mathbb{R}_{\geq 0}^{p \times 1} \quad \forall (v, i, j) \in \mathcal{A} \quad \forall t \in \mathcal{T} \quad \forall \xi \in \mathcal{K}$$

In this formulation, equation 80 is the objective function, which calculates the expected mission cost, where $q_{\xi} = 1/\|\mathcal{K}\|$. When evaluating the expected IMLEO, the cost coefficients for the launch arcs are set as one, while the rest are set as zero. Equation 81 is the mass balance constraint that limits commodity flows to satisfy the demands. The second term $Q_{v j i} \mathbf{x}_{\xi v j i (t - \Delta t_{j i})}$ represents commodity transformations during space transportation and space mission operations, including propellant burning, crew consumables, and resource generations by space infrastructures. The additional supply $\mathbf{u}_{\xi i t}$ is the interface variable connecting space logistics and decision rules. Equation 82 is the spacecraft concurrency constraint, which defines the upper bound of commodity flows limited by the spacecraft propellant capacity and the payload capacity. l is the number of concurrency constraints considered in mission planning. Equation 83 is the time window constraint defined by the time window vector $W_{\xi i j}$.

6.1.5 Operating Time Loss Evaluation through Decision Rules

This section introduces the decision rule method to determine the mission performance metric (i.e., crew operating time loss) Z . For a flexibility management problem for multiple space stations, decision rules need to be established independently for each space station. For simplicity, in this section, we only show the decision rule formulation for one space station. The decision rules for multiple space stations and the combination with space logistics will be discussed in the next section. Thus, we omit the node index in the additional supply variable and rewrite it as $\mathbf{u}_{\xi t}$.

For a space station, we define a set of rocket launches \mathcal{L} (index θ). The safety stock, denoted by \mathbf{R}_θ for the rocket launch θ , is the decision rule variable to be optimized. The decision rule can be expressed as “launch up to \mathbf{R}_θ kg safety stock in rocket launch $\theta - 1$ ”. After observing the delay in rocket launch $\theta - 1$, when the system is available to launch a rocket again, decision-makers prepare safety stock for the next mission. Now, since launch delay $\theta - 1$ has already occurred, decision-makers know the amount of remaining stock $\mathbf{B}_{\xi(\theta-1)}$ at the destination, where ξ is the index of uncertainty scenario. Based on the decision rule variable \mathbf{R}_θ , which is the safety stock we have to maintain for launch θ , we can determine the additional supply $\mathbf{u}_{\xi t}$ that should be launched in addition to the necessary mission demand in launch $\theta - 1$, which is $\mathbf{R}_\theta - \mathbf{B}_{\xi(\theta-1)}$. However, there is a possibility that the remaining stock $\mathbf{B}_{\xi(\theta-1)}$ is larger than \mathbf{R}_θ , where no additional supply is needed. Therefore, the expression of additional supply is $\mathbf{u}_{\xi t} = \max(\mathbf{R}_\theta - \mathbf{B}_{\xi(\theta-1)}, \mathbf{0}_{p \times 1})$, where t is the time index in space mission planning formulation. This expression works when t is the time step at which launch $\theta - 1$ happens. Then, for each mission scenario ξ , we know the available safety stock prepared for launch θ , defined as $\mathbf{r}_{\xi l} = \max(\mathbf{R}_\theta, \mathbf{B}_{\xi(\theta-1)})$. The available safety stock $\mathbf{r}_{\xi l}$ can also be written as $\mathbf{r}_{\xi l} = \mathbf{u}_{\xi t} + \mathbf{B}_{\xi(\theta-1)}$. Based on the available safety stock for each scenario ξ , we can calculate the length of the supply shortage $\mathbf{h}_{\xi \theta}$ for each launch delay, in the unit of days. In this

research, we measure mission performance through the total operating time loss \mathcal{Z} , which can be then calculated based on $\mathbf{h}_{\xi\theta}$. The optimization framework eventually outputs \mathbf{R}_θ as the decision rule result. Decision-makers can make decisions directly and immediately after a launch delay occurs based on the value of \mathbf{R}_θ .

Besides the aforementioned notations, we also need to define the following parameters for the decision rule formulation.

\mathbf{c}'' = operating time loss weighting coefficient for different commodities.

$D_{\xi l}$ = length of the launch delay, days.

$\boldsymbol{\eta}$ = commodity consumption rate, kg/day.

$\boldsymbol{\psi}$ = commodity shortage penalty.

Then, the decision rule optimization can be formulated as follows.

Minimize:

$$\sum_{\xi \in \mathcal{K}} q_\xi \mathcal{Z}_\xi = \sum_{\xi \in \mathcal{K}} q_\xi \sum_{\theta \in \mathcal{L}} \mathbf{c}''^T \mathbf{h}_{\xi\theta} \quad (84)$$

Subject to:

$$\begin{cases} \mathbf{u}_{\xi t} = \max(\mathbf{R}_\theta - \mathbf{B}_{\xi(\theta-1)}, \mathbf{0}_{p \times 1}) & \text{if } t = \zeta(\theta - 1) \\ \mathbf{u}_{\xi t} = \mathbf{0}_{p \times 1} & \text{otherwise} \end{cases} \quad \forall t \in \mathcal{T} \quad \forall \theta \in \mathcal{L} \quad \forall \xi \in \mathcal{K} \quad (85)$$

$$\begin{aligned} \mathbf{h}_{\xi\theta} &= \max((D_{\xi\theta} \mathbf{1}_{p \times 1} - (\mathbf{u}_{\xi t} + \mathbf{B}_{\xi(\theta-1)}) \oslash \boldsymbol{\eta}) \circ \boldsymbol{\psi}, \mathbf{0}_{p \times 1}) \quad \forall \theta \in \mathcal{L} \quad \forall t \\ &= \zeta(\theta - 1) \quad \forall \xi \in \mathcal{K} \end{aligned} \quad (86)$$

$$\mathbf{B}_{\xi\theta} = \max((\mathbf{u}_{\xi t} + \mathbf{B}_{\xi(\theta-1)}) - D_{\xi\theta}\boldsymbol{\eta}, \mathbf{0}_{p \times 1}) \quad \forall \theta \in \mathcal{L} \quad \forall t = \zeta(\theta - 1) \quad \forall \xi \in \mathcal{K} \quad (87)$$

$$\mathbf{R}_\theta, \mathbf{u}_{\xi t}, \mathbf{h}_{\xi\theta}, \mathbf{B}_{\xi\theta} \in \mathbb{R}_{\geq 0}^{p \times 1} \quad \forall \theta \in \mathcal{L} \quad \forall \xi \in \mathcal{K}$$

Equation 84 is the objective function, which calculates the expected operating time loss, where $q_\xi = 1/\|\mathcal{K}\|$. Equation 85 determines the value of the interface variable $\mathbf{u}_{\xi t}$. It connects the additional supply $\mathbf{u}_{\xi t}$ in launch θ and the remaining stock $\mathbf{B}_{\xi(\theta-1)}$ after launch $\theta - 1$ with the expected safety stock \mathbf{R}_θ for mission θ . $t = \zeta(\theta - 1)$ is the rocket launch time index function, which outputs the time step of each rocket launch. This function converts the time index t in the space logistics formulation into the rocket launch index θ in the decision rule section. Equation 86 calculates the operating time loss because of the shortage of certain commodities. Note that, \oslash and \circ are Hadamard operators. They are the division and product of each element with the same indices between two matrices. These two matrices should have the same dimension. If the safety stock is sufficient to support the space mission during delays, $D_{\xi\theta}\mathbf{1}_{p \times 1} - (\mathbf{u}_{\xi t} + \mathbf{B}_{\xi(\theta-1)}) \oslash \boldsymbol{\eta}$ is negative, which then enforces the operating time loss to be zero. Equation 87 calculates the level of remaining stock. If the safety stock is not sufficient to support a launch delay, the remaining supplies $\mathbf{B}_{\xi\theta}$ are zeros. But if there are enough available safety stock $\mathbf{r}_{\xi\theta} = \mathbf{u}_{\xi t} + \mathbf{B}_{\xi(\theta-1)}$ to support the mission during a launch delay, there are some remaining supplies after this delay. The remaining commodities become part of the safety stock for the next launch.

Note that, even though the constraints in the above decision rule optimization formulation are all equality constraints, they are all nonlinear functions. To solve this problem effectively, we can linearize the constraints by introducing two binary variable vectors $\boldsymbol{\mu}_{1,\xi\theta}$ and $\boldsymbol{\mu}_{2,\xi\theta}$ to represent whether there is enough safety stock to support the mission operation and whether additional supplies are needed for a specific rocket launch mission, respectively.

$$\boldsymbol{\mu}_{1,\xi\theta} = \begin{cases} 0 & \text{if } D_{\xi\theta} \leq (\mathbf{u}_{\xi\theta} + \mathbf{B}_{\xi(\theta-1)}) \oslash \boldsymbol{\eta} \\ 1 & \text{if } D_{\xi\theta} > (\mathbf{u}_{\xi\theta} + \mathbf{B}_{\xi(\theta-1)}) \oslash \boldsymbol{\eta} \end{cases}$$

$$\boldsymbol{\mu}_{2,\xi\theta} = \begin{cases} 0 & \text{if } \mathbf{B}_{\xi(\theta-1)} \leq \mathbf{R}_\theta \\ 1 & \text{if } \mathbf{B}_{\xi(\theta-1)} > \mathbf{R}_\theta \end{cases}$$

Define a large constant scalar \mathcal{M} , the decision rule formulation can be linearized as follows.

Minimize:

$$\sum_{\xi \in \mathcal{K}} q_\xi \mathcal{Z}_\xi = \sum_{\xi \in \mathcal{K}} q_\xi \sum_{\theta \in \mathcal{L}} \mathbf{c}''^T \mathbf{h}_{\xi\theta} \quad (88)$$

Subject to:

$$\begin{cases} \mathbf{u}_{\xi t} \geq \mathbf{R}_\theta - \mathbf{B}_{\xi(\theta-1)} \\ \mathbf{u}_{\xi t} \leq \mathcal{M} \boldsymbol{\mu}_{2,\xi\theta} + \mathbf{R}_\theta - \mathbf{B}_{\xi(\theta-1)} & \text{if } t = \zeta(\theta - 1) \\ \mathbf{u}_{\xi t} \leq \mathcal{M}(\mathbf{1}_{p \times 1} - \boldsymbol{\mu}_{2,\xi\theta}) \\ \mathbf{u}_{\xi t} = \mathbf{0}_{p \times 1} & \text{otherwise} \end{cases} \quad \forall t \in \mathcal{T} \quad \forall \theta \in \mathcal{L} \quad \forall \xi \in \mathcal{K} \quad (89)$$

$$\begin{cases} \mathbf{h}_{\xi\theta} \geq (D_{\xi\theta} \mathbf{1}_{p \times 1} - (\mathbf{u}_{\xi t} + \mathbf{B}_{\xi(\theta-1)}) \oslash \boldsymbol{\eta}) \circ \boldsymbol{\psi} \\ \mathbf{h}_{\xi\theta} \leq \mathcal{M}(\mathbf{1}_{p \times 1} - \boldsymbol{\mu}_{1,\xi\theta}) + (D_{\xi\theta} \mathbf{1}_{p \times 1} - (\mathbf{u}_{\xi t} + \mathbf{B}_{\xi(\theta-1)}) \oslash \boldsymbol{\eta}) \circ \boldsymbol{\psi} \\ \mathbf{h}_{\xi\theta} \leq \mathcal{M} \boldsymbol{\mu}_{1,\xi\theta} \end{cases} \quad \forall \theta \quad (90)$$

$$\in \mathcal{L} \quad \forall t = \zeta(\theta - 1) \quad \forall \xi \in \mathcal{K}$$

$$\begin{cases} \mathbf{B}_{\xi\theta} \geq (\mathbf{u}_{\xi t} + \mathbf{B}_{\xi(\theta-1)}) - D_{\xi\theta} \boldsymbol{\eta} \\ \mathbf{B}_{\xi\theta} \leq \mathcal{M} \boldsymbol{\mu}_{1,\xi\theta} + (\mathbf{u}_{\xi t} + \mathbf{B}_{\xi(\theta-1)}) - D_{\xi\theta} \boldsymbol{\eta} \\ \mathbf{B}_{\xi\theta} \leq \mathcal{M}(\mathbf{1}_{p \times 1} - \boldsymbol{\mu}_{1,\xi\theta}) \end{cases} \quad \forall \theta \in \mathcal{L} \quad \forall t = \zeta(\theta - 1) \quad \forall \xi \in \mathcal{K} \quad (91)$$

$$\begin{cases} D_{\xi\theta} \mathbf{1}_{p \times 1} - (\mathbf{u}_{\xi t} + \mathbf{B}_{\xi(\theta-1)}) \odot \boldsymbol{\eta} \geq \mathcal{M}(\boldsymbol{\mu}_{1,\xi\theta} - \mathbf{1}_{p \times 1}) \\ D_{\xi\theta} \mathbf{1}_{p \times 1} - (\mathbf{u}_{\xi t} + \mathbf{B}_{\xi(\theta-1)}) \odot \boldsymbol{\eta} \leq \mathcal{M} \boldsymbol{\mu}_{1,\xi\theta} \end{cases} \quad \forall \theta \in \mathcal{L} \quad \forall t \quad (92)$$

$$= \zeta(\theta - 1) \quad \forall \xi \in \mathcal{K}$$

$$\begin{cases} \mathbf{B}_{\xi(\theta-1)} - \mathbf{R}_\theta \geq \mathcal{M}(\boldsymbol{\mu}_{2,\xi\theta} - \mathbf{1}_{p \times 1}) \\ \mathbf{B}_{\xi(\theta-1)} - \mathbf{R}_\theta \leq \mathcal{M} \boldsymbol{\mu}_{2,\xi\theta} \end{cases} \quad \forall \theta \in \mathcal{L} \quad \forall \xi \in \mathcal{K} \quad (93)$$

$$\mathbf{R}_\theta, \mathbf{u}_{\xi t}, \mathbf{h}_{\xi\theta}, \mathbf{B}_{\xi\theta} \in \mathbb{R}_{\geq 0}^{p \times 1} \quad \boldsymbol{\mu}_{1,\xi\theta}, \boldsymbol{\mu}_{2,\xi\theta} \in \{0,1\}^{p \times 1} \quad \forall \theta \in \mathcal{L} \quad \forall \xi \in \mathcal{K}$$

In this formulation, all constraints become linear constraints. They are equivalently linearized constraints of the original nonlinear equality constraints. The additional constraints equations 92 and 93 determines the value of binary variables $\boldsymbol{\mu}_{1,\xi\theta}$ and $\boldsymbol{\mu}_{2,\xi\theta}$.

6.1.6 Flexibility Management Framework for Space Logistics

Substituting the formulations to calculate \mathcal{J} and \mathcal{Z} proposed in Sec. 6.1.4 and Sec. 6.1.5 into equation 77, we combine decision rule with space logistics and obtain a flexibility management framework for space logistics mission design under uncertainties, shown as follows.

Minimize:

$$\begin{aligned} & \sum_{\xi \in \mathcal{K}} q_\xi \mathcal{J}_\xi + \varphi \sum_{\xi \in \mathcal{K}} q_\xi \mathcal{Z}_\xi \\ & = \sum_{\xi \in \mathcal{K}} q_\xi \left(\sum_{t \in \mathcal{T}} \sum_{(v,i,j) \in \mathcal{A}} \mathbf{c}_{vijt}^T \mathbf{x}_{\xi vijt} \right) \\ & + \varphi \sum_{\xi \in \mathcal{K}} q_\xi \sum_{\theta \in \mathcal{L}} \mathbf{c}''^T \mathbf{h}_{\xi\theta} \end{aligned} \quad (94)$$

Subject to:

Constraint set 1 (space logistics model)

equations 81-83

Constraint set 2 (decision rule)

For each space station $\forall i \in \hat{\mathcal{N}}$

equations 89-93

Equation 94 is the objective function. The first term calculates the value of expected mission cost J (i.e., IMLEO) and the second term calculates the expected value of mission performance Z (i.e., operating time loss).

This framework models the space logistics problem considering uncertainties as a MILP formulation. It is a single objective optimization formulation with weighted sum objectives. The flexibility management framework introduced in this section is suitable to be directly used for mission design under uncertainties in rocket launch delay and spacecraft flight delay. It can also be extended to consider other traditional uncertainty factors in space logistics problems.

In the next section, the performance of this flexibility management framework for space logistics is evaluated based on a space station resupply mission case study.

6.2 Case Study: Space Station Resupply Logistics

6.2.1 Space Station Resupply Mission Background

In this chapter, the performance of the flexibility management framework is evaluated based on a crewed space station resupply example mission in a lunar orbit. The

mission scenario is developed based on the data of past resupply missions for ISS and the planned Gateway concept [84].

6.2.1.1 Mission Demand

The example mission planning case study is a one-year multi-mission logistics to the space station. The case study considers a crew of four with four missions per year: two missions with cargo and crew and two missions with cargo only. A crew rotation will be performed during each crew mission. Each group of crew stays on the space station for six months. The goal of flexibility management is to satisfy the cargo demand for space activities while guaranteeing astronaut safety during space station operations. The estimated yearly cargo needs for the space station is up to 16,750 kg based on ISS pressurized cargo needs defined in the CRS2 Request for information [85]. The crew consumable requirement is defined as 17.1 kg/day for 4 crew based on NASA Design Reference Architecture 5.0 [65]. The remaining cargo is split between science and maintenance cargo. A review of the recent NASA CRS mission overviews (12/6/2015 through 6/13/2017) shows a nearly even split between science (37.2%) and maintenance cargo mass (36.4%) of the total cargo [43, 86-94] detailed in Table 22. For this example mission case study, it is expected that the initial maintenance needs of the considered lunar orbital station will be lower than the ISS assuming that it is significantly smaller than the ISS. Therefore, the prescribed cargo split is 66% for science and 33% for maintenance for the example scenario. The consumption rate for the science and maintenance cargo is assumed to be evenly distributed over the mission duration of one year.

We also need to set penalties for the shortage of science instruments and maintenance spares to measure the influences of rocket launch delays and determine the operating time loss. This penalty is relevant to the importance of commodities to the mission operation. We assume astronauts will spend 80% of their time performing

scientific experiments and 20% of their time performing maintenance on the space station. Thus, one day shortage of scientific instruments will lead to a 0.8 day operating time loss, while one day shortage of maintenance spares will lead to a 0.2 day operating time loss. We will perform a sensitivity analysis to evaluate the impact of the crew operating time assignment later. Based on these assumptions, our goal is to find the optimal amount of safety stock to reduce operating time loss while balancing the mission cost at the same time.

Table 22 - ISS CRS Cargo Manifest Mass by Category (Dec. 2015 to Jun. 2017).

Category	Mass, kg	% of total
Crew Supplies	4,893	26.4
Science Investigations	6,881	37.2
Other	6,746	36.4
Total (Including Packaging)	19,334.1	100

The orbit of the space station is considered to be the Near Rectilinear Halo Orbit (NRHO). It takes about 5 days to fly from LEO or back to LEO. The total ΔV from LEO to NRHO is 3.53 km/s, while the ΔV from NRHO to LEO is 3.51 km/s [95].

Based on the consumption rates of science instruments, maintenance spares, and crew consumables introduced above, the demands and supplies of this space station resupply mission are listed in Table 23. The mission plan is shown in Figure 30.

This research focuses on decision rule optimization and analysis. Therefore, for simplicity, in this case study, no spacecraft design is considered and an existing spacecraft, Centaur, is used throughout the mission. Centaur is the upper stage for United Launch Alliance's Atlas V rocket, with a 2,316 kg structure mass and 20,830 kg propellant capacity [55]. It uses liquid oxygen and liquid hydrogen as the propellant, with a specific impulse of 450.5 seconds.

Table 23 - Demand and Supply of the Resupply Mission.

Payload Type	Node	Demand Time, day	Supply
Crew, no.	Earth	0, 182	4
Crew, no.	Space Station	0, 182	-4
Science instrument, kg	Space Station	0, 91, 182, 273	- 1729
Maintenance spares, kg	Space Station	0, 91, 182, 273	- 891
Crew consumables, kg	Space Station	0, 91, 182, 273	- 1556
Crew, no.	Space Station	183, 365	4
Crew, no.	Earth	183, 365	-4
Science, maintenance, and crew consumables, kg	Earth	0-365	+∞

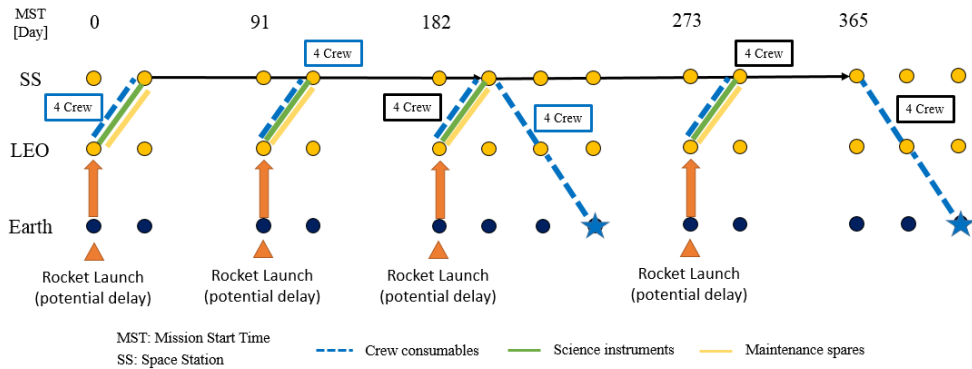


Figure 30 - Space Station Resupply Mission Plan.

6.2.1.2 Rocket Launch Delay Scenarios

Launch vehicle delay is one of the main uncertainty inputs for the flexibility management framework. For this case study, we build a cumulative distribution function (CDF) for rocket launch delay based on the available dataset in the format of a doubly truncated exponential function as shown in Appendix B, where the maximum delay is considered to be 90 days (i.e., the assumption is that if the delay is longer than 90 days, e.g., due to launch vehicle failures, we would replan the missions with a new optimization.)

For a multi-mission space campaign, we assume that the rocket launch delays are independent for each mission. The argument for this assumption is that rocket launches are typically scheduled to optimize cargo transportation following specific mission requirements and there can be multiple transportation service providers for a campaign. Thus, we perform inverse transform sampling for each rocket launch mission and combine generated launch delay sampling sets together to form mission scenarios.

For result analysis, the resulting decision rules and space logistics planning are evaluated using different sets of operating mission scenarios than those used for optimization. This is to ensure the generality of the resulting decision rules. Furthermore, when we generate the Pareto front of the expected mission cost and the expected mission performance, we evaluate all solutions on the Pareto front based on a common set of evaluation mission scenarios for a fair comparison.

6.2.2 Space Station Resupply Mission Analysis and Results

In this section, we analyze the performance of the proposed flexibility management framework and the regular pattern of decision rules for a space station resupply campaign. For this case study, the multi-stage stochastic problem is solved under uncertainty mission scenarios generated by the method as introduced above. Each scenario contains the launch delay information of four rocket launches.

In Figure 31, we first compare the Pareto fronts generated through different numbers of operating mission scenarios. The decision rules achieved through these mission scenario samples are evaluated based on the common evaluation sampling set with 256 mission scenarios. Results show that the sample size does not have much impact on the shape of the Pareto front. Thus, for computation efficiency, in the following analysis, we use a sample set with 128 operating mission scenarios to solve for decision rules and a different sample set with 256 evaluation scenarios to generate the Pareto front.

The decision rule strategies are also compared with traditional deterministic design strategies in Figure 31. When the mission performance weighting coefficient $\varphi = 0$, decision-makers only focus on the mission cost of the campaign. It is equivalent to the “design for the best case” scenario, where uncertainties are neglected during mission planning and the objective is to minimize the mission cost. It is the design with the most optimistic forecast. As the value of φ increases, mission performance becomes dominant in mission planning. The expected operating time loss decreases while the expected mission cost increases. When φ reaches infinity, decision-makers only focus on mission performance. It is equivalent to the “design for the worse case” scenario, where mission uncertainty is the only concern during mission planning and the objective is to minimize the operating time loss. As a result, the safety stocks are prepared to counter the longest possible launch delay scenario (i.e., 90 days delay in this case study). It is the design with the most conservative forecast. The design points considering the best and the worse uncertainty scenarios are at two ends of the Pareto front. They are the anchor points for the Pareto front.

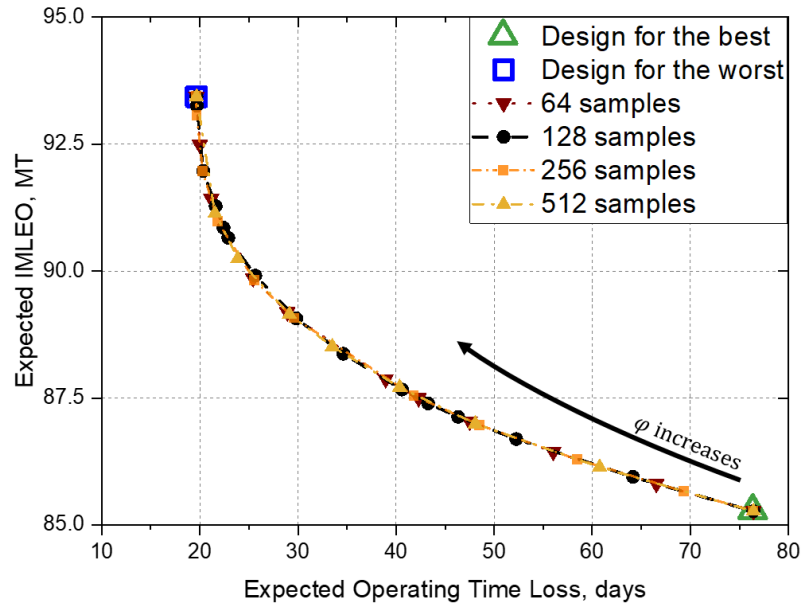


Figure 31 - Expected Operating Time Loss vs. Expected IMLEO Pareto Front.

Moreover, it is also interesting to observe how the slope of the Pareto front changes as φ increases. When the value of φ is small, as the decrease of the operating time loss, the mission cost increases almost linearly. However, when φ becomes large enough, the decreasing of the operating time loss leads to a much faster increase in the mission cost. To understand this slope change in the Pareto front, we conduct a sensitivity analysis to observe the variance of resultant decision rules with different values of φ , as shown in Figure 32.

In Figure 32, we only consider the logistics of cargo missions. One rocket launch represents one cargo transportation mission. The safety stock starts from rocket launch index 2 because we assume there is no initial safety stock available for the first rocket launch. This figure shows that when the value of φ is small (e.g., 100), the required safety stock for each launch decreases linearly as the procedure of the space campaign. This is because the redundant supplies that are not consumed for the earlier launches can be used for later missions. Thus, more safety stock will be transported in earlier missions. However,

there is an upper bound for the safety stock, where it is enough to support the longest launch delay for each mission. As the increase of φ , safety stocks for the first few launches reach the upper bound ($\sim 2,600$ kg) first. For the same amount of safety stock, it has less and less potential to counter the operating time loss. This is where the Pareto front bending begins. When φ is above 5000, only the safety stocks for the last few launches have not been fully filled. Increasing safety stock leads to negligible improvement in mission performance. The Pareto front approaches a vertical line eventually.

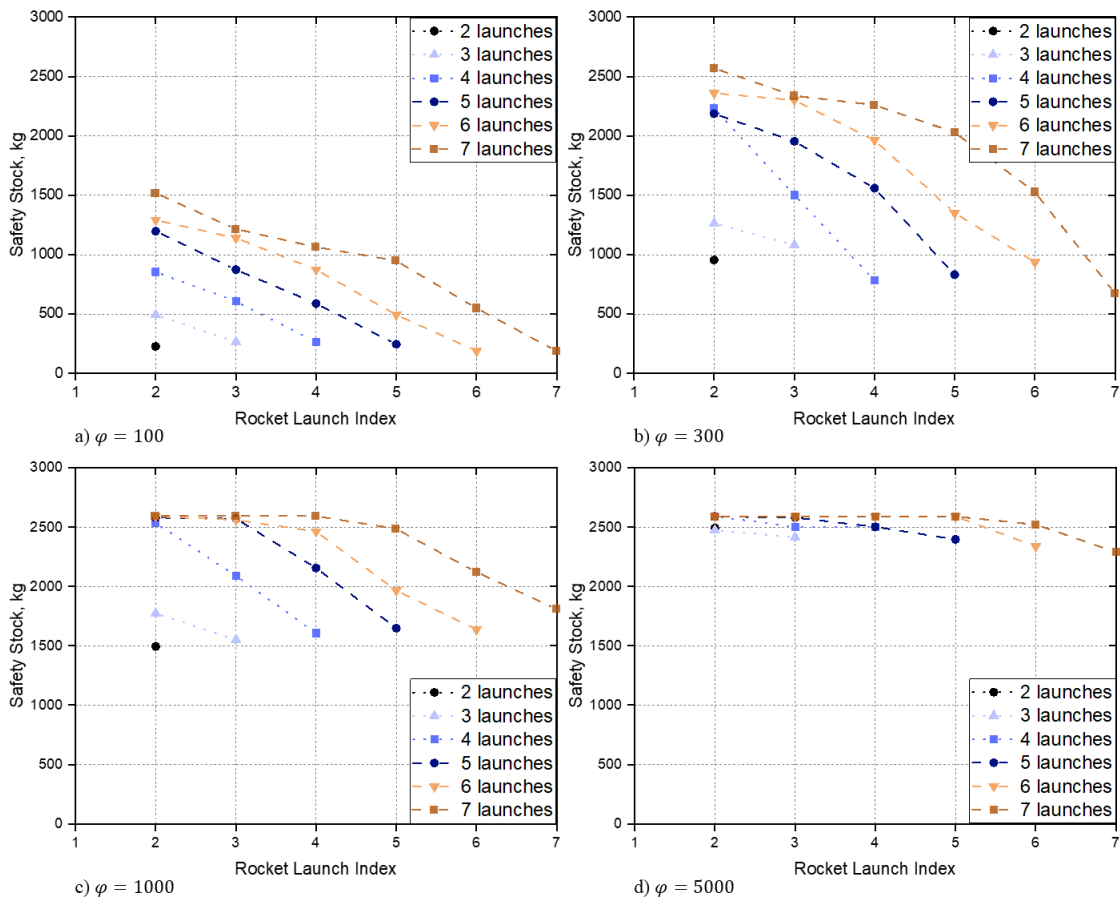


Figure 32 - Decision Rule Result Variance.

The impact of the number of missions is also illustrated in Figure 32. We keep the launch frequency and mission demands but elongate the time horizon of the space campaign. In this case, we only consider cargo missions without the logistics of the crew.

Longer space campaign provides larger potentials to the safety stock in the first few missions to counter the operating time loss in later missions. This means that the Pareto front bending begins later for a long-term space station operation campaign, as shown in Figure 33. This figure shows the expected mission cost and mission performance on average per cargo mission. For different numbers of missions with similar mission demands, the slope of the Pareto front is the same when φ is small. As φ increases, the Pareto front for shorter space campaign with fewer space missions starts to bend first. Eventually, the Pareto fronts all end up being vertical lines. The delayed bending of the Pareto front represents that decision-makers can reduce the operating time loss without a significant increase in the mission cost. Moreover, longer space campaigns also further reduce the average mission cost and improve average mission performance.

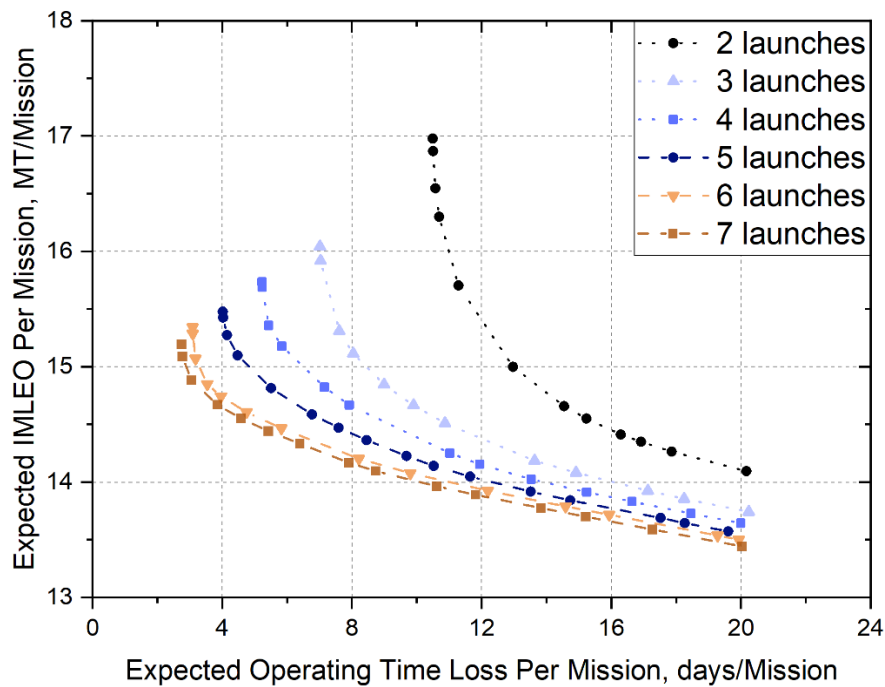


Figure 33 - Pareto Fronts Comparison with Respect to the Number of Launches.

Crew time assignment is another important factor that impacts the decision rules and the shape of the Pareto front. Its impact on the Pareto front is also correlated with the

material consumption rate. By default, we assume 80% of the crew operating time is used for scientific experiments and 20% of the time is used for maintenance. By varying the percentage of the crew operating time used for science, we conduct a sensitivity analysis on the crew operating time assignment. The result is shown in Figure 34. For this case study, the consumption rate for scientific experiments is twice of that for maintenance. Therefore, if 66% of the crew operating time is assigned for science, where science instruments and maintenance spares can support the same length of space station operation per unit mass, the Pareto front is the least convex, as shown in Figure 34. On the other hand, if the material with the lower consumption rate (i.e., maintenance spares) is dominant in supporting space station daily operations, the Pareto front contains a sharp turn when balancing mission cost and mission performance. For these Pareto fronts, we can identify an area of the “knee region”. For multi-objective optimization, a set of solutions on the Pareto-optimal front are called “knees” when a small improvement in one objective would lead to a large deterioration in at least one other objective [96]. Focusing on the search of the “knee region” can generate a smaller set of solutions that are more likely to be preferred by decision-makers during mission planning. As shown in Figure 34, outside this region, any improvement of mission performance leads to a dramatic increase in mission cost, and any decrease in mission cost leads to a dramatic deterioration of mission performance. When one of the materials is dominant in supporting space station daily operations, the “knee region” becomes smaller.

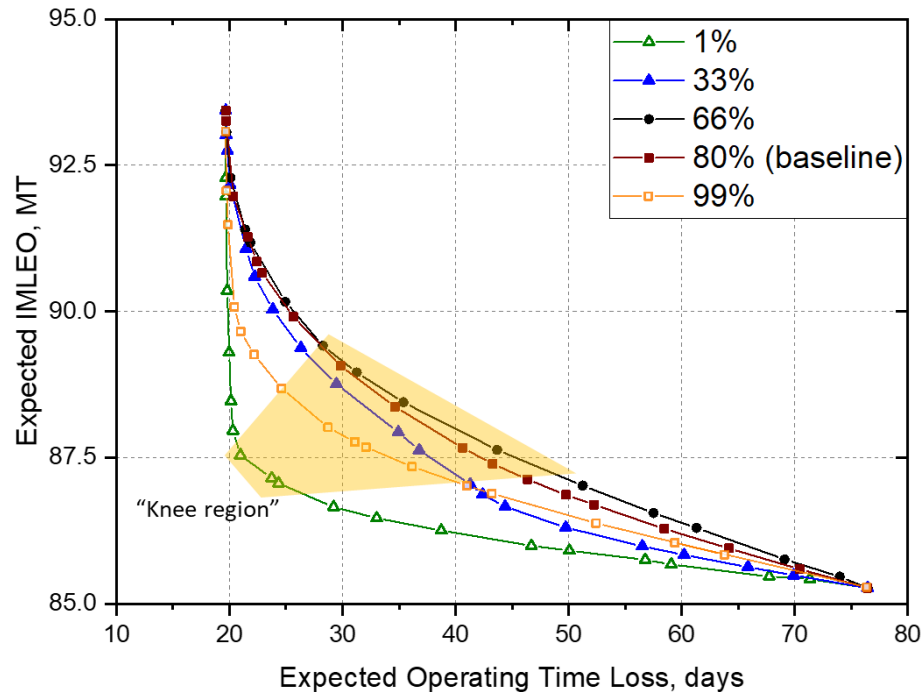


Figure 34 - Pareto Fronts for Different Percentages of Crew Operating Time for Science.

6.3 Chapter Summary

This chapter proposes a flexibility management framework to add built-in flexibility in space logistics mission planning through decision rules and multi-stage stochastic programming. It is formulated as an optimization problem with weighted sum objectives balancing mission cost and mission performance. Space logistics optimization is developed through a network-based commodity flow model. The decision rule formulation is established by combining condition-go and linear decision rule formats to take into account the level of available safety stock before each launch and determine the amount of additional supply to be delivered together with pre-determined mission demands. A mission planning Pareto front is generated as the output to analyze the tradeoff between mission cost and mission performance.

An example mission scenario about space station resupply is established to evaluate the performance of the proposed framework considering the rocket launch delay uncertainty. Results show that the relationship among safety stocks, expected mission cost, and expected mission performance can be analyzed with the proposed framework and illustratively presented on the Pareto front between the expected mission cost (i.e., initial mass in low-Earth orbit) and the expected mission performance loss (i.e., effective crew operating time loss). Changes in space mission demands, time horizon, mission operation patterns can be directly illustrated through the variation of the Pareto front. These observations of the Pareto front show the value of the proposed flexibility management framework. For decision-makers, the decision rule results and Pareto front achieved by the framework can help improve the understanding of impacts from stochastic mission operation environments and make directly implementable strategies to counter uncertainties.

The proposed framework can be extensively applied to problems with multiple different uncertainty sources, including demand changes, spacecraft flight delays, and infrastructure performance uncertainties, and the logistics for multiple destinations at the same time. Further applications can also be explored to consider large-scale human exploration and the implementation of other mitigation methods rather than only relying on the redundant supply.

CHAPTER 7. CONCLUSION

7.1 Thesis Summary

The goal of this thesis is to develop a series of space logistics optimization frameworks to resolve the grand challenges in multi-mission space campaign design for future large-scale space exploration. This thesis starts from an integrated space logistics optimization framework in Chapter 3 to enable concurrent optimization in space transportation scheduling, spacecraft design, and space infrastructure design. A piecewise-linear approximation method is proposed to handle nonlinear spacecraft and space infrastructure sizing models. As a result, the original mixed-integer nonlinear programming formulation is converted into a mixed-integer linear programming formulation, where the computational efficiency is significantly improved and the optimality gap can be guaranteed.

The integrated space logistics optimization formulation proposed in Chapter 3 takes a step forward in multi-mission space campaign design, but it also brings a scalability issue to the time dimension for long-term space exploration. In response to this challenge, a periodic time-expanded network is proposed in Chapter 4. It is developed by leveraging repeatability in multi-mission space campaign operations. The proposed framework can generate mission planning solutions with significantly less computation time compared to the full time-expanded network methods with solutions that are also preferred practically.

In Chapter 5, the focus switches to integrated architecture trade studies for space infrastructure technologies. Based on the network flow model proposed in Chapter 3, a full-size space infrastructure optimization framework is first proposed to take into account subsystem-level interactions between ISRU subsystems and their external synergistic effects with the space logistics system. Because the full-size optimization framework can

be computationally prohibitive due to the significant increase in variables and constraints from infrastructure subsystems, a multi-fidelity optimization framework is then proposed by varying the granularity of the commodity-type definition over the space transportation network. This method can lead to an approximate solution to the full-size problem in a computationally efficient manner with little sacrifice to the quality of the solution.

Frameworks and methods proposed in Chapters 3, 4, and 5 resolve the grand challenge of space logistics in multi-mission space campaign design, long-term space mission design, and space infrastructure trade studies, but mainly in deterministic mission operation environments. In Chapter 6, a flexibility management framework is established to handle uncertainties in space mission planning and operations. It is developed based on decision rules and multi-stage stochastic programming. The proposed decision rules focus on the uncertainties in rocket launch delay. However, the proposed methods can be used to handle the general stochastic mission operation environment. The generated decision rules can also be used as direct implementable policies for decision-makers whenever an uncertainty event occurs.

For all the frameworks and methods proposed in this thesis, case studies on multi-mission lunar exploration campaigns and Mars exploration missions are conducted to demonstrate the values of proposed methods and evaluate their performances. The proposed formulations in this thesis provide important steps to enable effective interdisciplinary space logistics optimization for future large-scale space exploration.

7.2 Broader Applications

The transportation planning and system design frameworks proposed in this thesis presume a space exploration environment. All the case studies conducted also mainly focus on space transportation planning in space flights to the moon or Mars. However, applications of the proposed methods are not limited to space transportation and logistics.

The integrated space logistics optimization framework can also be used for future multi-agent system design and performance evaluation for planetary surface exploration. Multi-agent planetary exploration is an emerging field that has attracted more and more attention. Technologies and algorithms have been developed to explore, detect, and exploit resources within certain areas through the collaboration of multiple agents. However, more studies are needed to consider detailed material flows and space infrastructure operational coordinations among agents and systems. The interdisciplinary space logistics frameworks developed in this thesis can be used to handle the existing challenges in planetary surface exploration fields.

Beyond the space field, the proposed space logistics optimization frameworks are also very useful to both traditional terrestrial transportation and air transportation domains. For example, the integrated space logistics optimization framework proposed in Chapter 3 can be used in terrestrial transportation planning when system design and sizing are also part of the decision space. The periodic time-expanded network proposed in Chapter 4 brings a new perspective to airline schedule recovery problems by considering the recovery period and the subsequent schedule at the same time. The multi-fidelity optimization framework introduced in Chapter 5 is also useful for architecture technology trade studies in general logistics and transportation optimization problems.

7.3 Future Work

Going forward, multiple directions are possible to continue research on astrodynamics and space system optimization in both methodology and application areas. The research can also branch out to investigate uncertainties, parallel computing, intelligent space systems, and on-orbit servicing.

On the astrodynamics side, integrated trajectory analysis and transportation planning is an important step to improve the mission design fidelity and explore a larger

trade space, such as the consideration of high-thrust and low-thrust trajectory analysis and the phasing of orbits. Current methods consider the entire orbit as a node, which ignore the impact of orbital resonances and optimal synchronization on transportation planning and trajectory evaluations. More studies are needed to closely look at the timing and phasing of orbital maneuvers during the transportation.

On the space architecture design and system engineering side, multiple areas need further analysis, including demand forecasting, inventory management, stochastic programming, cooperation and coordination in logistics, etc. Although many approaches that address problems in terrain transportation or the airline industry have been proposed, little has been implemented in space transportation. Future methodology development needs to be done leveraging state-of-the-art operations research, space system engineering, control theory, and machine learning. The developed space logistics methodology in this thesis can be further extended to contribute to the establishment of a sustainable space transportation system for cislunar space exploration and beyond. In addition to high-level mission planning framework development, we also need to explore its application in the early stage mission concept generation, autonomous supply chain management, and the transportation platform design considering both low-thrust and high-thrust space vehicles.

Another important direction is to focus on fundamental research in transportation science to handle uncertainties in space mission design and operations. The uncertainty sources are not limited to the rocket launch delay discussed in Chapter 6. It may also involve transportation flight delay, mission demand change, or ISRU system performance uncertainty after deployment. Further studies are crucial to understanding interactions and propagations between different uncertainty events in the transportation network. This type of research is not only useful to space logistics but also beneficial to traditional terrestrial and air transportation. The consideration of uncertainties also triggers the demand for large-scale computing and parallel computing to handle a significantly larger design space. It is

critical to understand how to parallelize mission planning optimization leveraging its particular structure.

In addition, intelligent space logistics is also an interesting direction to explore. System automation and robotics have been widely used in terrain and space programs. However, few studies have focused their implementations on logistics and supply chain management. Intelligent space logistics can create sustainable and reliable large-scale space transportation systems to improve mission operation efficiency, mitigate the impact of uncertain events, and guarantee astronaut safety. Considering space autonomous systems from the perspective of space logistics enables system-level evaluation and technology trade studies for the performance and impact of intelligent systems.

Finally, the proposed frameworks for space logistics in this thesis have the potential to support the development of on-orbit servicing. It is an emerging field that has attracted more and more attention from space agencies and commercial entities. Technologies have been developed to refuel, repair, manipulate, and assemble new satellites or space vehicles in orbit. However, little has been addressed at the detailed material flow level which is a key step to transit on-orbit servicing from concept and experiment to reality. Research can focus on methodology development and its application evaluation from the material flow level for on-orbit servicing leveraging interdisciplinary space logistics frameworks. More investigations need to be conducted to enable effective mission planning and architecture design in on-orbit servicing, considering the complex interactions among transportation elements (i.e., launcher, servicer, and storage depot), the constraints (i.e., time windows, trajectories, budget, and resources), and supply chain management (i.e., maintenance spares, components, propellant, and material flow monitoring).

In summary, space logistics research tries to enable holistic evaluations and technology trade studies throughout the entire life cycle of a multi-mission space

exploration campaign. As more space agencies and commercial entities participate in human space exploration, space logistics research is becoming increasingly impactful.

APPENDIX A. PARAMETRIC SPACECRAFT MODEL

This appendix lists preexisting spacecraft parameters upon which the spacecraft model of Taylor was based on Ref. [52]. Table A1 lists the fuel type and corresponding function values, and Table A2 lists the spacecraft parameters.

Table A1 - List of fuel and corresponding parameters used for spacecraft models. [52]

Fuel Type	ID	I_{sp}, s	α
LOX/kerosene	1	330	0.045
LOX/LH2	2	420	0.079
N2O4/UDMH	3	310	0.08
LCH4/LOX	4	318	0.958
MMH/N2O4	5	307	0.226
GOX/Ethanol	6	300	3.9353

Table A2 - List of spacecraft data used for spacecraft model. [52]

Spacecraft name	Fuel identification (ID)	Propellant mass, kg	Payload mass, kg	Structural mass, kg
Saturn V third stage	2	107,725	0	12,014
Apollo command module (CM)	3	0	524	4,841
Apollo service module (SM)	3	18,413	60	6,053
Apollo LM DS	3	8,804	500	2,770
Apollo LM AS	3	2,358	250	1,719
Lunar crew exploration vehicle (CEV) CM	6	363	500	8,034
Lunar CEV SM	5	7,222	0	3,027
Altair DS	2	28,932	2,200	6,182
Altair AS	4	5,257	100	4,964
Earth departure stage (EDS)	2	226,693	0	22,500
Altair Cargo Carrier	0	0	15,000	1,000
Soyuz TM	3	900	255	7,250
Soyuz TMA	3	900	355	7,220
Progress M	3	900	2,350	7,450
Progress M1	3	900	1,800	7,150
Zvezda service module	0	0	10,000	20,000
STS-stage 2 (orbiter)	2	12,412	18,000	78,498
Soyuz-stage 2 (upper)	1	22,845	0	2,355
Proton-stage 2	3	46,562	0	4,115
ISS CEV CM (3 crew + cargo)	6	2,000	400	8,008
ISS CEV CM (6 crew)	6	2,000	0	8,079
ISS CEV (pressurized cargo)	0	0	3,500	7,683
ISS CEV SM	4	2,033	0	3,997
ATV: Automated transfer vehicle	5	2,613	5,500	10,470
HTV:H-II Transfer Vehicle	5	2,000	6,000	10,000
ISS CEV CM Prop	5	2,000	400	8,008
EDS (75 mt)	2	129,500	0	19,986

APPENDIX B. PROBABILITY DISTRIBUTION GENERATION FOR THE CASE STUDY

The launch vehicle delay distribution used in the case study is a hypothetical distribution created based on ISS past data. This Appendix includes the data source and how the used distribution is generated from the data.

The data source for the ISS USOS mission launch data is the ISS Flight Plan from the Flight Planning Integration Panel (FPIP) and includes ISS flights from the NASA CRS program, European Space Agency (ESA), and Japan Aerospace Exploration Agency (JAXA). The ISS Flight Plans provide a multi-year look ahead at planned mission dates for ISS activities including the CRS and international partner missions. While the complete revision history of the ISS Flight Plans is not publicly available, these plans are frequently incorporated in other NASA presentations related to ISS status and planning.

For each revision of the ISS Flight Plan at a defined baseline plan date, the planned launch for each ISS mission in the multi-year planning window is defined. These data provide insight into changes to the near and long-term missions over planning periods approaching the actual launch date. The actual launch dates for each of the ISS USOS missions were obtained from the NASA website [41]. For each ISS USOS mission, the number of days from the baseline planning date to the planned launch date was compared to the number of days the mission was delayed from the planned launch date for launches planning within 1 year of the planning, the resulting data is shown in Figure B1. The data provided in Table B1 contains 21 launches spanning from March 2013 to February 2017 and 16 ISS Flight Plans spanning from November 2012 to January 2017 [97-99] (See Table B1). It is important to note there are more data points in Figure B1 than ISS USOS missions because there are multiple revisions of the ISS Flight Plan between the first planning date

for a given mission and the final planning date for the mission prior to launch. Additionally, the data in Figure B1 includes the total delay between the planned mission date and the actual launch date and does not include any segregation of data for different reasons for launch delays.

Table B1 - Summary of FPIP Planning Dates.

FPIP Dates
11/13/2012 [97, 98]
3/26/2013 [98]
7/17/2013 [99]
10/15/2013 [98]
11/25/2013 [98]
2/6/2014 [98]
4/23/2014 [98]
7/3/2014 [98]
8/8/2014 [98]
9/25/2014 [98]
12/8/2014 [98]
2/20/2015 [98]
10/26/2015 [98]
2/18/2016 [98]
9/20/2016 [98]
1/20/2017 [98]

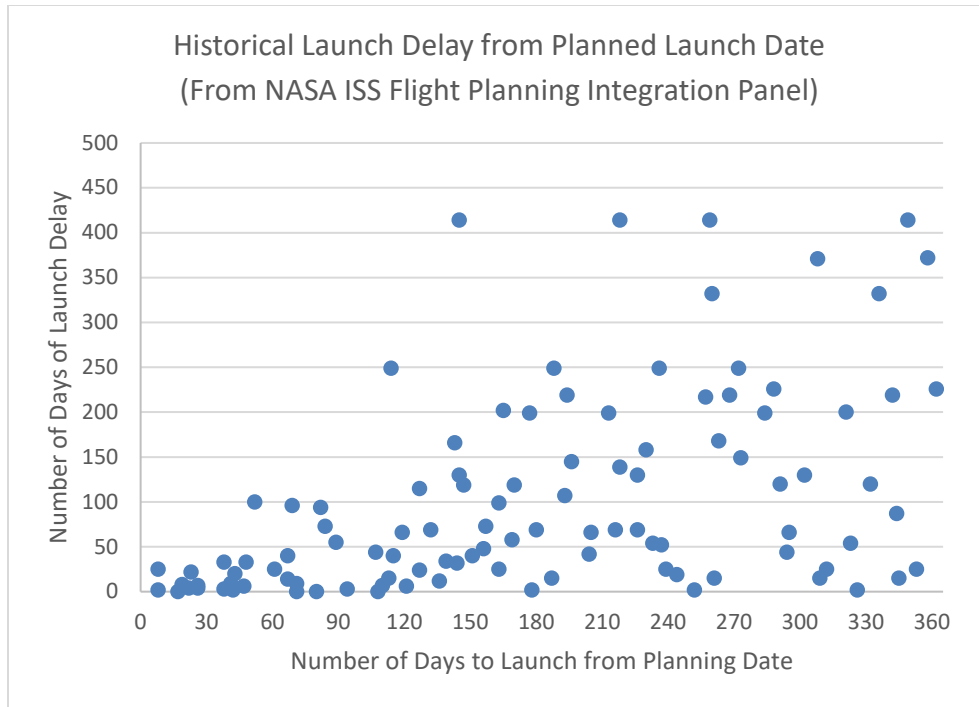


Figure B1 - Historical Error in CRS Launch Date Planning (within 1 Year of Planned Launch).

The data in Figure B1 shows an expected trend that as the mission planning date is closer to the planned launch date, the accuracy of the planned launch date improves. Additionally, variation in the launch delay increases as the number of days between the mission planning date and the launch date increases. The data points with delays exceeding 350 days are associated with return to flight missions for Orbital ATK and SpaceX after the Orb-3 and SpX-7 launch failures, respectively, and the HTV4 and HTV5 missions from JAXA.

For a multi-mission space station resupply campaign, based on the available data, the launch delay for each mission is assumed to be independent in the scenario generation. There are two reasons for this assumption. Firstly, the ISS Flight Plan provides mission

plans based on planned ISS needs well in advance of the actual mission date. As the ISS planning is adjusted based on ISS needs, the mission dates may shift to optimize cargo delivery to maximize total delivered mass, providing the best value for NASA and the taxpayer. Secondly, the CRS program has two launch providers, so if one provider experiences a significant launch delay, NASA can reorganize launches to minimize delay in providing cargo to the ISS.

Because the launch delays are assumed as independent for each mission, we only need to discuss the launch delay model for one mission first and implement it directly to other missions in the campaign. In this case study, we assume four missions per year as a campaign; so we only use the data within a 90-day planning period for the launch vehicle delay model. For simplicity in this case study, we consider 90 days as the longest possible delay; we assume that if the delay is longer than 90 days, we would replan the missions with a new optimization. The data for the 90-day planning window is shown in Figure B2. The cumulative density function of launch delay (in the number of days) within a 90-day planning window is determined from the data in Figure B2. The resulting discrete probability is a curve fit to find a continuous function to represent the launch delay. The resulting curve fit is a doubly, truncated exponential curve shown in Figure B3. Based on the launch delay cumulative density function as shown in Figure B3, we can do the inverse transform sampling to generate uncertainty scenarios input for the space station resupply mission example.

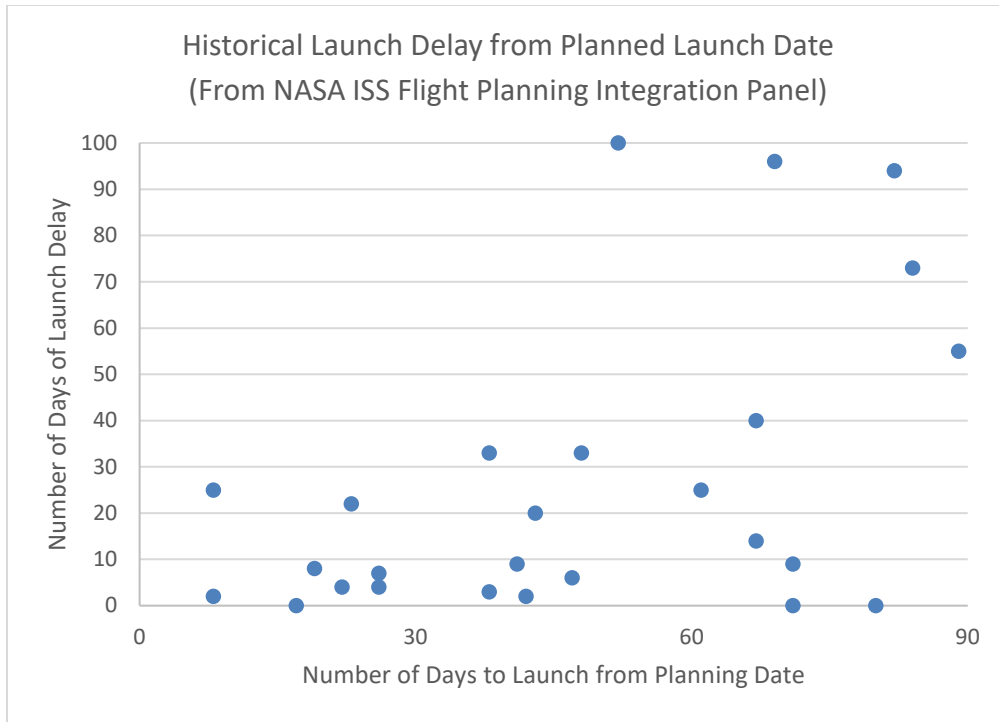


Figure B2 - Historical Error in CRS Launch Date Planning (within 90 days of planned launch).

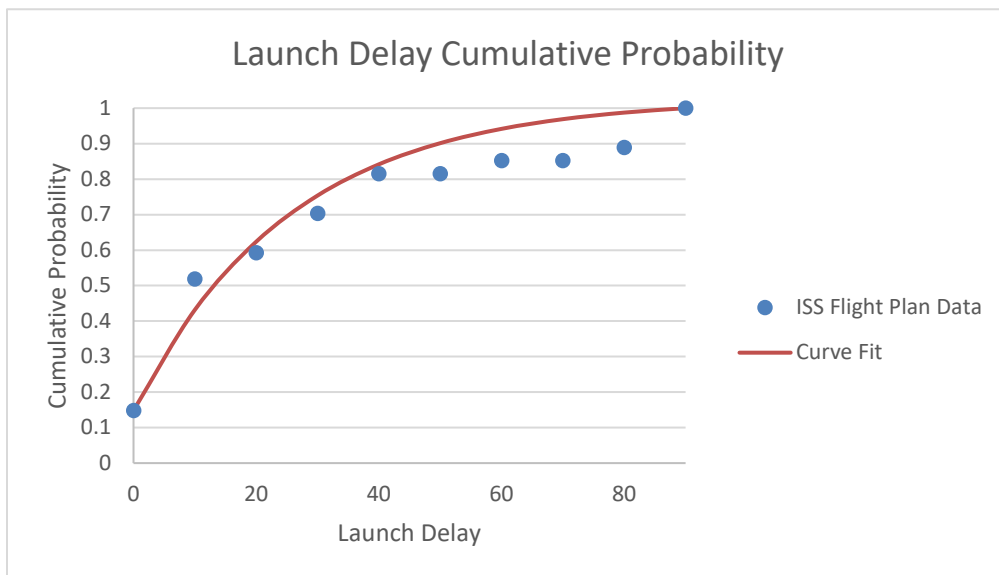


Figure B3 - Launch Delay Cumulative Distribution Function.

REFERENCES

- [1] Ishimatsu, T., de Weck, O. L., Hoffman, J. A., Ohkami, Y., and Shishko, R., "Generalized Multicommodity Network Flow Model for the Earth–Moon–Mars Logistics System," *Journal of Spacecraft and Rocket*, Vol. 53, No. 1, Jan. 2016, pp. 25-38.
doi: 10.2514/1.A33235
- [2] Ho, K., de Weck, O. L., Hoffman, J. A., and Shishko, R., "Dynamic Modeling and Optimization for Space Logistics Using Time-Expanded Networks," *Acta Astronautica*, Vol. 105, No. 2, Dec. 2014, pp. 428-443.
doi: 10.1016/j.actaastro.2014.10.026
- [3] Taylor, C., Song, M., Klabjan, D., de Weck, O. L., and Simchi-Levi, D., "A Mathematical Model for Interplanetary Logistics," *Logistics Spectrum*, Vol. 41, No. 1, Jan-Mar 2007, pp. 23-33.
- [4] Komar, D. R., Hoffman, J., Olds, A., and Seal, M., "Framework for the Parametric System Modeling of Space Exploration Architectures," *AIAA Space 2008 Conference & Exposition*, AIAA 2008-7845, San Diego, CA, Sep. 2008.
doi: 10.2514/6.2008-7845
- [5] Arney, D. C. and Wilhite, A. W., "Modeling Space System Architectures with Graph Theory," *Journal of Spacecraft and Rockets*, Vol. 51, No. 5, Mar. 2014, pp. 1413-1429.
doi: 10.2514/1.A32578
- [6] Oeftering, R. C., "A Cis-Lunar Propellant Infrastructure for Flexible Path Exploration and Space Commerce", *AIAA SPACE 2011 Conference & Exposition*, AIAA 2011-7113, Long Beach, CA, Sep. 2011.
doi: 10.2514/6.2011-7113
- [7] Schreiner, S. S., "Molten Regolith Electrolysis Reactor Modeling and Optimization of In-Situ Resource Utilization Systems," M.S. Thesis, Aeronautics and Astronautics Dept., MIT, Cambridge, MA, 2015.
- [8] Howell, J. T., Mankins, J. C., and Fikes, J. C., "In-Space Cryogenic Propellant Depot Stepping Stone," *Acta Astronautica*, Vol. 59, No. 1-5, Jul.-Sep. 2006, pp. 230-235.
doi: 10.1016/j.actaastro.2006.02.019

- [9] Notardonato, W., "Active Control of Cryogenic Propellants in Space", *Cryogenics*, Vol. 52, No.4-6, Apr.-Jun. 2012, pp. 236-242.
doi: 10.1016/j.cryogenics.2012.01.003
- [10] Liggett, M. W., "Space-Based LH2 Propellant Storage System: Subscale Ground Testing Results", *Cryogenics*, Vol. 33, No.4, Apr. 1993, pp. 438-442.
doi: 10.1016/0011-2275(93)90174-M
- [11] Taylor, T., Kistler, W. P., and Citron, B., "On-Orbit Fuel Depot Deployment, Management and Evolution Focused on Cost Reduction," *AIAA SPACE 2009 Conference & Exposition*, AIAA 2009-6757, Pasadena, CA, Sep. 2009.
doi: 10.2514/6.2009-6757
- [12] Woodcock, G. R., "Logistics Support of Lunar Base," *Acta Astronautica*, Vol. 17, No. 7, Jul. 1988, pp. 717-738.
doi: 10.1016/0094-5765(88)90186-5
- [13] Charania, A. C., and DePasquale, D., "Economic Analysis of a Lunar In-Situ Resource Utilization (ISRU) Propellant Services Market", *58th International Astronautical Congress*, IAC-07-A5.1.03, Hyderabad, India, Sep. 2007.
- [14] Musk, E., "Making Humans a Multi-Planetary Species," *New Space*, Vol. 5, No. 2, Jun. 2017, pp. 46-61.
doi: 10.1089/space.2017.29009.emu
- [15] Grogan, P. T., Yue, H. K., and de Weck, O. L., "Space Logistics Modeling and Simulation Analysis using SpaceNet: Four Application Cases," *AIAA Space 2011 Conference & Exposition*, AIAA 2011-7346, Long Beach, CA, Sep. 2011.
doi: 10.2514/6.2011-7346
- [16] Cornes, O. and de Weck, O. L., "Design of executable space mission architectures using discrete network flow optimization," *Proceedings of the International Astronautical Congress*, IAC, Vol. 14, Sep. 2017, pp. 9423-9436.
- [17] Chen, H., and Ho, K., "Integrated Space Logistics Mission Planning and Spacecraft Design with Mixed-Integer Nonlinear Programming," *Journal of Spacecraft and Rockets*, Vol. 55, No. 2, Apr. 2018, pp. 365-381.
doi: 10.2514/1.A33905

- [18] Steinzen, I., Gintner, V., Suhl, L., and Kliewer, N., “A Time-Space Network Approach for the Integrated Vehicle- and Crew-Scheduling Problem with Multiple Depots,” *Transportation Science*, Vol. 44, No. 3, Aug. 2010, pp. 367-382.
doi: 10.1287/trsc.1090.0304
- [19] Belanger, N., Desaulniers, G., Soumis, F., and Desrosiers, J., “Periodic Airline Fleet Assignment with Time Windows, Spacing Constraints, and Time Dependent Revenues,” *European Journal of Operational Research*, Vol. 175, No. 3, Dec. 2006, pp. 1754-1766.
doi: 10.1016/j.ejor.2004.04.051
- [20] Zeghal, F. M., Haouari, M., Sherali, H. D., and Aissaoui, N., “Flexible Aircraft Fleeting and Routing at TunisAir,” *Journal of the Operational Research Society*, Vol. 62, No. 2, Feb. 2011, pp. 368-380.
doi: 10.1057/jors.2010.100
- [21] Ben Ahmed, M., Ghroubi, W., Haouari, M., and Sherali, H. D., “A Hybrid Optimization-Simulation Approach for Robust Weekly Aircraft Routing and Retiming,” *Transportation Research Part C: Emerging Technologies*, Vol. 84, Nov. 2017, pp. 1-20.
doi: 10.1016/j.trc.2017.07.010
- [22] Carbajal, J. A., Erera, A., and Savelsbergh, M., “Balancing Fleet Size and Repositioning Costs in LTL Trucking,” *Annals of Operations Research*, Vol. 203, Mar. 2013, pp. 235-254.
doi: 10.1007/s10479-011-0924-1
- [23] Bard, J. F., Yu, G., and Arguello, M. F., “Optimizing Aircraft Routings in Response to Groundings and Delays,” *IIE Transactions*, Vol. 33, No. 10, Oct. 2001, pp. 931-947.
doi: 10.1023/A:1010987008497
- [24] Sinclair, K., Cordeau, J.-F., and Laporte, G., “Improvements to a Large Neighborhood Search Heuristic for an Integrated Aircraft and Passenger Recovery Problem,” *European Journal of Operational Research*, Vol. 233, No. 1, Feb. 2014, pp. 234-245.
doi: 10.1016/j.ejor.2013.08.034
- [25] Kornuta, D., Abbud-Madrid, A., Atkinson, J., Barr, J., Barnhard, G., Bienhoff, D., Blair, B., Clark, V., Cyrus, J., DeWitt, B., Dreyer, C., Finger, B., Goff, J., Ho, K., Kelsey, L., et. al, “Commercial Lunar Propellant Architecture: A Collaborative Study

- of Lunar Propellant Production,” *REACH - Reviews in Human Space Exploration*, Vol. 13, Mar.2019, 100026.
doi: 10.1016/j.reach.2019.100026
- [26] Lee, K. A., Oryshchyn, L., Paz, A., Reddington, M., and Simon, T. M., “The ROxygen Project: Outpost-scale Lunar Oxygen Production System Development at Johnson Space Center,” *Journal of Aerospace Engineering*, Vol. 26, No. 1, 2013, pp. 67-73.
doi: 10.1061/(ASCE)AS.1943-5525.0000230
- [27] Clark, D. L., Keller, B. W., and Kirkland, J. A., “Field Test Results of the PILOT Hydrogen Reduction Reactor,” *AIAA Space 2009 Conference and Exposition*, AIAA 2009-6475, Pasadena, CA, Sep. 2009.
doi: 10.2514/6.2009-6475
- [28] Gustafson, R. J., White, B. C., and Fidler, M. J., “2010 Field Demonstration of the Solar Carbothermal Regolith Reduction Process to Produce Oxygen,” *49th AIAA Aerospace Sciences Meeting including the New Horizons Forum and Aerospace Exposition*, Aerospace Sciences Meetings, AIAA 2011-434, Orlando, FL, Jan. 2011.
doi: 10.2514/6.2011-434
- [29] Meyen, F. E., “System modeling, design, and control of the Mars Oxygen In-Situ Resource Utilization Experiment (MOXIE) and implications for atmospheric ISRU processing plants,” Ph.D. dissertation, Aeronautics and Astronautics Dept., MIT, Cambridge, MA, 2017.
- [30] Parrish, J., “Robotic servicing of geosynchronous satellites (RSGS).” DARPA, URL: <http://www.darpa.mil/program/robotic-servicing-of-geosynchronous-satellites>. [cited 15 January 2020].
- [31] NASA, “In-space robotic manufacturing and assembly (IRMA),” 2016. URL: https://www.nasa.gov/sites/default/files/atoms/files/nac_tkortes_irma_nov2016_tagged.pdf. [cited 15 January 2020].
- [32] Verstraete, A. W., Anderson, D., St. Louis, N. M., and Hudson, J., “Geosynchronous Earth orbit robotic servicer mission design,” *Journal of Spacecraft and Rockets*, Vol. 55, No. 6, Nov. 2018, pp. 1444-1452.
doi: 10.2514/1.A33945
- [33] Verstraete, A., St. Louis, N., Kolosa, D., and Hudson, J., “GEO robotic servicer trajectory optimization,” *AIAA Space 2016 Conference & Exposition*, AIAA 2016-5242, Long Beach, CA, Sep. 2016.

doi: 10.2514/6.2016-5242

- [34] Sarton du Jonchay, T. and Ho, K., “Quantification of the Responsiveness of On-Orbit Servicing Infrastructure for Modularized Earth-Orbiting Platforms,” *Acta Astronautica*, Vol. 132, Mar. 2017, pp. 192-203.
doi: 10.1016/j.actaastro.2016.12.021
- [35] Kutter, B. F., “Cislunar-1000: Transportation Supporting a Self-Sustaining Space Economy,” *AIAA Space 2016 Conference & Exposition*, AIAA 2016-5491, Long Beach, CA, Sep. 2016.
doi: 10.2514/6.2016-5491
- [36] Ho, K., de Weck, O. L., Hoffman, J. A., and Shishko, R., “Campaign-level Dynamic Network Modelling for Spaceflight Logistics for the Flexible Path Concept,” *Acta Astronautica*, Vol. 123, Jun. 2016, pp. 51-61.
doi: 10.1016/j.actaastro.2016.03.006
- [37] Chen, H., Lee, H., and Ho, K., “Space Transportation System and Mission Planning for Regular Interplanetary Missions,” *Journal of Spacecraft and Rockets*, Vol. 56, No. 1, Jan. 2019, pp. 12-20.
doi: 10.2514/1.A34168
- [38] Sanders, G. B., “Comparison of Lunar and Mars In-Situ Resource Utilization for Future Robotic and Human Missions,” *49th AIAA Aerospace Sciences Meeting including the New Horizons Forum and Aerospace Exposition*, AIAA 2011-120, Orlando, FL, Jan. 2011.
doi: 10.2514/6.2011-120
- [39] Arney, D. C., Jones, C. A., Klovstad, J., Komar, D.R., Earle, K., Moses, R., Bushnell, D., and Shyface, H., “Sustaining Human Presence on Mars Using ISRU and a Reusable Lander,” *AIAA SPACE 2015 Conference and Exposition*, AIAA 2015-4479, Pasadena, CA, 31 Aug.-02 Sep. 2015.
doi: 10.2514/6.2015-4479
- [40] Little, R. G., “Controlling Cascading Failure: Understanding the Vulnerabilities of Interconnected Infrastructures,” *Journal of Urban Technology*, Vol. 9, No. 1, 2002, pp. 109-123.
doi: 10.1080/106307302317379855

- [41] “Visiting Vehicle Launches, Arrivals and Departures,” NASA, URL:<http://www.nasa.gov/feature/visiting-vehicle-launches-arrivals-and-departures> [cited 06 May 2020].
- [42] “Orbital CRS-3 Mission Overview,” NASA, URL:https://www.nasa.gov/sites/default/files/files/Orbital_CRS3_mission_overview.pdf [cited 06 May 2020].
- [43] “SpaceX CRS-7 Mission Overview,” NASA, URL:https://www.nasa.gov/sites/default/files/atoms/files/spacex_crs7_mission_overview.pdf [cited 06 May 2020].
- [44] Foust, J. “Progress Docking Called Off.” *SpaceNews.com*, 29 Apr. 2015, URL:<https://spacenews.com/progress-docking-called-off> [cited 17 Feb 2017].
- [45] “NASA’s Response to Orbital’s October 2014 Launch Failure: Impacts on Commercial Resupply of the International Space Station,” NASA Office of Inspector General, Washington, D.C., IG-15-023, Sep. 2015.
- [46] Shull, S. A., “Integrated Modeling and Simulation of Lunar Exploration Campaign Logistics,” M.S. Thesis, Aeronautics and Astronautics Dept., MIT, Cambridge, MA, 2013.
- [47] Stromgren, C., Goodliff, K., Cirillo, W., and Owens, A., “The Threat of Uncertainty - Why Using Traditional Approaches for Evaluating Spacecraft Reliability Are Insufficient for Future Human Mars Missions,” *AIAA Space 2016 Conference & Exposition*, AIAA 2016-5307, Long Beach, CA, Sep. 2016.
doi: 10.2514/6.2016-5307
- [48] Cardin, M.-A., “Enabling Flexibility in Engineering Systems: A Taxonomy of Procedures and a Design Framework,” *Journal of Mechanical Design*, Vol. 136, No. 1, Jan. 2014.
doi: 10.1115/1.4025704
- [49] Cardin, M.-A., Kolfshoten, G. I., Frey, D. D., de Neufville, R., de Weck, O. L., and Geltner, D. M., “Empirical Evaluation of Procedures to Generate Flexibility in Engineering Systems and Improve Lifecycle Performance,” *Research in Engineering Design*, Vol. 24, No. 3, July 2013, pp. 277-295.
doi: 10.1007/s00163-012-0145-x

- [50] Wang, T., "Real Options "in" Projects and Systems Design – Identification of Options and Solution for Path Dependency," Ph.D. Dissertation, Aeronautics and Astronautics Dept., MIT, Cambridge, MA, 2005.
- [51] Cardin, M.-A., Xie, Q., Ng, T. S., Wang, S., and Hu, J., "An Approach for Analyzing and Managing Flexibility in Engineering Systems Design Based on Decision Rules and Multistage Stochastic Programming," *IISE Transactions*, Vol. 49, No. 1, 2017, pp. 1-12.
doi: 10.1080/0740817X.2016.1189627
- [52] Taylor, C., "Integrated Transportation System Design Optimization," Ph.D. Dissertation, Aeronautics and Astronautics Dept., MIT, Cambridge, MA, 2007.
- [53] Ho, K., "Dynamic Network Modeling for Spaceflight Logistics with Time-Expanded Networks," Ph.D. Dissertation, Aeronautics and Astronautics Dept., MIT, Cambridge, MA, 2015.
- [54] Ishimatsu, T., "Generalized Multi-Commodity Network Flows: Case Studies in Space Logistics and Complex Infrastructure Systems," Ph.D. Dissertation, Aeronautics and Astronautics Dept., MIT, Cambridge, MA, 2013.
- [55] "Atlas V Launch Services User's Guide," United Launch Alliance, <http://www.ulalaunch.com/uploads/docs/AtlasVUsersGuide2010.pdf> [retrieved 31 May 2017].
- [56] Miki, Y., Abe, N., Matsuyama, K., Masuda, K., Fukuda, N., Sasaki, H., "Development of the H-II Transfer Vehicle (HTV)," *Mitsubishi Heavy Industries Technical Review*, Vol. 47, No. 1, Mar. 2010, pp. 58-64.
- [57] de la Bourdonnaye, O. and Kinnersley, M., "The Automated Transfer Vehicle – A Valuable Asset for ISS Logistics," *AIAA SPACE 2010 Conference & Exposition, AIAA 2010-8620*, Anaheim, CA, Sep. 2010.
doi: 10.2514/6.2010-8620
- [58] Zegler, F. and Kutter, B., "Evolving to a Depot-Based Space Transportation Architecture", *AIAA SPACE 2010 Conference & Exposition, AIAA 2010-8638*, Anaheim, CA, Sep. 2010.
doi: 10.2514/6.2010-8638

- [59] Schreiner, S. S., Sibille, L., Dominguez, J. A., Hoffman, J. A., Sanders, G. B., and Sirk, A. H., "Development of a Molten Regolith Electrolysis Reactor Model for Lunar In-Situ Resource Utilization," *8th Symposium on Space Resource Utilization, AIAA SciTech Forum*, AIAA 2015-1180, Kissimmee, FL, 2015.
doi: 10.2514/6.2015-1180
- [60] Vielma, J. P., Ahmed, S., and Nemhauser, G., "Mixed-Integer Models for Nonseparable Piecewise Linear Optimization: Unifying Framework and Extensions," *Operations Research*, Vol. 58, No. 2, Oct. 2009, pp. 303-315.
doi: 10.1287/opre.1090.0721
- [61] Vielma, J. P., Nemhauser, G. L., "Modeling disjunctive constraints with a logarithmic number of binary variables and constraints," *Mathematical Programming*, Vol. 128, No. 1, Jun. 2011, pp. 49-72.
doi: 10.1007/s10107-009-0295-4
- [62] "Apollo 17 Mission Report," Apollo 17 Mission Evaluation Team, NASA Lyndon B. Johnson Space Center, JSC-07904, Houston, TX, March 1973.
- [63] Wickman, L., Nota, B., Keates, S., "Lunar Life Support System Study: Metabolic Energy and Water Considerations," *Space 2004 Conference and Exhibit*, AIAA 2004-6025, San Diego, CA, Sep. 2004.
doi: 10.2514/6.2004-6025
- [64] Jones, H. W., "Ultra Reliable Space Life Support," *AIAA SPACE 2012 Conference & Exposition*, AIAA 2012-5121, Pasadena, CA, Sep. 2012.
doi: 10.2514/6.2012-5121
- [65] Drake, B. G., "Human Exploration of Mars Design Reference Architecture 5.0," NASA-SP-2009-566, NASA Johnson Space Center, Houston, TX, 2009.
- [66] Sanders, G., "Current NASA Plans for Mars In Situ Resource Utilization," NASA Johnson Space Center, Houston, TX, 20 February 2018.
- [67] Surampudi, R., Carpenter, B., EI-Genk, M., Herrera, L., Mason, L., Mondt, J., Nesmith, B., Rapp, D., and Wiley, R., "Advanced Radioisotope Power System Report," NASA's Office of Space Science, D-20757, March 2001.
- [68] Zipkin, P. H., "Bounds on the Effect of Aggregating Variables in Linear Programs," *Operations Research*, Vol. 28, No. 2, Mar.-Apr. 1980, pp. 403-418.

- [69] Zipkin, P. H., "Bounds for Row-Aggregation in Linear Programming," *Operations Research*, Vol. 28, No. 4, Jul.-Aug. 1980, pp. 903-916.
- [70] Rogers, D. F., Plante, R. D., Wong, R. T., and Evans, J. R., "Aggregation and Disaggregation Techniques and Methodology in Optimization," *Operations Research*, Vol. 39, No. 4, Jul.-Aug. 1991, pp. 553-582.
- [71] Evans, J. R., "Model Simplification in Multicommodity Distribution Systems Through Aggregation," *Proceedings of The American Institute for Decision Sciences 11th*, Vol. 2, New Orleans, Louisiana, Nov. 1979, pp. 77-79.
- [72] Anon., "SpaceNet," URL: http://strategic.mit.edu/spacelogistics/space_net.php. [retrieved 08 June 2019].
- [73] Chen, H., Sarton du Jonchay, T., Hou, L., and Ho, K. "Integrated In-Situ Resource Utilization System Design and Logistics for Mars Exploration," *Acta Astronautica*, Vol. 170, May 2020, pp. 80-92.
doi: 10.1016/j.actaastro.2020.01.031
- [74] Landis, G. A., Kerslake, T. W., Scheiman, D. and Jenkins, P., "Mars solar power," *2nd International Energy Conversion Engineering Conference*, AIAA 2004-5555, Providence, Rhode Island, Aug. 2004.
doi: 10.2514/6.2004-5555
- [75] Toman, M., Cipin, R., Cervinka, D., Vorel, P., and Prochazka, P., "Li-ion Battery Charging Efficiency," *ECS Transactions*, Vol. 74, No. 1, 2016, pp. 37-43.
doi: 10.1149/07401.0037ecst
- [76] "Energy Storage Technologies for Future Planetary Science Missions," JPL D-101146, Jet Propulsion Laboratory, La Cañada Flintridge, CA, Dec. 2017.
- [77] Zakrajsek, J. F., Woerner D. F., and Fleurial J.-P., "NASA Special Session: Next-Generation Radioisotope Thermoelectric Generator (RTG) Discussion," NASA, URL: <https://rps.nasa.gov/resources/69/next-generation-radioisotope-thermoelectric-generator-presentation> [cited 15 November 2018].
- [78] Buurman, J., Zhang, S., and Babovic, V., "Reducing Risk Through Real Options in Systems Design: The Case of Architecting a Maritime Domain Protection System," *Risk Analysis*, Vol. 29, No. 3, Mar. 2009, pp. 366-379.
doi: 10.1111/j.1539-6924.2008.01160.x

- [79] Jiao, J., “Product Platform Flexibility Planning by Hybrid Real Options Analysis,” *IIE Transactions*, Vol. 44, No. 6, Jun. 2012, pp. 431-445.
doi: 10.1080/0740817X.2011.609874
- [80] de Neufville, R., Scholtes, S., and Wang, T., “Real Options by Spreadsheet: Parking Garage Case Example,” *Journal of Infrastructure Systems*, Vol. 12, No. 2, Jun. 2006, pp. 107-111.
doi: 10.1061/(ASCE)1076-0342(2006)12:2(107)
- [81] Garstka, S. J. and Wets, R. J.-B., “On Decision Rules in Stochastic Programming,” *Mathematical Programming*, Vol. 7, No. 2, 1974, pp. 117–143.
doi: 10.1007/BF01585511
- [82] Caunhye, A. M. and Cardin, M.-A., “An Approach Based on Robust Optimization and Decision Rules for Analysis Real Options in Engineering System Design,” *IIE Transactions*, Vol. 49, No. 8, 2017, pp. 753–767.
doi: 10.1080/24725854.2017.1299958
- [83] Beuchat, P. N., Warrington, J., Summers, T. H., and Morari, M., “Performance Bounds for Look-Ahead Power System Dispatch Using Generalized Multistage Policies,” *IEEE Transactions on Power Systems*, Vol. 31, No. 1, 2016, pp. 474–484.
doi: 10.1109/TPWRS.2015.2394354
- [84] Gerstenmaier, B., “Progress in Defining the Deep Space Gateway and Transport Plan,” Presented at the NASA Advisory Council, NASA Headquarters, March 2017, URL: https://www.nasa.gov/sites/default/files/atoms/files/nss_chart_v23.pdf [cited 06 May 2020].
- [85] “Extending the Operational Life of the International Space Station Until 2024,” NASA Office of Inspector General, Washington, D.C., IG-14-031, Sep. 2014. URL: <https://oig.nasa.gov/docs/IG-14-031.pdf> [cited 18 July 2020].
- [86] “Orbital ATK CRS-4 Mission Overview”, NASA, URL: https://www.nasa.gov/sites/default/files/atoms/files/orbital_atk_crs-4_mission_overview.pdf [cited 06 May 2020].
- [87] “Orbital ATK CRS-5 Mission Overview”, NASA, URL: https://www.nasa.gov/sites/default/files/atoms/files/orbital_atk_crs-5_mission_overview.pdf [cited 06 May 2020].

- [88] “Orbital ATK CRS-6 Mission Overview,” NASA, URL: https://www.nasa.gov/sites/default/files/atoms/files/orbital_atk_crs-6_mission_overview-1.pdf [cited 06 May 2020].
- [89] “Orbital ATK CRS-7 Mission Overview,” NASA, URL: https://www.nasa.gov/sites/default/files/atoms/files/orbital_atk_crs-7_mission_overview.pdf [cited 06 May 2020].
- [90] “SpaceX CRS-6,” NASA, April 2015, URL: [https://www.nasa.gov/sites/default/files/files/SpaceX_CRS-6_Mission_Overview\(1\).pdf](https://www.nasa.gov/sites/default/files/files/SpaceX_CRS-6_Mission_Overview(1).pdf) [cited 06 May 2020].
- [91] “SpaceX CRS-8 Mission Overview,” NASA, URL: https://www.nasa.gov/sites/default/files/atoms/files/spacex_crs-8_mission_overview.pdf [cited 06 May 2020].
- [92] “SpaceX CRS-9 Mission Overview,” NASA, URL: https://www.nasa.gov/sites/default/files/atoms/files/spacex_crs-9_mission_overview.pdf [cited 06 May 2020].
- [93] “SpaceX CRS-10 Mission Overview,” NASA, URL: https://www.nasa.gov/sites/default/files/atoms/files/spacex_crs-10_mission_overview.pdf [cited 06 May 2020].
- [94] “SpaceX CRS-11 Mission Overview,” NASA, URL: https://www.nasa.gov/sites/default/files/atoms/files/spacex_crs-11_mission_overview.pdf [cited 06 May 2020].
- [95] Whitley, R. and Martinez, R., “Options for Staging Orbits in Cislunar Space,” *Aerospace Conference, 2016 IEEE*, Big Sky, MT, Mar. 2016.
doi: 10.1109/AERO.2016.7500635
- [96] Branke, J., Deb, K., Dierolf, H., and Osswald, M., “Finding Knees in Multi-objective Optimization,” *International Conference on Parallel Problem Solving from Nature, Parallel Problem Solving from Nature - PPSN VIII*. PPSN 2004, Lecture Notes in Computer Science, vol 3242, Springer, Berlin, Heidelberg, 2004.
doi: 10.1007/978-3-540-30217-9_73

[97] Suffredini, M. T. , “International Space Station Program Overview,” November 2012, URL: https://www.nasa.gov/pdf/707197main_Suffredini_ISS_NAC_20121114.pdf [cited 06 May 2020].

[98] L2 International Space Station Forum, URL: <https://forum.nasaspaceflight.com/> [cited 06 May 2020].

[99] Scimemi, S., “International Space Station Program Status,” July 2013, URL: [https://www.nasa.gov/sites/default/files/files/HEOC_ISSStatus_July2013\(1\).pdf](https://www.nasa.gov/sites/default/files/files/HEOC_ISSStatus_July2013(1).pdf) [cited 06 May 2020].